2002

The Zintl chemistry of the heavy tetrel elements

Michael Thomas Klem
Iowa State University

INFORMATION TO USERS

This manuscript has been reproduced from the microfilm master. UMI films the text directly from the original or copy submitted. Thus, some thesis and dissertation copies are in typewriter face, while others may be from any type of computer printer.

The quality of this reproduction is dependent upon the quality of the copy submitted. Broken or indistinct print, colored or poor quality illustrations and photographs, print bleedthrough, substandard margins, and improper alignment can adversely affect reproduction.

In the unlikely event that the author did not send UMI a complete manuscript and there are missing pages, these will be noted. Also, if unauthorized copyright material had to be removed, a note will indicate the deletion.

Oversize materials (e.g., maps, drawings, charts) are reproduced by sectioning the original, beginning at the upper left-hand corner and continuing from left to right in equal sections with small overlaps.

ProQuest Information and Learning
300 North Zeeb Road, Ann Arbor, MI 48106-1346 USA
800-521-0600

The Zintl chemistry of the heavy tetrel elements

by

Michael Thomas Klem

A dissertation submitted to the graduate faculty

in partial fulfillment of the requirements for the degree of

DOCTOR OF PHILOSOPHY

Major: Inorganic Chemistry

Program of Study Committee:
John D. Corbett, Major Professor
David P. Cann
Robert A. Jacobson
Gordon J. Miller
L. Keith Woo

Iowa State University

Ames, Iowa

2002

ProQuest Information and Learning Company
300 North Zeeb Road
P.O. Box 1346
Ann Arbor, MI 48106-1346

Graduate College
Iowa State University

This is to certify that the doctoral dissertation of

Michael Thomas Klem

has met the dissertation requirements of Iowa State University

Signature was redacted for privacy.

Major Professor

Signature was redacted for privacy.

For the Major Program

TABLE OF CONTENTS

CHAPTER 1. GENERAL INTRODUCTION AND EXPERIMENTAL METHODS

Introduction

Exploration of the alkali metal / alkaline-earth metal / heavy tetrel (Sn or Pb) systems has revealed a vast array of new chemistry and novel structure types. The structures and properties of these new materials have been studied in an attempt to understand the chemistry of these and other related systems. Most of these materials possess a metallic luster indicative of an intermetallic compound, which is correct in some cases, but upon further analysis, a majority of these compounds exhibit closed-shell bonding along with the corresponding semiconducting and diamagnetic properties. The latter properties are more consistent with valence (salt-like) compounds and thus may be considered as a link between valence and intermetallic structures. The latter category of materials has become known as Zintl phases[1] and traditionally formed between elements of type A, where A = alkali-metal, alkaline-earth, or rare-earth metals, and of type B, where B = group 13, 14, or 15 elements. Zintl phases are traditionally viewed as compounds that have discrete isolated anions or anionic frameworks that are held together by 2-center–2-electron bonds. Some of the more recently examined heavy tetrel clusters exhibit delocalized bonding that would be considered deficient by the 2-center-2-electron bond scheme provided by the Zintl-Klemm classification,[2] but they still possess a closed shell configuration, identical in characteristics to those attributed to deltahedral polyboranes whose electronic requirements were first described via Wade's rules.[3]

The electron counting rules developed by Wade have become an incredibly useful tool for the electron counting in boranes and carboranes. These rules state that the number of

skeletal electrons required for bonding in a *closo*-cluster depends only on the number of vertices (n) in the structure and is equal to 2n + 2. This sum also remains the same, even when vertices are removed, i.e. 2n + 4, and 2n + 6 for the corresponding (n – 1) *nido*- and (n – 2) *arachno*- types.

The group 14 elements present an interesting problem in the search for novel clusters. The *closo*-deltahedron from a tetrel element (Si, Ge, Sn, or Pb) would have a total charge of -2 for n independent vertices. The problem is obvious, only two alkali metal cations are now needed for charge balance and, therefore, not enough of them may be present to pack around the clusters (especially larger ones), and separate them in the solid.

A variety of solutions to this problem present themselves. One of the first is the formation of *nido*- or *arachno*-deltahedra of small clusters. This would give an overall charge of 4- and 6- respectively, and allow for 4 or 6 A^+ cations to separate them. One example of this is the *nido*-Tt_4^{4-} (Tt = Si, Ge, Pb) known to form with all alkali metals in a simple one-to-one binary ATt (A = Na-Cs; Tt = Si-Pb).[4] The use of larger monovalent cations, such as K, Rb, or Cs, has been used to isolate the *closo*-Tt_9^{4-}.[5] This work reports one such example of a Tt_9^{4-} cluster phase, Rb_4Pb_9.

It is, of course, possible to produce new Zintl compounds of the tetrel elements without resorting to cluster formations. Examples in binary systems would include such phases as $Ca_{31}Sn_{20}$, $Sr_{31}Pb_{20}$, and $Yb_{31}Pb_{20}$.[6] These phases possess isolated M^{4-} atoms, M_2^{6-} dimers, and linear M_5^{12-} pentamers (M = Sn or Pb). Another example of a binary Zintl phase lacking recognizable clusters of the tetrel elements is Na_7Sn_{13}, which has a complex three-dimensional structure built from mainly 4-bonded tin atoms in interbonded pentagons.[7] Also, it is possible to isolate tetrel clusters with relatively few cations, as was demonstrated in the

Zintl phase $BaGe_2$ which contains Ge_4^{4-} tetrahedra separated by Ba cations in the $BaSi_2$ structure type.[8]

It has been discovered that structural stability can be "tuned" by using a mixture of alkali-metal cations to obtain phases that are not available in ordinary binary systems. The use of mixed cations allows one to tune for electron count and packing requirements simultaneously. This was exploited initially in the heavier triel (In, Tl) systems to obtain new phases.[9] Recently this has been expanded to include the heavier tetrels (Sn or Pb) with such examples as $Ca_{2-x}Mg_xTt$ (Tt = Sn, Pb),[10] $Ca_{6.2}Mg_{3.8}Sn_7$,[11] $A_4Li_2Sn_8$ (A = K, Rb),[12] $RbLi_7Ge_8$,[13] and $Ba_{16}Na_{204}Sn_{310}$, the last of which contains an isolated gigantic tin cluster of 56 atoms making it the largest known main group cluster, besides fullerenes, in the solid state.[14] Interestingly, there is only one reported case known for lead with mixed alkali-metals, $Cs_{10}K_6Pb_{36}$.[15]

Another method at obtaining novel cluster materials is to synthesize the clusters from solution in which large countercations, such as crypt-$(A)^+$ (A = alkali-metal; crypt = 4, 7, 13, 16, 21, 24-hexaoxa-1, 10-diazobicyclo-(8,8,8)hexacosane) are available. Reported cluster examples from cryptated salts include the *closo*-M_5^{2-},[16] *nido*-M_9^{4-},[17] *closo*-M_9^{3-} (M = Ge, Sn, Pb),[18] *closo*-Ge_9^{2-},[19] and *closo*-Ge_{10}^{2-}.[20]

The introduction of a third element, particularly an electron poorer one, may aid in the formation of clusters by increasing the number of counter cations required for closed shell bonding. The group 13 elements at first glance seem ideal for this purpose. These elements are frequently called electron poor-elements, because they only have one p-electron per atom and have to share it with as many atoms as possible to achieve good bonding. This, of course, is a prerequisite for cluster bonding. The combination of Group 13/14 elements

could give rise to unknown heteroatomic clusters that could adequately be separated by cations like those of the alkali metals and has been somewhat successful in solution chemistry giving rise to $TlSn_8^{3-}$ and $TlSn_9^{3-}$.[21] Other such examples in "neat" systems would include $Ca_5In_9Sn_6$.[22] This work reports another "neat" example A_5InPb_8 (A = K, Rb) which has $InPb_8^{5-}$ clusters consisting of two Pb_4 tetrahedra linked by a μ_6-In atom in a D_{3d} arrangement.

Attempts to include group 15 elements in a heteroatomic cluster present their own difficulties. These elements are relatively rich in electrons compared to the triels, and only require 3 bonds to gain an octet. These elements readily form nondeltahedral clusters where each vertex is 2- or 3-bonded like Bi_4^{2-} and Sb_7^{3-}.[23-24] Wade's rules are generally not valid for such formations because they contain simple 2-center–2-electron bonds. By mixing Group 14/15 elements it may be conceivable to produce small clusters of the arachno or higher classes of deltahedra. This has led to the formation of $K_5As_3Pb_3$, a new phase that consists of As_3Pb_3 crown-shaped clusters that form 1-dimensional chains via intercluster bonds.

The stabilities of ionic cluster salts in the solid are often influenced by packing as well as electronic effects. The modification of cation or anions along with the formal charge on either can lead to new structure types, although typically, this often leads to apparent instability of a cluster species. This work reports on a series of compounds (Sr_3Sn_5, Ba_3Pb_5, and La_3Sn_5) in the Pu_3Pd_5 structure type that contains varying numbers of nominally free metal electrons beyond the requirements imposed by the Tt_5^{4-} clusters. These clusters behave differently than what would be expected in molecular systems, because the free electrons in the later would normally further reduce the clusters present. The limited number of cations

and the excess electrons also allow for appreciable intercluster interactions that are mediated by the cations.

Exploratory synthesis is, and will continue to be, an important aspect of the pursuit of novel compounds. The continual discovery of new cluster formations and unusual properties, some of which are reported herein, provide an incentive for new synthetic work. The best results are often unexpected and arrive from plausible, but incorrect ideas about the structures one can target, such as the attempted substitution of In into a Pb_9^{4-} cluster that gave rise to the new phase K_5InPb_8.

Experimental Techniques

Starting Materials. Almost all of the compounds reported were prepared starting with stoichiometric amounts of the elements except for a few instances in which a binary hydride were loaded. Elemental sodium (Fisher, 99.9%) in the form of a large block (approximately 5 x 5 x 10 cm) that was stored in an gas-tight mason jar inside of a N_2-filled glove box. The surface of the block became oxidized and the oxidized part was removed with a scalpel. The other alkali-metals were used as received from the manufacturer, potassium (Aesar, 99.95%, Strem 99.9995%), rubidium (Aesar 99.95%, Strem 99.999+%), and cesium (Aesar 99.95%). Small ampoules of these metals were stored inside mason jars that had an excess of alkali-metal present to act as a getter. The alkaline-earth metals used were strontium (Aesar, distilled, 99.8%) and barium (Aesar distilled, 99.8%). The rare earth-metal lanthanum (Ames Lab, 99.99%) was obtained as thin sheets and was stored inside of a N_2- or He-filled glove box. The cold-rolled sheets were scraped with a scalpel to remove any accumulated oxide coating before use. The other main group elements used included lead

(Aesar, 99.9999%), tin (Aesar 99.99%), indium (Aesar, 99.99%), and arsenic (Aldrich, 99.9999%).

Inert Atmospheres. The air-sensitive nature of most starting materials and of all the products required the use of several specialized procedures. All reactions were loaded in either a N_2- or He-filled glove-box from Vacuum Atmospheres Co., model PC-1 or model DLX-001-S-P respectively. Product containers were opened in either a Blickman N_2-filled box or one of the glove-boxes mentioned above. The atmosphere was maintained in all three glove-boxes by a Vacuum Atmospheres DRI-TRAIN regeneration system, model HE-493. The moisture and oxygen content of the glove boxes were maintained at <1 ppm by volume by the circulation of the inert gas through an activated Cu/molecular sieve catalyst. The moisture levels were monitored via a Panametrics Systems 3A hygrometer. All of the starting materials were handled either in glass petri dishes or in molybdenum weighing boats while inside of the glove boxes.

Reaction Vessels. The reactivity of the materials required the use of 3/8" tantalum or niobium tubing. The tubing was cut into approximately 1.25–2.00" lengths and cleaned with an acid mixture containing (by volume) 55% sulfuric acid (95% w), 25% nitric acid (70% w), and 20% hydrofluoric acid (49% w) and then rinsed with distilled water. The tubes were then allowed to air dry at which point each tube had one end crimped shut in a vise and sealed by arc welding. The air-cooled welder was evacuated with a rough pump and back filled with an argon atmosphere before welding.

Reaction Loading. The starting materials were placed into the prepared niobium or tantalum tubing inside of a glove-box. The open end of the tube was crimped shut and placed inside of a capped glass container which was then covered with parafilm for transport

to the arc welder. The time outside of the inert environment of the glove-box was minimized (<5 minutes) to reduce the possibility of contamination. The sample tubes were then arc welded as previously described. In order to protect the sealed tubes from oxidation at the high reaction temperatures, the sample tubes were cleaned in a weak acid solution before being enclosed in a silica jacket. The silica jacket was then evacuated with the aid of a mercury diffusion pump. The jacket was heated with a natural gas/oxygen fueled torch to remove moisture from the silica and then to seal it. The vacuum level in the silica jacket was checked with a tesla coil. The jacket was sealed when no discharge was observed.

Heating. The reactions were then generally carried out in a Marshal tube furnace for temperatures < 1000° C. The temperatures were monitored by J-type thermocouples and adjusted by programmable Eurotherm controllers. In order to insure a complete reaction, the tube furnaces were tilted approximately 25° to collect all of the materials at one end of the tantalum tube. A vacuum furnace from Thermal Technology Inc., Model # 100-2560-FP20, was used for temperatures > 1000 °C and/or a dynamic vacuum to achieve the desired phases. A Eurotherm programmable temperature controller and an Aeropak T/C thermocouple were used to control and monitor the respective temperature cycles.

Binary Metal Hydride Preparation. Binary metal hydrides were prepared by the direct reactions between hydrogen gas and the metals. Small pieces of the metal were placed in a cleaned tantalum tube that was then crimped and welded shut as described previously. The tantalum tube was then placed inside a fused silica vessel connected to a vacuum line. The reaction vessel was then evacuated three times and filled with H_2 gas before initiating the reaction. Each metal was slowly heated to a temperature ranging between 400° and 500° C at a constant hydrogen pressure of approximately 600 to 700 torr. The specific conditions

to hydrogenate the metal were based upon their reported AH_x decomposition isotherms.[25] The start of the reaction was recognized by a 100+ torr drop in the gas pressure, and was considered finished when an increase in temperature was followed by an increase in pressure. The binary products were annealed under H_2 at about 20 to 50°C below the maximum reaction temperature for 24 hours. Identification was made by Guinier x-ray powder pattern, and the cell dimensions of the prepared hydrides agreed with the reported values.[26] All products were single phase.

Product Identification. Completed reactions were opened inside a nitrogen-filled glove box that had an optical microscope (objective removed) mounted on the plexiglass top. The reaction tube was opened by cutting off one of the welded ends with a tube cutter. The products were then poured out of the tube or scraped from the tubing walls with a spatula into a glass Petri dish. The sample was then visually inspected for morphology, color, brittleness, crystallinity, and whether the sample was sticky because of any excess of alkali metal. If crystals suitable for single crystal x-ray diffraction experiments appeared, they were sealed into 0.3 mm diameter capillary tubes with grease, and later sealed with a gas microtorch outside the glove box. The remaining sample was then ground into chunks and powder using a mortar and pestle in the glove box. The majority of the ground sample was then later sealed in a evacuated Pyrex tube using a natural gas/oxygen torch, while a small amount was separated from the bulk and mixed with NIST (SRM-640b) standard silicon. The latter sample was fixed between two sheets of aluminized polyester film, (from MPI Outdoors) by means of a thin centered film of Apiezon L vacuum grease which also sealed the outer edge of the sheets to prevent decomposition of the air sensitive products.[27] This was done to reduce the otherwise frequent appearance of broad patterns for elemental Pb, Sn,

or In from subsequent accidental oxidation of the sample surface. The foil wrapped sample was put into a closed container and transferred to a rotating sample holder inside an X-ray powder camera. The Guinier cameras, Enraf-Nonius model FR552, utilized monochromated Cu $K\alpha_1$ radiation ($\lambda = 1.540562$ Å), with the samples held under continuous rough pump evacuation (~150 mTorr). The X-ray powder diffraction patterns were recorded with Kodak BIOMAX MR Scientific Imaging Film.

The resulting patterns were visually compared against calculated patterns of known elements and compounds (or hypothetical compounds of known structure types). The calculated powder patterns were obtained through the use of the program POWDER[28] on a VAX computing system or a MS-DOS native version.[29] The yield of specific phases could be qualitatively estimated based on relative intensities of the strongest diffraction lines through comparisons of the experimental and calculated patterns. This method requires care, because differing symmetries, preferred orientation, sampling, and other factors can contribute to the relative intensities observed.

An LS20 Line Scanner from KEJ Instruments allowed for a more precise measurement of line positions and intensities. The program SCANPI8[30] was used in the digitizing process to adjust the data to account the individual camera and film variations and the Si standardization. The process of matching and refining the experimental diffraction lines to the theoretical model was done in one of two ways. The first method uses the program COMPARE[31] to match the experimental and theoretical patterns. The lattice constants and associated errors were then calculated from the former via least squares refinement using the program LATT.[32] The other method was to use the program U-FIT V1.3 to carry out the matching and refining process.[33]

Single Crystal X-ray Diffraction. After identifying an unknown in a powder pattern, the quality of single crystals obtained was evaluated through Laue photographs on either a Weissenburg or precession camera obtained with Cu $K\alpha_1$ radiation. The best crystals were selected for further study and were transferred to one of two diffractometers, a Rigaku AFC6R with a rotating anode, or a Bruker CCD Smart System 3 equipped with an area detector and a sealed x-ray tube. Both diffractometers utilized graphite-monochromated Mo $K\alpha$ radiation (λ=0.71069 Å). Single-crystal data sets were acquired and analyzed using the associated software packages for each machine, controller software (Molecular Structure Corp.) for the AFC6R, and SMART (Bruker AXS) for the Bruker CCD. The data were then manipulated and refined in either TEXSAN[34] or SHELXTL[35]. Details of the data collection and analysis may be found in the experimental section of each of the chapters.

Energy Dispersive X-ray Spectroscopy (EDS). The elemental compositions of crystals and powdered samples were occasionally evaluated via energy-dispersive X-ray spectroscopy (EDS) on a JEOL system 840A scanning electron microscope (SEM), equipped with an IXRF X-ray analyzer system and a Keverex Quantum light element detector. Typical data collections utilized a beam of approximately 20kV and 0.3nA to gain a count rate of about 2500 s^{-1}.

Magnetic Susceptibility Measurements. Molar susceptibilities were measured with respect to temperature on a SQUID magnetometer from Quantum Design. The air-sensitive nature of the samples required the use of a special container. The powdered samples were held between two fused silica rods (3 mm outer diameter) which were sealed within a fused silica tube (3 mm inner diameter and approximately 15-20 cm long).[36] All samples were

loaded in a He-filled glove box. The raw data obtained were then corrected for the sample holder and for the diamagnetic cores.

Electrical Resistivity Measurements. The electrical resistivities of powdered samples were measured by the electrodeless Q-method.[37] This technique relies on the surface conduction of a sample to change the quality factor of a coil. The powder sample was sieved through a 250 μm mesh onto a 150 μm mesh sieve to obtain a sample with an average 200 μm particle size. The sample was then diluted with dry chromatographic Al_2O_3 (approximately 1 cm^3) to isolate the individual particles from one another. Each sample was loaded inside a He-filled dry box and later sealed inside the Pyrex tube with a natural gas/oxygen torch.

To measure the resistivities, the sample was placed inside a copper coil operating at 34 MHz, and the quality factor (Q) of the coil was measured with a Hewlett-Packard model 4342A Q meter over a temperature range of approximately 100 to 298K. At each temperature, the sample was then removed from the coil, and the quality factors (Q_o) measured each time. This change in the quality factor ΔQ (normally $Q > Q_o$) was used to calculate the sample resistivity (ρ) using the formula:[38]

$$\rho = \frac{B(Va)}{\Delta(1/Q)}$$

where B is a constant that is calibrated for every coil (4.84×10^5), V is the sample volume (m^3), a is the average particle radius (m), and $\Delta(1/Q)$ is $1/Q - 1/Q_o$. This equation assumes that the samples are diamagnetic or only weakly paramagnetic; various corrections need to be included otherwise. The average resistivity values obtained from this method are approximately within a factor of three of those measured by four-probe methods.[39]

The resistivity values in this work are reported in units of micro-ohm centimeters ($\mu\Omega \cdot$cm) and the temperature resistivity coefficients are calculated from the slope of the ρ versus T curves [$\delta\rho/(\rho_o\delta T)$] in K^{-1},[40] where ρ_o is the resistivity of the sample at the average temperature measured.

Electronic Structure Calculations. Molecular orbital and band calculations were made with the CAESAR EHTB software package.[41] The calculations were carried out within the tight-binding approximation for the full structure at k-points spread out over the irreducible wedge and used to produce the energy densities-of-states (DOS) and crystal orbital overlap populations (COOPs). The H_{ii} values and orbital coefficients used are listed in the respective chapters. Occasionally it was necessary to charge iterate the starting H_{ii} parameters to self consistency, in order to obtain a more satisfactory and reasonable answers, and this was done with the associated Iterate program.[42]

Thesis Organization. The thesis has been arranged in the form of papers suitable for publication. Each chapter corresponds to one paper. The second paper has been published, while the remaining chapters are ready for submission. The author has also contributed to another publication that is not directly related to the thesis topic. This paper reported the synthesis, single crystal x-diffraction study, and theoretical considerations of $A_8Tl_{11}Pd$ (A = Cs, Rb, K).[43] The author was involved with running and analyzing the extended Hückel calculations.

References

(1) *Chemistry, Structure, and Bonding of Zintl Phases and Ions*; Kauzlarich, S.; Ed.; VCH Publishers: New York, **1996**.

(2) Klemm, W.; Busmann, E. *Z. anorg. allg. Chem.* **1963**, *319*, 297.

(3) Wade, K. *Adv. Inorg. Chem. Radiochem.* **1976**, *18*, 1.

(4) Lambert, G.J.; Dicks, L.; Crowther, P. *J. Phys. Chem.* **1968**, *72*, 1439.

(5) Quenéau , E; Sevov, S. C. *Angew. Chem. Int. Ed. Engl.* **1997**, *36, 1754.; b.)* Quenéau, E; Sevov, S.C., *Inorg. Chem.* **1998**, *37*, 1350.; Todorov, E.; Sevov, S.C. *Inorg. Chem.* **1998**, *37*, 3889; c.) Xu, L.; Sevov, S.C. *J. Am. Chem. Soc.* **1999**, *121*, 9245.

(6) Ganguli, A.K.; Guloy, A.M.; Leon-Escamilla, E.A.; Corbett, J.D. *Inorg. Chem*, **1993**, *32*, 4349.

(7) Vaughey, J.T.; Corbett, J.D. *Inorg. Chem.* **1997**, *36*, 4316.

(8) Vaughey, J.T.; Miller, G.J.; Gravelle, S.; Leon-Escamilla, E.A.; Corbett, J.D. *J. Solid State Chem.* **1997**, *133*, 501.

(9) Dong, Z.-C.; Corbett, J.D. *J. Am. Chem. Soc. 1994, 116,* 3429.

(10) Ganguli, A.K.; Guloy, A.M.; Corbett, J.D. *J. Solid State Chem.* **2000**, *152*, 474.

(11) Ganguli, A.K.; Corbett, J.D. *J. Am. Chem. Soc.* **1998**, *120*, 1223.

(12) Bobev, S.; Sevov, S.C. *Angew. Chem. Int. Ed.* **2000**, *39*, 4108.

(13) Bobev, S.; Sevov, S.C. *Angew. Chem. Int. Ed.* **2001**, *40*, 1507.

(14) Bobev, S.; Sevov, S.C. *J. Am. Chem. Soc.* **2002**, *124*, 3359.

(15) Bobev, S.; Sevov, S.C., *Polyhedron*, **2002**, *21*, 641.

(16) Edwards, P.A.; Corbett, J.D. *Inorg. Chem.* **1977**, *16*, 903.; b.) Campbell, J.; Schrobilgen, G. *Inorg. Chem.* **1997**, *36*, 4078.

(17) Belin, C.; Corbett, J.D.; Cisar, A. *J. Am. Chem. Soc.* **1977**, *99*, 7163; b.) Corbett, J.D.; Edwards, P.A. *J. Am. Chem. Soc.* **1977**, *99*, 3313.; c.) Burns, R.C.; Corbett, J.D. *Inorg. Chem.* **1985**, *24*, 1489.; d.) Campbell, J.; Dixon, D.A.; Mercier, H.P.; e.) Schrobligen, G.J. *Inorg. Chem.* **1995**, *34*, 5798.

(18) Angilella, V.; Belin, C. *J. Chem. Soc. Faraday Trans.* **1991**, *87*, 203.; b.) Fässler, T; Hunziker, M. *Inorg. Chem.* **1994**, *33*, 5380.; c.) Critchlow, S.C.; Corbett, J.D. *J. Am. Chem. Soc.* **1983**, *105*, 5715.

(19) Belin, C.; Corbett, J.D.; Cisar, A. *J. Am. Chem. Soc.* **1977**, *99*, 7163.

(20) Belin, C.; Mercier, H.; Angilella, V. *New J. Chem.* **1991**, *15*, 931.

(21) Burns, R.C.; Corbett, J.D. *J. Am. Chem. Soc.* **1982**, *104*, 2804.

(22) Xu, Z.; Guloy, A.M. *J. Am. Chem. Soc.* **1998**, *120*, 7349.

(23) Cisar, A.; Corbett, J.D. *Inorg. Chem.* **1977**, *16*, 2482.

(24) Adolphson, D.G.; Corbett, J.D.; Merryman, D.J. *J. Am. Chem. Soc.* **1976**, *98*, 7234.

(25) Magee, C.B., in *Metal Hydrides*, Mueller, W.M.; Backledge, J.P.; Libowitz, G.G., eds., Academic Press, NY, **1968**, Ch 6.

(26) Villars, P.; Clavert, L.D., *Pearson's Handbook of Crystallographic Data for Intermetallic Phases*, 2nd ed., American Society for Metals International, Metals Park, OH, **1991**.

(27) Kaskel, S.; Corbett, J.D. *Inorg Chem.* **2000**, *39*, 778.

(28) Clark, C.M.;. Smith; D. K; Johnson, G.J. A Fortran IV Program for Calculating X-Ray Powder Diffraction Patterns –Version 8, Department of Geosciences, Pennsylvania State University: University Park, PA, **1973**.

(29) MS-DOS version uses the POWDER calculation routines with a front-end written and compiled by Martin Köckerling.

(30) Werner, P.-E. Arrhenius Laboratory, University of Stockholm, Stockholm, Sweden, **1990**.

(31) Maggard, P. Ames Laboratory, Iowa State University, unpublished research, **1995**.

(32) Takusagawa, F, Ames Laboratory, Iowa State University, unpublished research, **1981**.

(33) Michel, E. Institut des Matériaux de Nantes. Nantes, France. **1992**.

(34) TEXSAN for Windows, Version 1.04, Molecular Structure Corp., The Woodlands, Texas, **1997**.

(35) SHELXTL. Version 5.1. Bruker AXS, Inc. Madison, Wisconsin. **1997**.

(36) Guloy, A.M. Corbett, J.D., *Inorg Chem.* **1996**, *35*, 4669.

(37) El-Hanany, U. *Rev. Sci. Instrum.* **1973**, *44(8)*, 1067.

(38) Zhao, J.-T.; Corbett, J. D. Inorg. Chem. **1995**, *34*, 378.

(39) van der Pauw, L.J., *Phillips Res. Rep.* **1958**, *13*, 1.

(40) Dong, Z.C.; Corbett, J.C., *J. Cluster Sci.*, **1995**, *6*, 187.

(41) Ren, J.; Liang, W.; Whangbo, M.-H. *CAESAR*; PrimeColor Software, Inc. Raleigh, NC, **1998**.

(42) Charge iterations utilized a local variant of the EHMACC suite of programs written and modified by students in R. Hoffmann's group at Cornell University and adapted to the PC by Martin Köckerling

(43) Kaskel, S.; Klem, M. T.; Corbett, J. D. *Inorg Chem.* **2002**, *41*, 3457.

CHAPTER 2. SYNTHESIS AND STRUCTURE OF Rb_4Pb_9, A ZINTL PHASE WITH TWO DIFFERENT ISOLATED Pb_9^{4-} CLUSTER GEOMETRIES.

Michael T. Klem and John D. Corbett*

Department of Chemistry and Ames Laboratory —DOE,[1]

Iowa State University, Ames IA 50011

Abstract

The title phase, isostructural with the previously reported Zintl phase K_4Pb_9, was synthesized by direct fusion of a stoichiometric amount of the elements at 800 °C for 24 hours and then annealed at 350 °C for 4 weeks. The compound crystallizes in a monoclinic space group, $P2_1/m$, Z = 4, with a = 9.8969(16), b = 13.408(2), c = 16.250(3) Å, and β = 103.009(3). The compound contains two different types of Pb_9^{4-} deltahedra, a monocapped square antiprism and a distorted tricapped trigonal prism. Both cluster geometries correspond to a nido assignment even though the tricapped trigonal prism is not the classic Wade's rules nido deltahedron expected. The geometries and their relationships are discussed, and reasons given for the unusual electron count of the tricapped trigonal prism.

Introduction

Until recently, the Zintl chemistry of the heaviest congener of the Group 14 elements, lead, was unknown. The exploration of the alkali-metal—lead binary systems has only produced three types of isolated clusters to date; the tetrahedron found in APb^2 and the nine atom deltahedra (two types) in the A_4Pb_9 type phases (A = K, Cs)[3,4]. The title phase represents the second known alkali-metal—Pb binary which contains two different types of deltahedra, the *nido*-monocapped square antiprism, and the distorted tricapped trigonal prism. Previous to K_4Pb_9, the only known examples of nine atom deltahedra were found in compounds in solution[5] or with cryptated alkali-metals.[6]

The use of the concepts put forth by Zintl–Klemm and Wade are useful because of their ability to form correlations between the geometric and electronic structures of clusters.[7] The title phase is interesting because it possesses a *closo*-like cluster (the tricapped trigonal prism) but has a *nido* (2n + 4) electron count. Molecular orbital studies on the tricapped trigonal prism have indicated closed-shell bonding at 40 electrons per formula unit which is in excess of the 38 predicted from Wade's rules. A study of the effects on the molecular orbital diagram as one goes from a perfect tricapped trigonal prism (D_{3h}) to one that approximates the observed cluster (C_{2v}) points to the substantial role the a_2'' orbital plays in the bonding of the now distorted deltahedron. It is these distortions that permit the 2 extra electrons to occupy a now lowered bonding orbital and allow for the characterization of Rb_4Pb_9 as a Zintl phase.

Experimental Section

Synthesis. The general techniques involving welded Nb containers sealed within evacuated silica jackets have been described elsewhere.[8] An improved method for sample mounting for powder pattern measurements was employed. The sample was held between two sheets of aluminized polyester film by means of a thin centered film of vacuum grease that also sealed the outer edge of the sheets to prevent decomposition of the air sensitive products.[9] Thus the appearance of broad patterns for elemental Pb from subsequent accidental oxidation of the sample surface was greatly reduced over that previously achieved with cellophane tape mounting. All operations were carried out in a N_2- or He-filled glove boxes.

The sample was synthesized from the neat elements (all from Aesar) in sealed niobium tubes. The surfaces of the Rb (99.95%) and Pb (99.9999%) were cut and cleaned with a scalpel before use. The sample was then equilibrated at 800 °C, quenched, and annealed at 350 °C for 4 weeks. The Guinier powder pattern of the products showed Rb_4Pb_9 and a trace amount of elemental Pb.

X-ray Diffraction. A single crystal of the dark grey, brittle compound was mounted in a glass capillary inside a glove box. The crystal was first checked by Laue photography for its singularity and then transferred to a Bruker SMART 1000 CCD-equipped X-ray diffractometer for data collection. A total of 1818 frames was collected with an exposure time of 30 s each. The reflection intensities were then integrated with the SAINT subprogram in the SMART software package.[10] A monoclinic unit cell was initially indicated from 322 indexed reflections, and the data collection process yielded a total of

12799 reflections out of which 11773 had intensities greater than $2\sigma(I)$ and 1935 were independent. The program SADABS was applied for an empirical absorption correction.[11]

The SHELXTL software package was used for space group determination. Systematic absences led to the indicated primitive cell with the possible space groups being $P2_1$ (4) or $P2_1/m$ (11). The intensity statistics showed a clear indication of centrosymmetric space group ($<E^2 - 1> = 0.917$), and the centrosymmetric space group $P2_1/m$ gave satisfactory refinement results. The refinement was carried out via direct methods, and the final residuals were $R(F^2)/R_w = 5.0/11.8$ with the highest residual in the ΔF map, of 2.824 e/Å^3, located 1.85 Å from Pb4.

Calculations. Theoretical calculations were made over 326 k-points in the irreducible wedge with the aid of the CAESAR EHTB program of Whangbo, et al.[13] Only the lead atoms were included (H_{ii} and ζ_1 for Pb 6s: -15.70 eV and 2.35, for Pb6p: -8.00 eV and 2.06).[14]

Results and Discussion

Structure. This phase crystallizes in the K_4Pb_9 structure type.[3] Details of the refinement as well as important Pb-Pb distances are listed in Tables 1 and 2 respectively. The structure can be described as isolated nine-atom clusters of lead in two different, but closely related, geometries (Figure 1) with the same formal charges of 4-.

The type A cluster (Pb2, 4-6, 9, 11) is a distorted nido-monocapped square antiprism, Figure 2a, with the expected charge of -4 as predicted by Wade's Rules ($2n$+4). The square of atoms Pb2, 5, 9 is capped by Pb6, while the square of Pb4, 11 is left open. The distances within the cluster range from 3.064(2) to 3.539(2) Å. The largest distances occur within the

capped square of the antiprism and the shorter distances occur from the capping atom and in the open square of the antiprism. As usual, there appears to be some association between the bonding associated with the capping atom and the distances within the capped square. This inverse relationship gives rise to distances that are on average 0.35 Å longer within the capped square as compared to the uncapped face.

The Type B cluster (Pb 1, 3, 7-8, 10, 12) is an elongated tricapped trigonal prism, Figure 2b, with two long vertical edges of the trigonal prism (3.835 Å) and a shorter third one (3.441 Å). The other distances within this cluster range from 3.070(2) to 3.323(2) Å. This geometry for a cluster of nine atoms and 22 electrons is quite uncommon in neat solids with other known examples including the A_4Tt_9, $A_{12}Tt_{17}$[15] (A = alkali metal and Tt = group 14 minus carbon), and $Cs_{10}K_6Pb_{36}$.[16] The alkali-metal about each cluster adopts the expected configuration. The alkali-metal caps and bridges the faces and edges of the polyhedra, respectively.

In order to assign a cluster to a specific geometry (square-prism or trigonal prism) one needs some criteria to compare. What has traditionally been done is to compare important distance ratios and dihedral angles in a series of related clusters. Listed in table 4 is the paramagnetic closo-Pb_9^{3-} tricapped trigonal prism in [2, 2, 2–crypt-K]$_3Pb_9$·0.5en,[17] a monocapped square antiprism from [2, 2, 2,-crypt-K]$_3$[KPb_9],[18] the monocapped square antiprism from Cs_4Pb_9,[4] and the elongated tricapped trigonal prism of Bi_9^{5+}.[19] The two cluster types found in the present compound were also included for comparison. The table clearly shows that the type-A clusters have parameters that correlate with the nido-monocapped square antiprism classification. The type-B clusters, however, appear to be closer to the tricapped trigonal prism classification.

Bonding. The clusters are found in a ratio of 1:1 in the full structure so the formula could be written as $K_8[Pb_9$ (type A) Pb_9 (type B)]. Since the type A is a normal nido-cluster, the formal charge should be -4, and this in turn implies that type B also has a -4 formal charge to give a total that is consistent with the number of cations present. This also implies that both clusters have 2n + 4 skeletal electrons instead of the 2n + 2 prescribed for tricapped trigonal prisms by Wade. Extended Hückel calculations show similar HOMO-LUMO gaps at about 3.0 and 2.6 eV for the A- and B-type clusters at 40 electrons (22 skeletal electrons + 18 lone pair electrons). Analysis of the COOP curves for the full structure show that both cluster geometries are optimized (all bonding levels filled) at 40 electrons per formula unit, as expected.

There has been extensive discussion in the literature on the bonding adopted within 9 atom deltahedra with monocapped square antiprism or tricapped trigonal antiprism geometries.[3,17,18,20] The stabilization of a tricapped trigonal prism with a 2n + 4 electron count can be understood by looking at the changes in a MO diagram when one goes from a regular tricapped trigonal prism to a distorted one as in the title compound which is shown in Figure 3. The MO diagram for the regular tricapped trigonal prism (at 2n + 2 electrons) shows a relatively large gap above the a_2'' LUMO. This LUMO would be attractive for additional electrons if it could be lowered, and this is what happens when the cluster is allowed to distort. This a_2'' orbital has been discussed before and is bonding within the triangular bases, but antibonding between them with the capping atoms not participating.[21] This bonding character makes the orbital particularly sensitive to the height of the prism, and thus is the controlling factor in the distortions that are observed in the title compound. Elongating two (or three) of the three prism edges causes the a_2'' orbital to drop in energy as

the antibonding component between the two triangular bases is greatly reduced. This lowered orbital is now only 0.26 eV above the previous molecular orbital and below a gap of more than 2.5 eV.

The closest intercluster distance in Rb_4Pb_9 is 3.774 Å which occurs between Pb4 and Pb11 of the type-A clusters. This distance is longer than that found in the isostructural K_4Pb_9 (3.669 Å) due to the larger rubidium cations. An overlap population of 0.01 confirms that there is no intercluster bonding between the type-A clusters. For comparison, the intracluster overlap populations for Pb5-Pb9 at 3.539 Å is 0.15 and the overlap for Pb2 – Pb5 at 3.403 Å is 0.22. It was observed for K_4Pb_9 that these intercluster interactions caused a broadening of the valence p-band which gave rise to a small band gap of 0.30 eV. The larger intercluster separation found in Rb_4Pb_9 lessens this interaction somewhat and the band gap grows to 0.7 eV. Care must be taken when considering these results because the calculations fail to include any cation contributions to the bonding.

Conclusions.

The isolated clusters in the title phase can best be thought of as a monocapped square antiprism and a tricapped trigonal prism with two elongated edges. They both carry a 4- charge which is consistent with their assignment as *nido* species (2n + 4 electrons). The distorted tricapped trigonal prism is able to achieve this configuration by lowering the LUMO of the idealized *closo* cluster by elongating two of its three edges. The ability to correlate the structure with a delocalized closed-shell bonding scheme allows Rb_4Pb_9 to be classified as a Zintl phase.

References

(1) This research was supported by the Office of the Basic Energy Sciences, Materials Sciences Division, U. S. Department of Energy (DOE). The Ames Laboratory is operated for DOE by Iowa State University under Contract No. W-7405-Eng-82.

(2) Lambert, G.J.; Dicks, L.; Crowther, P. *J. Phys. Chem.* **1968**, *72*, 1439.

(3) Quenéau, E; Sevov, S.C., *Inorg. Chem.* **1998**, *37*, 1350.

(4) Todorov, E.; Sevov, S.C. *Inorg. Chem.* **1998**, *37*, 3889.

(5) Wilson, W.L.; Rudolph R. W.; Lohr, L. L.; Taylor, R.C.; Pyykkö, P. *Inorg. Chem.* **1986**, *25*, 1535.

(6) Corbett, J.D. *Chem. Rev.* **1985**, *85*, 383.

(7) Zintl E. *Angew. Chem.* **1939**, *52*, 1; b) Klemm, W.; Bussmann, E. *Z. Anorg. Allg. Chem.* **1963**, *319*, 297; c) Schäfer, H. *Ann. Rev. Mater. Chem.* **1985**, *15*, 1; d) Wade, K. *Adv. Inorg. Chem. Radiochem.* **1976**, *18*, 1.

(8) Dong, Z.-C.; Corbett, J. D. *J. Am. Chem. Soc.* **1993**, *115*, 11299.

(9) Kaskel, S.; Corbett, J.D. *Inorg Chem.* **2000**, 39, 778.

(10) *Smart*; Bruker AXS, INC.; Madison, WI, **1996**.

(11) Blessing, R. H. *Acta Crystallogr.* **1995**, *A*51, 33.

(12) *Shelxtl*; Bruker AXS, Inc.; Madison, WI, **1997**.

(13) Ren, J.; Liang, W.; Whanbgbo, M.-H. *CAESAR*; PrimeColor Software, Inc.: Raleigh, NC, **1998**.

(14) Alvarez, A. Tables of Parameters for Extended Hückel Calculations, Parts 1 and 2, Barcelona, Spain, **1987**.

(15) Quenéau, V.; Todorov E.; Sevov, S.C. *J. Am. Chem. Soc.* **1998**, *120*, 3263.

(16) Bobev, S.; Sevov, S.C., *Polyhedron*, **2002**, *21*, 641.

(17) Fässler, T.F.; Hunziker, M. *Inorg Chem.* **1994**, *33*, 5380.

(18) Cambell, J.; Dixon, D.A.; Mercier, H.P.A.; Schrobilgen, G.J. *Inorg. Chem.* **1995**, *34*, 5798.

(19) Friedman, R.M.; Corbett, J.D. *Inorg Chem.*, **1973**, *2*, 979.

(20) Fässler, T.F.; Hoffman, R. *Angew. Chem. Int. Ed. Engl.* **1999**, *38*, 543.

(21) Corbett, J.D.; Rundle, R.E. *Inorg. Chem.* **1964**, *3*, 1408.

Table 1. Selected Details of Data Collection and Structural Refinement for Rb_4Pb_9

	Rb_4Pb_9
Formula Weight	2206.59
Crystal system, space group, Z	monoclinic, $P2_1/m$, 4
lattice constants	
a (Å)	9.8969(16)
b (Å)	13.408(2)
c(Å)	16.250(3)
β(°)	103.009(3)
V(Å^3)	2101.0(6)
Calc. density, Mg m^{-3}	6.976
Absorp. coeff. μ (Mo Kα, cm^{-1})	810.08
R, R_w[a]	0.050, 0.118

[a] $R = \Sigma||F_o| - |F_c||/\Sigma|F_o|$; $R_w = [\Sigma w(|F_o| - |F_c|)^2/\Sigma w(F_o)^2]^{1/2}$; $w = \sigma_F^{-2}$.

Table 2. Refined atomic positions (x 10^4) for Rb_4Pb_9.

	x	y	z	U_{eq}
Pb1	624(2)	2500	2426(1)	42(1)
Pb2	1387(2)	2500	4976(1)	45(1)
Pb3	-37(1)	618(1)	1220(1)	51(1)
Pb4	-3905(1)	1333(1)	6198(1)	50(1)
Pb5	3108(1)	650(1)	6218(1)	52(1)
Pb6	1808(2)	2500	6911(1)	51(1)
Pb7	-2291	1353(1)	2159(1)	54(1)
Pb8	-2407(2)	1337(1)	-250(1)	55(1)
Pb9	-5031(2)	2500	7566(1)	69(1)
Pb10	627(2)	2500	309(1)	52(1)
Pb11	3895(1)	1337(1)	4536(1)	54(1)
Pb12	-4252(2)	2500	737(1)	85(1)
Rb1	-2581(5)	2500	4321(3)	59(2)
Rb2	3823(3)	772(3)	2139(2)	59(1)
Rb3	-521(3)	28(3)	6294(2)	52(1)
Rb4	-3265(4)	-989(3)	909(3)	67(1)
Rb5	-1146(5)	2500	7947(3)	74(2)

Table 3. Atom Separations (Å) in Rb_4Pb_9.

Atoms	Distance	Atoms	Distance
Pb1 – Pb3 x2	3.1719(13)	Pb4 – Pb11 x2	3.064(2)
Pb1 – Pb7 x2	3.211(2)	Pb5 – Pb6 x2	3.118(2)
Pb1 – Pb10	3.441(3)	Pb5 – Pb9 x3	3.539(2)
Pb2 - Pb5 x2	3.4025(19)	Pb5 – Pb11	3.145(2)
Pb2 – Pb6	3.077(3)	Pb6 – Pb9 x2	3.069(3)
Pb2 – Pb11 x2	3.147(2)	Pb7 – Pb7	3.075(3)
Pb3 – Pb7	3.132(2)	Pb7 – Pb12 x2	3.075(2)
Pb3 – Pb8	3.1001(19)	Pb8 – Pb8	3.119(3)
Pb3 – Pb10 x2	3.070(2)	Pb8 – Pb10 x2	3.323(2)
Pb4 – Pb4	3.129(3)	Pb8 – Pb12 x2	3.107(3)
Pb4 – Pb5 x2	3.1022(18)	Pb11 – Pb11	3.119(3)
Pb4 – Pb9 x2	3.122(2)		

Table 4. Selected Edge Ratios and dihedral angles in some Nine-atom Clusters.

Cluster	Symmetry	Edge Ratios[a]		Angle[b]	Ref.
		h_3:h_1	h_2:h_1		
Pb_9^{3-}	$\approx D_{3h}$	1.05	1.01	14	17
Pb_9^{4-}	$\approx C_{4v}$	1.31	1.03	0.7	18
Pb_9^{4-}	$\approx C_{2v}$	1.28	1.05	5.3	4
Bi_9^{5+}	$\approx D_{3h}$	1.07	1.00	16	19
Pb_9^{4-} (A)	$\approx C_{2v}$	1.29	1.04	0	c
Pb_9^{4-} (B)	$\approx C_{2v}$	1.13	1.13	13.1	c

[a] h_3:h_1 and h_2:h_1 are the ratios of the longest height to the shortest height and the second longest height to the shortest respectively.

[b] The angle listed is the smallest dihedral angle in the waist of trigonal prism or the dihedral angle in the base of the square antiprism.

[c] This work.

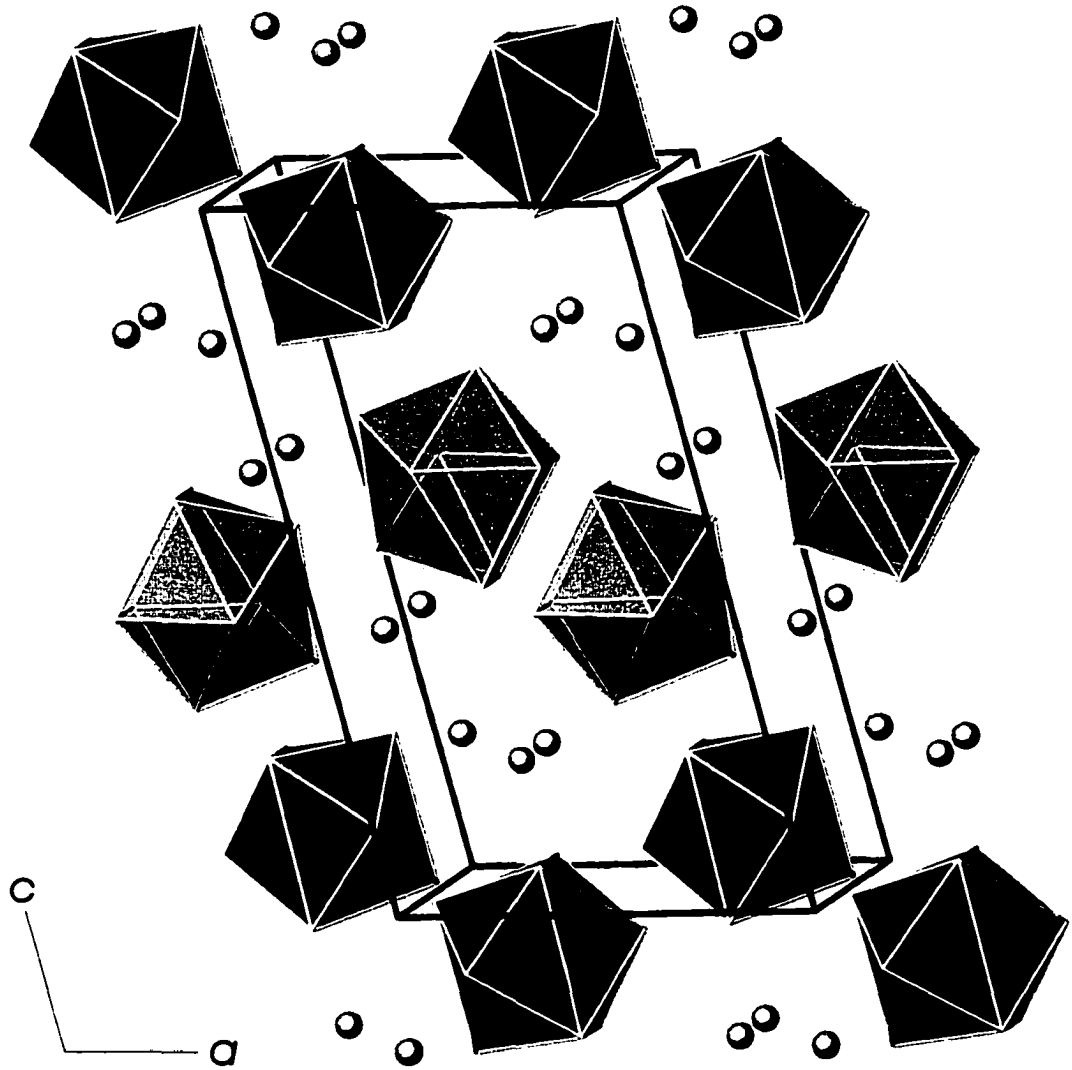

Figure 1. A view along *b* of the structure Rb_4Pb_9 showing the two types of nine-atom clusters: the A-type are lighter than the B-type. The rubidium cations are shown as isolated spheres, and the unit cell is outlined.

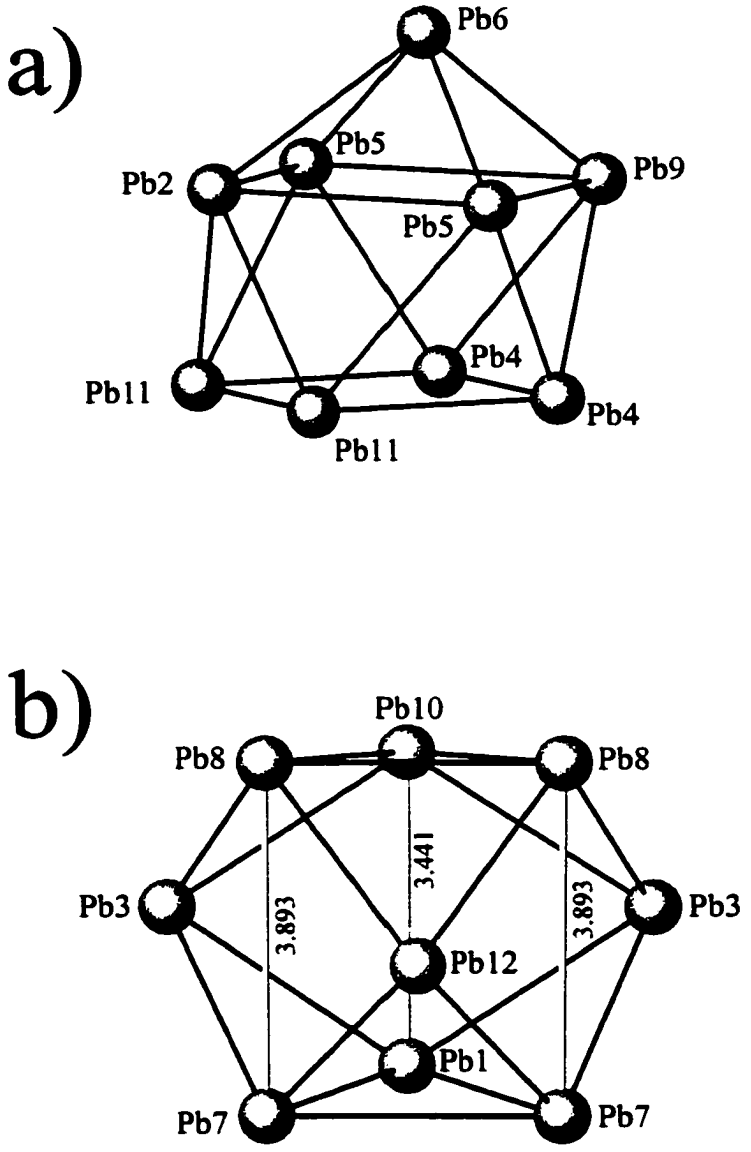

Figure 2. Drawing of the two types of Pb_9^{4-} clusters in Rb_4Pb_9: (a) the A-type, a monocapped square antiprism, and (b) the B-type, an elongated tricapped trigonal prism.

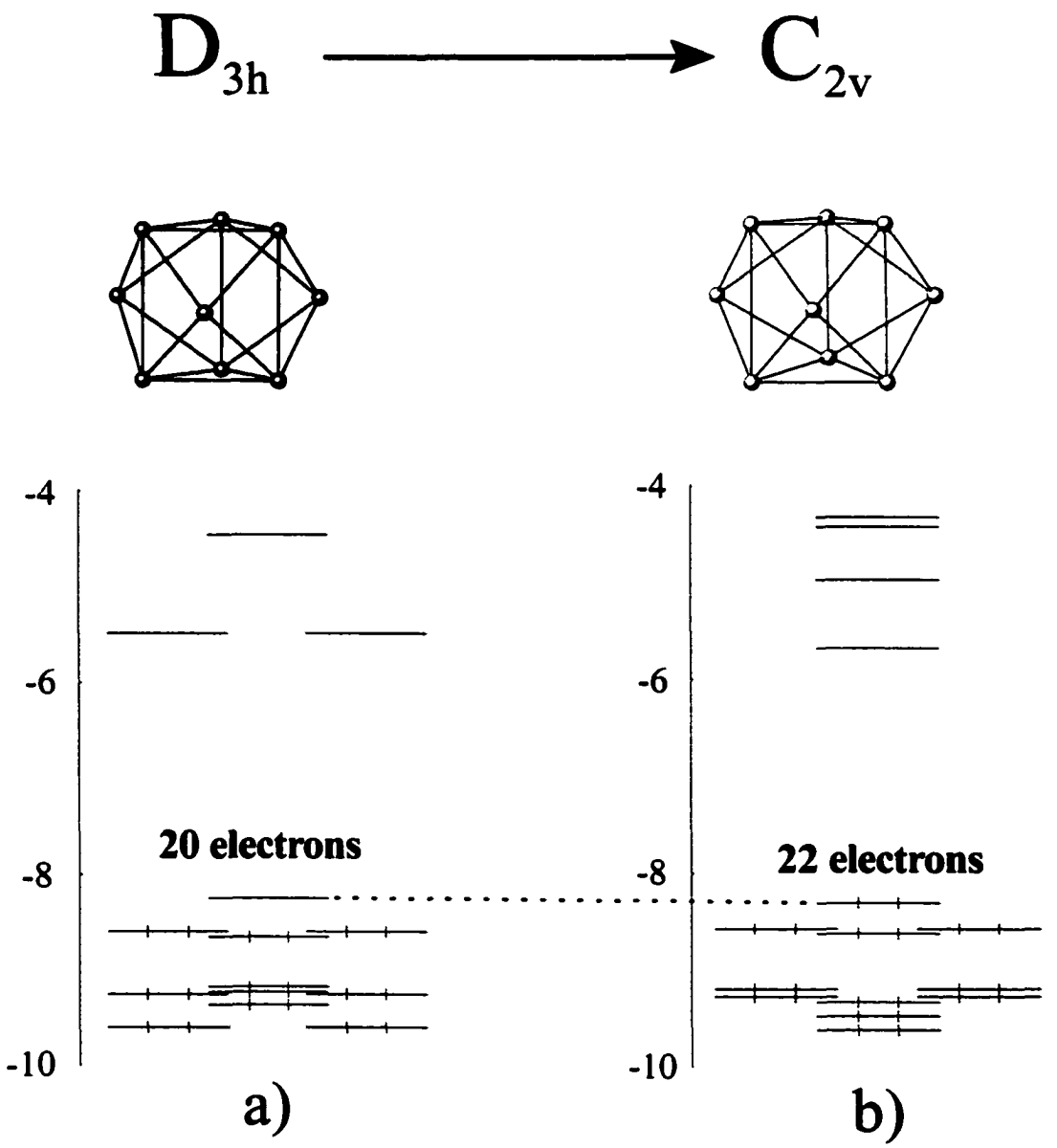

Figure 3. A MO representation of the consequences of distorting a tricapped trigonal prism starting from: (a) the ideal cluster (D_{3h}) to (b) a tricapped trigonal prism with two of three edges elongated.

Table S1. Details of data collection and refinement for Rb_4Pb_9

	Rb_4Pb_9
Formula Weight	2206.59
Crystal system, space group, Z	monoclinic, $P2_1/m$, 4
Unit cell dimensions (Å)[a]	
a	9.8969(16)
b	13.408(2)
c	16.250(3)
β (°)	103.009(3)°
V (Å^3)	2101.0(6)
Calculated density, Mg m^{-3}	6.976
Diffractometer	Bruker Smart CCD
Octants, $2\theta_{max}$ (deg)	$-11 \le h \ge 10, 0 \le k \ge 14, 0 \le l \ge 18$
Observ. refl. ($>2\sigma_I$)	3163
unique	1935
Absorp. coeffic. (Mo Kα, mm^{-1})	81.008
variables	131
R, R_w[b]	0.0495, 0.1180
GOF on F^2	0.722
Extinction coefficient	0.00010(3)
Largest ΔF, e$^-$/Å^3	2.824 at 1.85 Å from Pb4

[a] Guinier powder pattern data, $\lambda = 1.540.562$, 23 °C.
[b] $R = \Sigma||F_o| - |F_c||/\Sigma|F_o|$; $R_w = [\Sigma w(|F_o| - |F_c|)^2/\Sigma w(F_o)^2]^{1/2}$; $w = \sigma_F^{-2}$.

Table S2. Anisotropic displacement parameters[a] ($Å^2$ x 10^3) for Rb_4Pb_9

Rb_4Pb_9	U_{11}	U_{22}	U_{33}	U_{12}	U_{13}	U_{23}
Pb1	47(1)	38(1)	37(1)	0	-1(1)	0
Pb2	37(1)	52(1)	42(1)	0	2(1)	0
Pb3	53(1)	44(1)	51(1)	-6(1)	3(1)	13(1)
Pb4	40(1)	39(1)	69(1)	-2(1)	9(1)	5(1)
Pb5	47(1)	38(1)	73(1)	15(1)	18(1)	-4(1)
Pb6	48(1)	70(2)	42(1)	0	22(1)	0
Pb7	56(1)	37(1)	75(1)	8(1)	28(1)	0(1)
Pb8	67(1)	45(1)	44(1)	1(1)	-7(1)	-11(1)
Pb9	48(1)	128(2)	31(1)	0	14(1)	0
Pb10	50(1)	74(2)	37(1)	0	14(1)	0
Pb11	62(1)	53(1)	49(1)	-21(1)	19(1)	-5(1)
Pb12	39(1)	191(3)	32(1)	0	6(1)	0
Rb1	51(3)	90(5)	41(3)	0	20(2)	0
Rb2	53(2)	67(3)	57(3)	14(2)	13(2)	0(2)
Rb3	45(2)	48(2)	60(3)	-3(2)	8(2)	-2(2)
Rb4	83(3)	46(2)	65(3)	4(2)	1(2)	-15(2)
Rb5	50(3)	149(7)	23(3)	0	9(2)	0

[a] $T = \exp(-2\pi^2(h^2a^{*2}U_{11} + \ldots + 2h\,k\,a^*b^*U_{12}]$

CHAPTER 3. A_3Tt_5 PHASES Sr_3Sn_5, Ba_3Pb_5, La_3Sn_5. STRUCTURE AND BONDING IN A SERIES OF ISOTYPIC METALLIC COMPOUNDS WITH INCREASED ELECTRON COUNT AND THEIR COMPARISON WITH THE NOMINAL ZINTL PHASE La_3In_5

A paper published in Inorganic Chemistry

Michael T. Klem, J. T. Vaughey, Jason G. Harp and John D. Corbett*

Reprinted by permission: *Inorg. Chem.* **2001**, *40*, 7020-7026.

Department of Chemistry and Ames Laboratory —DOE,[1]

Iowa State University, Ames IA 50011

Abstract

A series of compounds that contain square pyramidal Tt_5 polyanions of tin and lead has been obtained in alkaline-earth or rare-earth metal–tetrel systems by direct fusion of the elements at 570 °C (Sr_3Sn_5), 1000 °C (Ba_3Pb_5), or 1300 °C (La_3Sn_5) followed by slow cooling or annealing. The crystal structures for all three have been refined in the Pu_3Pd_5 structure type (orthorhombic, Cmcm, Z = 4) with cell dimensions of a = 10.644(2) , 11.154(7), 10.352(5) Å, b = 8.588(1), 9.049(7), 8.290(6) Å, c = 10.895(2), 11.370(5), 10.652(5) Å for Sr_3Sn_5, Ba_3Pb_5 and La_3Sn_5, respectively. Square pyramidal clusters of the tetrel elements are weakly interlinked into chains via two types of longer intercluster interactions that are mediated by bridging cations and substantially influenced by cation size

and the free electron count. The new compounds are all metallic (ρ_{295} ~10 (Sr_3Sn_5) to ~25 (La_3Sn_5) $\mu\Omega$·cm), in agreement with simple valence considerations that predict two and five extra electrons per formula unit, respectively, beyond that necessary for closed shell nido-Tt_5^{4-} anions. Extended Hückel tight-binding calculations on the new compounds, as well as on La_3In_5, reveal that bonding in the regions below and around the Fermi energies are dominated by general cation–anion interactions, that is, lattice covalency. Closed-shell bonding features for the classical Sn_5^{4-}, In_5^{9-}, etc. ions are also obvious but subsidiary to the heteroatomic interactions with the cations. The intercluster contacts are relatively unimportant in bonding.

Introduction

Both Zintl–Klemm and Wade's principles are useful in inorganic chemistry because of their utility in the correlations of geometric and electronic structures and compositions. Zintl's approach also has predictive power and offers insights into properties and bonding considerations for many main-group solid state materials. Some years ago we considered this correlation between electron count and cluster geometry for two new compounds with the novel Pu_3Pd_5 structure type, La_3In_5 and β-Y_3In_5, in which there are chemically distinctive cluster anions of square pyramidal In_5. According to Wade's rules (or simple MO calculations), the indium square pyramids would be classified as nido deltahedra with 2n + 4 skeletal electrons (14) and a charge of 9–, thereby matching the expected contribution from three rare-earth metal atoms and making these salts structurally Zintl phases. Although the fact that both phases are poor metals (La_3In_5: ρ_{295} = 90 $\mu\Omega$·cm, χ_{Pauli} = ~4 × 10^{-4} emu·mol^{-1}) may seem to deny their strict classification as Zintl (valence) compounds, this situation is in

various degrees common at least among alkali-metal–triel systems relative to analogous compounds of later main-group elements. Diminishing band gaps and increased covalency may be important in these systems. Nonetheless, the compositions of numerous cluster compounds, and their properties when known, still encourage useful and meaningful descriptions of most of them in terms of low lying valence electron pair bonding of the post-transition components, often in clusters, that clearly reflect significant and nominally closed-shells in regular and predictable patterns.[5]

The stabilities of diverse ionic cluster salts in solids are clearly often influenced by packing as well as electronic effects. Chemical modifications of the sizes of the cations or anions along with perhaps the formal charge on either can lead to new structure types, although these perhaps more often lead to instability of the cluster species. In the particular examples of Pu_3Pd_5 structure type reported here, variations in the electron requirements of the main-group polyanions together with charges on the countercations have been found to lead to a novel series of salts in which different numbers of nominally free, metallic electrons remain beyond Tt_5^{4-} clusters, namely, $Sr_3Sn_5 + 2e^-$, $Ba_3Pb_5 + 2e^-$, and $La_3Sn_5 + 5e^-$ to add to the earlier electron-precise examples La_3In_5 and β-Y_3In_5. This structure type also raises other issues in that the limited number of countercations allow appreciable interanionic interactions that are mediated by the cations. This article reports structural, property, and bonding details of this series, and some ramifications of adding electrons to a series of isostructural compounds that included the valence-precise La_3In_5. These compounds present a clearly different regime than do many more molecular systems wherein such metallic characteristics would be quite foreign, and free electrons would normally be expected to reduce or "open up" homoatomic bonds.

Experimental Section

The general techniques utilized welded Ta containers, glove-box operations, and Guinier powder diffraction, as have been described earlier.[6,7] An improved method for sample mounting for powder pattern measurements was employed. Samples were held between two sheets of aluminized polyester film by means of a thin centered film of vacuum grease that also sealed the outer edge of the sheets to prevent decomposition of the air-sensitive products.[7] Thus the appearance of broad patterns of Sn or Pb metals in the patterns from subsequent accidental oxidation of the sample surface was greatly reduced over that previously achieved with cellophane tape mounting. All operations were carried out in N_2- or He-filled glove-boxes.

Syntheses. The synthesis of Sr_3Sn_5 was carried out by mixing stoichiometric amounts of strontium (Aesar, distilled, 99.8%) and tin (Aesar, 99.99%), allowing these to prereact at 900 °C and then quenching and equilibrating the material at 570 °C for 3 weeks. The product was brittle and grey. An X-ray powder pattern of the product could be entirely indexed on the basis of the Pu_3Pd_5 structure type. The composition of this phase, 37.5 a/o Sr, falls close to the boundary between two earlier studies of the Sr–Sr system, 35%, but neither saw evidence for it.[8] It's furthermore not clear whether otherwise assigned isothermal events at 580 – 598° or 820 °C in this region might be the peritectic decomposition or melting temperature for Sr_3Sn_5, although the higher value seems more likely.

The synthesis of Ba_3Pb_5 was similarly carried out by direct fusion of stoichiometric amounts of barium (Aesar distilled, 99.8%) and lead (Aesar, 99.9999%) at 1000 °C for 2 hours, after which the mixture was cooled at 6 °C/hr to 550 °C and held for 2 hours. The X-

ray powder pattern likewise revealed only the Pu_3Pd_5 type product, and the refined lattice constants were in good agreement with those reported by Bruzzone and coworkers.[9] The La_3Sn_5 was also made by direct combination of lanthanum (Ames Lab, 99.999%) and tin at 1300 °C, where it was held for 12 hours and then slowly cooled to room temperature over 2 days. Its X-ray powder pattern revealed the expected Pu_3Pd_5-type pattern in an apparent quantitative yield (>95%), and the lattice dimensions are close to those reported earlier for a phase thought to be related to Pu_3Pd_5.[10] More importantly, intensity distributions in all three patterns were in excellent agreement with those calculated on the basis of the refined structural data (below).

Hydride errors can be particularly serious with many commercial alkaline-earth metals.[11] The absence of significant hydride in what we identify as Sr_3Sn_5 and Ba_3Pb_5 was ensured by production of materials with the same dimensions in each case whether these were made (a) with a SrH_2 or BaH_2 source, (b) when a dynamic vacuum was applied to the Sr–Sn system in Ta at temperature to remove H, or (c) carefully sublimed Ba was used in that synthesis.

Attempts to prepare a number of other isotypic, cation-precise or excess electron phases with the same anions were not successful, i.e., KSr_2Sn_5, $RbSr_2Sn_5$, Rb_2SrSn_5, Sr_3Sn_4As. Sr_3Sn_4Ga, $CsSr_2Sn_5$, Cs_2SrSn_5, Cs_2BaPb_5, Rb_2BaPb_5. Antimony analogues were not found, and cation-richer phases such as $Cs_3La_2In_5$ that might provide better separation of In_5^{9-} units were not achieved either. It was possible, however, to mix alkaline-earth with rare-earth metal cations to prepare other isotypic phases that presumably had 2 – 5 electrons in excess of the expected closed shell values, e.g., YSr_2Sn_5 + 3e. It was also possible to substitute up to ~20% Ga for Sn2 in $La_3Sn_{4.6}Ga_{0.4}$.

X-ray diffraction. Powder diffraction data obtained by an Enraf-Nonius Guinier camera and Cu Kαl radiation were used for phase identification. The films were usually first compared semiquantitatively with the patterns calculated for phases with known structures. The compositions of mixed products were estimated visually from relative powder pattern intensities, considering unit cell contents as well. The cell parameters listed in Table 1 were obtained by least squares refinement of measured and indexed 2θ values utilizing NIST silicon as an internal standard.

Several small grey crystals of Sr_3Sn_5 were first isolated from a $K_{10}Sr_5Sn_{14}$ reaction mixture, placed into thin-walled capillaries, and checked by Laue photographs. Diffraction data from one specimen (0.25 × 0.13 × 0.15 mm) were collected at room temperature using a Rigaku AFC6 diffractometer with monochromated Mo Kα radiation. Routine indexing of 25 centered reflections gave a C-centered orthorhombic cell. Systematic extinctions led to the selection of space group Cmcm and this, rather than the acentric alternate Cmc2, was confirmed in a refinement carried out with the aid of the TEXSAN package.[12] The data were corrected for absorption empirically according to three ψ-scans of strong reflections with different θ values. The final residuals were $R(F)/R_w = 3.6/6.0$ with the largest residual in the ΔF map of 3.6 e/Å^3, located 0.9 Å from Sn2. Potassium was not found in the structure, as further confirmed by the high yield syntheses later achieved from stoichiometric reactions in the binary system.

Similarly, small silvery crystals of Ba_3Pb_5 and La_3Sn_5 were mounted into thin-walled capillaries in a glove box, checked by Laue photographs, and diffractometer data collected from each. The routine indexing and cell reduction procedures indicated C-centered orthorhombic cells for both, and this was verified during collection of a full data set for each.

Systematic absences indicated Cmcm (no. 63) or $Cmc2_1$ (no. 36), and since a Pu_3Pd_5-type structure was already indicated by the powder diffraction data, the former was chosen. Each data set was corrected for absorption with the aid of psi-scans of three reflections. Their refinements were uneventful. Anomalous dispersion and secondary extinction were both taken into account. Because of the strong absorption and the inadequate corrections obtained, particularly at higher θ, an additional correction was applied to each data set by means of DIFABS, starting with isotropic atom displacement values and unaveraged intensity data, as recommended.[13] The final residual R/R_w values and largest peaks in the difference maps were: Ba_3Pb_5: 4.2/5.1% and 3.96 $e^-/Å^3$ 1.6 Å from Pb2; La_3Sn_5: 3.6/4.1% and 2.8 $e^-/Å^3$ 2.1 Å from La2. Most of the published estimates of fractional positional parameters in Ba_3Pb_5 made on the basis of powder diffraction data[9] were off by 0.01 to 0.02, too much to be useful.

Selected crystallographic and refinement data for the three studies are given in Table 2, and more detailed information and displacement ellipsoid parameters are given in the Supporting Information, Tables S1, S2. Refined atom positions for the three structures are listed in Table 3. All three are the first structural refinements.

Calculations. Theoretical calculations were made over 216 k-points in the irreducible wedge with the aid of the CAESAR EHTB program of Whangbo, et al.[14] Orbital coefficients for all elements and H_{ii} values for the main group atoms were taken from Alvarez.[15] Use of La energy values from the same source in the La_3In_5 and La_3Sn_5 calculations gave some nonsensical results, including reverse charge transfer from the anions and to lanthanum. Therefore, the La H_{ii} data were charge-iterated to self-consistency versus In with the aid of a package in the program EHMACC[16] and the charge coefficients from

Alvarez.[15] This raised the La values by 2.5 (s) to 3.3 (d) eV. The same was done for Ba_3Pb_5 starting with H_{ii} estimates for Ba from Seo.[17] The H_{ii} values for valence d orbitals on Sr and Ba were obtained following Burdett's method for making multiplicity corrections to the spectroscopic data for neutral atoms.[18,19] All the parameters employed are listed in Table 4.

Property measurements. Resistivities of Sr_3Sn_5 and La_3Sn_5 were measured by the electrodeless Q method[4] on 66.7 (44.8) mg that had each been sieved to 250 - 425 μm powder and diluted with chromatographic Al_2O_3. Measurements were made at 34 MHz over 120 - 240 K. The resistivity of Sr_3Sn_5 extrapolated to 298 K was 11 $\mu\Omega\cdot$cm with a temperature coefficient $[(\delta\rho/\delta T)/\rho]$ of $2.8(3) \times 10^{-2}$ K^{-1}, while La_3Sn_5 yielded 24 $\mu\Omega\cdot$cm at 298 K with about twice the temperature dependence, $5.5(7) \times 10^{-2}$ K^{-1}. The absolute resistivities may be off by a factor of two or three.

Results and Discussion

The present article reports three newly structured members of the Pu_3Pd_5 structure type that are especially novel because of the clear persistence of square pyramidal cluster groups of the elements Sn and Pb in spite of the apparent presence of excess electrons in them. These become more significant chemically when taken together with the prior example of the isotypic La_3In_5.[4] The last had been given the easy assignment as a Zintl phase structurally[21] in response to the evident valence balance between the expected cation oxidation numbers and the nominal closed-shell nido-In_5^{9-} anion. The fact that this phase is actually a poor metal will receive further consideration later. The new examples Sr_3Sn_5, Ba_3Pb_5 and La_3Sn_5 are on the same basis 2, 2, and 5 electrons rich, respectively, with regard to valence closure. Most important for the moment is what we can deduce about the bonding

in these compounds, including possible or perceptible intercluster bonding interactions as well as, it turns out, significant heteratomic cation–anion bonding or lattice covalence. The fact that the pentatomic anions are not well separated in the presence of a cation:anion ratio of only 3:1, and the relative sizes of the component ions, play significant roles in these secondary interactions. The metallic character of La_3In_5 was earlier attributed to intercluster bonding effects.[4] Although we will not consider Madelung energies per se, it must be recognized that the ultimate stability of every particular ion packing must in detail be significantly dependent on this factor as well.

The Structures. The structure description will start with the Sr_3Sn_5 phase as representative of the lot. The previously reported La_3In_5 will be incorporated into the discussion as well, so critical distances in all four phases are listed in Table 5. Near-[100] and -[001] views of the Sr_3Sn_5 (Pu_3Pd_5-type) unit cell are shown in Figure 1, with the Sn_5 units as blue polyhedra and the separate Sr atoms red. The polyanions all have mm (C_{2v}) symmetry with the 2-fold axes parallel to and vertical in the Figure. The basal Sn2 and Sn3 atoms do not lie in the same plane, doubtlessly because of the several factors that go into the packing and bonding; the separations between these two atoms parallel to range from 0.17 to 0.29 Å with that in La_3Sn_5 at the upper limit. The ranges of the three independent dimensions within the "square" pyramids, marked at the upper right in Figure 1 for Sr_3Sn_5, reflect this distortion and vary from 0.12 to 0.22 Å, being more nearly proportional for the pairs Sr_3Sn_5 vs Ba_3Pb_5 and La_3In_5 vs La_3Sn_5, larger for the latter in each pair. There are two types of generally longer intercluster distances that are influenced both by the main-group cluster element and the size (and presumably field) of the intervening cations, M2–M2 and M1–M3. The Sn2–Sn2 (base-to-base) separations are marked in Figure 1 with the narrower

solid lines, and the usually larger Sn1–Sn3 (base to apex, clearer at the bottom), with lighter lines. These are 0.26 and 0.72 Å longer, respectively, than the largest intracluster distance. The more important intercluster d(M2–M2) values are with one exception longer than all distances within the clusters, by 0.20 Å (La_3In_5) to 0.45 Å (Ba_3Pb_5). In the exceptional La_3Sn_5, bridging by the smaller cations is evidently responsible for an intercluster d(Sn2–Sn2) that is 0.07 Å shorter than the opposed elongated intracluster d(Sn1–Sn2), 3.235 Å. But the only significant intercluster bonding via M1–M3 is in La_3In_5 in which the separation is only 0.15 Å longer than d(In2–In2) and comparable in bonding.

Distances between the two independent cations and atoms in the anions are fairly regular. These also allow some comparative measures of anion sizes. The differences in specific d(A–Tt) pairs in Sr_3Sn_5 vs Ba_3Pb_5 are generally close to 0.16 Å, with lead naturally the larger. Since the cation crystal radii (CN8) differ by 0.14 Å,[21] this suggests that the contact radii for the lead atoms in the anion are only slightly greater than for tin. Coincidently, the same numerical differences apply to comparable bond lengths within the two polyanions. In the more important lanthanum salts, the coordination numbers of the cations are generally a little larger for La2 with tin (7–10, depending on cutoff) than for indium, and the distances are correspondingly about 0.1 Å longer (3.28 and 3.44 Å) for A2 vs A1 in both. Because of appreciable conformational changes, distance comparisons for In_5^{9-} vs Sn_5^{4-} (+5e) and the La–M interactions are rather erratic (below).

Bonding. The details of the intercluster and cation–anion bonding need some better basis for interpretation than can be obtained through simple distance tabulations. The two cations in this structure interbridge four to six clusters with seven or eight good A–M interactions each. Because of the limited number of cations and their higher oxidation states,

these appear to bring or hold clusters in relatively close proximity compared with internal distances in the Tt_5 units. These somewhat complex interplays are more important to our understanding of these structures and their bonding than just simple descriptions of polyhedra about individual cations. Furthermore, as we have recently noted elsewhere, distances alone may be poor descriptors of bond strength because of exterior limitations on distances brought on by atom sizes and packing sometimes produce atom separations that have little to do with bonding, i.e., matrix effects.[22,23]

Thus, a more useful catalog of the pair-wise bonding interactions in these four structures was already included in Table 5, the corresponding Mulliken overlap populations (OP) for each distance from EHTB calculations (below). The larger OP values and the cation bridging effects are best illustrated in Figure 2 for the extreme case of La_3Sn_5. Here "bonds" between atoms are shown with line widths proportional to OP, black for Sn–Sn and orange for La–Sn. (Remember that these are not intercomparable because of overlap integrals that are included. Also, the use of Hamiltonian COHP values, which better approximate bond energies, would underweight the listed heteratomic values.[24]) Figure 2 contains one complete cluster and the parts of four neighboring clusters (blue, with Sn2 darker) that have significant intercluster interactions therewith plus the bridging lanthanum atoms (La1 orange, La2 red) that are involved with these tin atoms. (The whole cluster is equivalent to that at the upper left in Figure 1.) Particularly striking here is the strength (OP) of the Sn2 – Sn2 intercluster bonding in La_3Sn_5, in which each pair of Sn2 atoms is bridged by two La1 and two La2. A substantial role of La1 in strong interactions with four different clusters is also seen at the bottom center. (There are, of course, many other packing components that lead to this structural result.)

The DOS (densities of states) and COOP (crystal orbital overlap populations) output from extended Hückel calculations give better overall insights as to the nature of, and the bonding in, these unusual compounds. They also offer a critical look at both the easy assumption of a Zintl phase classification for La_3In_5 and the question as to whether the new members of the electron-rich series reported here somehow fit into a different scheme. The existence of a fairly uniform and seemingly dominant heteroatomic lattice covalency is the most striking revelation.

Continuing with Sr_3Sn_5, the DOS curve (solid) plus the PDOS projections of Sn (dotted), Sr s+p (dashed), and Sr d (dash–dot) contributions are shown in Figure 3, left. The broad intracluster valence peaks for Sn centered around −10 eV also involve some Sr (covalent) contributions. The low DOS at about −7.8 eV corresponds to filling of the classic Sn_5^{4-} bonding orbitals, 24 e^-/f.u., (and certainly not that appropriate to a 26-electron arachno-Sn_5^{6-} [25]), whereas appreciable Sn 4p and, increasingly, Sr 4d states are involved above there. The latter do not reach a maximum until about 4 eV about E_F (−6.34 eV in this approximation), in contrast to what we shall see below with lanthanum cations. (The Sn 5s is dominant below about −13 eV. Note its importance according to intracluster COOP data, showing that simple "s cores" are not appropriate to this picture. On the other hand, the Sr 5s is generally not important anywhere.)

A clearer understanding of bonding in Sr_3Sn_5 comes from plots of the COOP data — overlap-weighted (Mulliken) bond populations, Figure 3 right, in which the Sn–Sn results are separated into intra- (dotted) and intercluster (dashed) portions. The former component shows a switch from bonding to antibonding contributions just at the point at which the classical valence shell is filled, as it should. The individual types of intercluster interactions

(not shown) are slightly bonding for Sn2 – Sn2 and antibonding for Sn1 – Sn3 near –8 eV, but both are small.

There is clearly nothing significant in the way of a Sr – Sr band (dash-dot curve) compared with the evidently dominant effect of heteratomic Sr – Sn bonding (solid line) that occurs throughout what could be called the valence band and around and above E_F. Plots of the individual Sr_i – Sn_j functions therein (not shown) indicate fairly uniform contributions across all of the bands. The clear bonding peak near –7 eV arises mainly from most of the Sr–Sn pairs that have appreciable overlap populations, Table 5. The charge distributions (from atom populations) are about +1.1 for Sr1, and +1.4 for Sr2 with its higher CN and longer d(Sr – Sn). These would be larger were the Mulliken approximation not to divide bond populations equally.

The bottom line is that a Sn_5^{4-} anion does not exist in any isolated sense in Sr_3Sn_5 because of both the extra electrons and the overarching lattice band (covalency) from multiple and strong Sr – Sn interactions. Nonetheless, that well-bonded closed-shell cluster anion persists in this somewhat complex lattice. There's no a priori reason that would preclude the existence of this electride salt either, but its prediction (or not) has much to do with the effects of efficient packing of the extra cation.

The comparable data for Ba_3Pb_5 are not sufficiently different to detail. The heteroatomic distances and bond populations are naturally longer and less, respectively, whereas Pb–Pb populations in the nominal anions are comparable. Expectations for Ba 5d energy (Table 4) put this much closer to its 6s level (~1.2 eV difference vs. 2.6 eV for Sr 4d vs 5s). Shapes of the DOS and COOP curves are very similar to those for Sr_3Sn_5.

Retention of the nominal Sn_5^{4-} anions but a switch to lanthanum cations increases the magnitude of several effects just described for strontium. This change increases the excess electron count to five per formula unit, but the major effects seem to be associated with the smaller size and higher charge of La^{3+} (1.30 Å vs 1.40 Å for Sr^{2+} and 1.56 Å for Ba^{2+} for CN8 [19]) and the greater proximity of the La 5d valence orbitals, all of which seem to increase what we designate as the lattice covalency substantially. The size decrease naturally increases the intercluster interactions significantly via the tighter interbridging of clusters by the cations; see Sr_3Sn_5 in Figure 2. Figure 4 illustrates the theory results, starting with the DOS for La_3Sn_5 together with PDOS for Sn (dotted) and La (dashed). The minimum in the Sn contributions near −7.8 eV corresponds to the (not quite) closed shell for internal bonding in the square pyramids, whereas both Sn and, increasingly, La are involved in the bonding up to E_F, −5.68 eV. The latter are substantially all La 5d, whereas La 6s is not appreciably involved below ~−3.5 eV by these approximations. The COOP results (Figure 4, right) can now be anticipated — a more emphatic and wider involvement of the lattice covalency (solid line), from the start of the Sn p-band and extending to appreciably higher energies. The antibonding Sn–Sn states components over the last $5e^-$ below E_F are principally intracluster, with the intercluster contributions being slightly antibonding for Sn2 – Sn2 (3.16 Å) and distinctly so for Sn1 – Sn3 (3.63 Å) just below E_F. The charges on the La ions in this approximation are each about 0.1 less than found in Sr_3Sn_5, in parallel with the greater evident La–Sn bonding and in contrast to their higher oxidation state.

We can now return to the original member La_3In_5, for which oxidation state and cluster valence rules predict it to be a valence (Zintl) phase according to the simplest, structural viewpoint. This is in reality a poor assignment, basically because of the strong

La–In covalency. Differences in the comparison with La_3Sn_5 include In states that lie 3.6 (s) and 2.1 (p) eV higher than for Sn, and La–M distances and OP values that are ~0.01 Å larger and very similar, respectively, for In relative to Sn. Changes in packing and bonding lead to a significant intracluster OP for In1–In3 although the separation is only 0.05 Å shorter than for Sn1 – Sn3, whereas In2 – In2 lengthens by 0.26 Å relative to Sn2 – Sn2 but the O.P. decreases only modestly. Projection of the In and La orbital contributions in DOS, Figure 5, show a familiar pattern except that there are closer to three valence bands, but no sign of a gap near E_F for In_5^{9-}. Large lanthanum contributions are spread throughout the upper pseudo-valence band, and this is seen clearly in the dominance of La – In bonding in the COOP data, the solid line in the right part of Figure 5. The intracluster In – In bonding is again optimized at E_F, the closed shell for the isolated In_5^{9-} anion, but the total In – In bonding is optimal somewhat lower because the now-shorter intercluster In1 – In3 (Figure 2, Table 5) is substantially antibonding around E_F (not shown). Both intercluster interactions (dashed line) make comparable and mainly bonding contributions at lower energies.

We have, by the way, not considered the isotypic β-Y_3In_5[4] here because the smaller cation results in markedly shorter intercluster distance relative to those within the In_5 units, and we expect that these, as well as appreciably greater lattice covalence, will make this even further from a classical Zintl phase.

The collective results above provide useful information and education on the all-too-easy Zintl phase classification afforded by the simplest bonding ideas. These seem to work fairly well for alkali-metal–tetrel and –pnictide examples, which are often semiconductors when resistivities are measured (which is fairly seldom). On the other hand, most valence-precise cluster phases for alkali-metal–triel phases are found to be metallic, although at the

same time often diamagnetic, probably because of the unusual diamagnetic components that contribute to the magnetic susceptibilities for these heavy elements.[5] Metallicity in the triel examples may arise in general because of the virtual disappearance of an electronic gap, reflecting the lower electron affinities of the triel elements. We have also recently noted a significant covalence entering into alkaline-earth metal–triel phases with network structures according to theoretical considerations.[17] The greater Madelung energies in most of the latter salts are apparently an increasingly important factor, and good accommodation of the higher field cations becomes more important as well. In addition, achievement of formal closed-shell electronic structures for the alkaline-earth metal examples appears to be less frequent with these higher charged cations, most being slightly electron deficient. It would appear that the Madelung energy must play an important role in the stabilities of the cation and electron-rich compounds considered here as well, the great numbers of, and high effective charges on, the extra cation in Sr_3Sn_5, etc. being significant relative to the unknown Sr_2Sn_5. Of course, much more subtle factors of alternate phase stability also come into play here, and treatment of the delocalized electrons in a Madelung energy sense is problematic.

A novel variation of these mixed salt–metal characteristics is found in $Ca_5In_9Sn_6$.[26] Here close packed metallic layers of $AuCu_3$ and Ni_3Sn types alternate with Zintl layers containing In_3^{5-} and Ca^{2+}.

There is another meaningful chemical viewpoint regarding the electron-rich phases, evidently first expressed by Nesper.[27,28] We find here, and many places elsewhere, well segregated clusters whose compositions, configurations, and evident formal charges agree well with classic Wade's rule or more theoretical MO descriptions, giving us useful ways to understand and correlate these features. Some of these may coincidentally also be metallic, a

property of the least bound electrons, whereas the clusters that chemists readily see represent strong interactions of more tightly bound electrons. In the present work we see that such units and the chemistry they represent persist in the presence of stoichiometrically excess electrons. This seems important. Nesper has aptly likened this to structures that may be found in the oceans, buried by the sea — conduction electrons in this case. Things are just harder to sort out under these circumstances.

Finally, to dispense with another supposed problem — the lack of further reduction of the Tt_5^{4-} anions in these metallic Zintl phases.[28] Most other possibilities are less reduced (Tt_4^{4-}, Tt_9^{4-}, etc.) except for formal isolated monoanions Tt^{4-} found in few examples in the presence of dipositive or higher charged cations, e.g., Ca_2Sn (Co_2Si) and Ca_5Ge_3 (Cr_5B_3). We believe the question is just not that simple in dense polar solids in which strong interactions and packing are much more important. Quantitative explanations of relative phase stabilities in the latter are not possible even when you know the alternate structure types, and they are impossible when you don't. Exploratory synthesis is still essential to progress.

Acknowledgements: We are indebted to D.-K. Seo for help and advice on the calculations and their interpretations.

Added during thesis preparation. Additional calculations were carried out on Sr_3Sn_5 to determine the effects, if any, of the size of the alkaline-earth metal. The Sr orbitals were contracted to a size comparable to La orbitals. There was no appreciable change in the shape and makeup of the Density of States or COOP curves when this was performed. The minor changes included a slight reduction of the overall intensity of the heteroatomic conduction

band and a shifting of the onset of the Sr d-orbital band to a slightly higher energy. The x-ray refinement data for $La_3Sn_{4.6}Ga_{0.4}$ are also included in the supplemental information.

Note. Supporting Information Available. Tables of additional crystallographic and refinement information and anisotropic displacement parameters for the three structures. The material is available free-of-charge via the Internet at http://pubs.acs.org.

References

(1) This research was supported by the Office of the Basic Energy Sciences, Materials Sciences Division, U. S. Department of Energy (DOE). The Ames Laboratory is operated for DOE by Iowa State University under Contract No. W-7405-Eng-82.

(2) Zintl E. *Angew. Chem.* **1939**, *52*, 1; b) Klemm, W.; Bussmann, E. *Z. Anorg. Allg. Chem.* **1963**, *319*, 297; c) Schäfer, H. *Ann. Rev. Mater. Chem.* **1985**, *15*, 1; d) Wade, K. *Adv. Inorg. Chem. Radiochem.* **1976**, *18*, 1.

(3) Cromer, D. *Acta Cryst.* **1976**, *B32*, 1930.

(4) Zhao, J.-T.; Corbett, J. D. *Inorg. Chem.* **1995**, *34*, 378.

(5) Corbett, J. D., in Chemistry, Structure and Bonding in Zintl Phases and Ions, Kauzlarich, S., Ed., VCH: New York, **1996**, Chap. 3.

(6) Dong, Z.-C.; Corbett, J. D. *J. Am. Chem. Soc.* **1993**, *115*, 11299.

(7) Kaskel, S.; Corbett, J. D. *Inorg. Chem.* **2000**, *39*, 778.

(8) Binary Alloy Phase Diagrams; 2nd ed.; T. B. Massalski, ed.; ASM International: Materials Park, OH, **1990**; p. 3400.

(9) Bruzzone, G. L.; Franceschi, E. *J. Less-Common Met.*, **1977**, *52*, 211.

(10) Borzone, G.; Borsese, A; Ferro, R. *Z. Anorg. Allg. Chem.* **1983**, *501*, 199.

(11) (a) Leon-Escamilla, E. A.; Corbett, J. D. *Inorg. Chem.* ***2001***, *40*, 1226; (b) Leon-Escamilla, E. A.; Corbett, J. D. *J. Solid State Chem.* **2001**, *159*, 149.

(12) TEXSAN, Windows version 1.02; Molecular Structure Corp. The Woodlands, TX, **1997**.

(13) Walker, N.; Stuart, D. *Acta Crystallogr.* A **1983**, *39*, 158.

(14) CAESAR: Ren, J.; Liang, W.; Whangbo, M.-H. PrimeColor Software, Inc., Raleigh, N.C., **1998**.

(15) Alvarez, A. Tables of Parameters for Extended Hückel Calculations, Parts 1 and 2, Barcelona, Spain, **1987**.

(16) Charge interactions utilized a local variant of the EHMACC suite of programs written and modified by students in R. Hoffmann's group at Cornell University and adapted to the PC by Martin Köckerling.

(17) Seo, D.-K.; Corbett, J. D. *J. Am. Chem. Soc.*, accepted.

(18) Brennan, T. D.; Burnett, J. K. *Inorg. Chem.* **1993**, *32*, 746.

(19) Moore, C. E. Atomic Energy Levels, Nat'l Standard Ref. Data Service, **1971**.

(20) Hughbanks, T. in Inorganometallic Chemistry, Fehlner, T., Ed.; Plenum Press, New York, **1992**, p. 291.

(21) Shannon, R. D. *Acta Crystallogr.* **1976**, *32A*, 751.

(22) Maggard, P. A.; Corbett, J. D. *J. Am. Chem. Soc.*, **2000**, *122*, 832 and references therein.

(23) Herle, P. S.; Corbett, J. D. *Inorg. Chem.* **2001**, *40*, 1858.

(24) Glassey, W. V.; Hoffmann, R. *J. Chem. Phys.* **2000**, *113*, 1698.

(25) Fässler, T. F.; Hoffmann, S. *Z. Kristallogr.* **1999**, *214*, 722.

(26) Xu, Z.; Guloy, A. M. *J. Am. Chem. Soc.* **1998**, *120*, 7349.

(27) Nesper R. Prog. *Solid State Chem.* **1990**, *20*, 1.

(28) A "metallic Zintl phase" appellation was evidently first applied to "valence" compounds containing excess electrons.[27] We use it in the same sense here, this seeming to be preferable to its application to valence precise phases that are coincidentally metallic.[5]

Table 1. Cell Parameters (Å, Å^3) of Orthorhombic Pu_3Pd_5-type phases[a]

compound	*a*	*b*	*c*	*V*
La_3In_5[b]	10.345(4)	8.424(6)	10.643(6)	927(2)
Sr_3Sn_5	10.644(2)	8.588(1)	10.895(2)	995.9(3)
YSr_2Sn_5	10.638(3)	8.581(3)	10.886(4)	993.7(6)
Ba_3Pb_5[c]	11.154(7)	9.049(7)	11.370(5)	1147(1)
La_3Sn_5	10.352(5)	8.290(6)	10.652(2)	914(1)

[a] From Guinier data with Si as an internal standard, 23 °C, λ = 1.540562 Å.

[b] Ref. 4.

[c] Ref. 8 gives 11.148, 9.049, 11.368 Å, respectively.

[d] Ref. 10 gives 10.35, 8.29, 10.63 Å, respectively.

Table 2. Selected Details of Data Collection and Structural Refinement for Sr_3Sn_5, Ba_3Pb_5, and La_3Sn_5[a]

	Sr_3Sn_5	Ba_3Pb_5	La_3Sn_5
Formula Weight	856.31	1449.47	1018.18
Crystal system, space group, Z	orthorhombic, *Cmcm* (No. 63), 4		
Calc. density, g cm^{-3}	5.719	8.391	7.333
Absorp. coeff. μ (Mo Kα, cm^{-1})	281.93	838.34	271.47
R, R_w[b]	0.036, 0.060	0.042, 0.051	0.036, 0.041

[a] Cell dimensions in Table 1.

[b] $R = \Sigma||F_o| - |F_c||/\Sigma|F_o|$; $R_w = [\Sigma w(|F_o| - |F_c|)^2/\Sigma w(F_o)^2]^{1/2}$; $w = \sigma_F^{-2}$.

Table 3. Refined atomic positions for Sr_3Sn_5, Ba_3Pb_5 and La_3In_5.

	x	y	z	B_{eq}
Sr_3Sn_5				
Sn1	0	0.0432(2)	0.25	1.20(4)
Sn2	0	0.3134(1)	0.4461(1)	1.24(3)
Sn3	0.1986(1)	0.2907(2)	0.25	1.30(3)
Sr1	0	0.6482(3)	0.25	1.12(5)
Sr2	0.2974(2)	0	0	1.33(3)
Ba_3Pb_5				
Pb1	0	0.0381(2)	0.25	0.46(7)
Pb2	0	0.3051(2)	0.4460(1)	0.4(1)
Pb3	0.2009(1)	0.2847(2)	0.25	0.57(7)
Ba1	0	0.6361(3)	0.25	0.4(1)
Ba2	0.2069(2)	0	0	0.4(1)
La_3Sn_5				
Sn1	0	0.0273(2)	0.25	0.81(5)
Sn2	0	0.3198(2)	0.4509(1)	0.76(7)
Sn3	0.2082(1)	0.2848(2)	0.25	0.86(5)
La1	0	0.6371(2)	0.25	0.66(6)
La2	0.2019(1)	0	0	0.73(4)

[a] Site symmetries in A_3M_5 phases (*Cmcm*): M1 4*c* *mm*.; M2 8*f* *m*..; M3 8*g* ..*m*; A1 4*c* *mm*.; A2 8*e* 2.
[b] $B_{eq} = 8/3\ \pi^2\ [U_{11}(aa^*)^2 + U_{22}(bb^*)^2 + U_{33}(cc^*)^2]$.

Table 4. Atom Parameters used for A_3M_5 Extended Hückel Calculations[a]

atom	orbital	ς_{i1}	H_{ii} (eV)	C1	ς_{i2}	C2
Sr	5s	1.214	−5.69			
	5p	1.214	−3.87			
	4d	3.047	−3.37	0.7492	0.9885	0.5467
Ba	6s	1.21	−5.21			
	6p	1.21	−3.43			
	5d	4.33	−3.99	0.688	1.64	0.595
La	6s	2.14	−5.15			
	6p	2.08	−2.97			
	5d	3.78	−4.90	0.7766	1.380	0.4587
In	5s	1.90	−12.60			
	5p	1.68	−6.19			
Sn	5s	2.12	−16.16			
	5p	1.82	−8.32			
Pb	6s	2.35	−15.70			
	6p	2.06	−8.00			

[a]Data from Alvarez[15] except for H_{ii} for Sr, Ba and La (see text).

Table 5. Atom Separations (Å) and Overlap Populations in A_3Tt_5 Compounds (Pu_3Pd_5-type) (A = Sr, Ba, La; M = In, Sn, Pb; d< 4.1 Å)

atom		Sr_3Sn_5		Ba_3Pb_5		La_3Sn_5		La_3In_5	
A1 – M1		3.390(4)	0.26	3.635(4)	0.21	3.234(3)	0.23	3.228(3)	0.23
A1 – M2 ×2		3.325(2)	0.33	3.497(3)	0.30	3.211(3)	0.29	3.263(3)	0.29
A1 – M2 ×2		3.580(3)	0.07	3.732(4)	0.07	3.392(2)	0.09	3.449(2)	0.12
A1 – M3 ×2		3.432(6)	0.32	3.600(3)	0.29	3.259(2)	0.31	3.285(1)	0.31
A1 – M3 ×2		3.726(9)	0.09	3.889(3)	0.07	3.629(2)	0.10	3.619(2)	0.11
A2 – M1	×2	3.492(2)	0.17	3.679(3)	0.13	3.395(2)	0.16	3.400(1)	0.15
A2 – M2	×2	3.496(8)	0.15	3.650(3)	0.12	3.416(2)	0.15	3.391(2)	0.17
A2 – M2	×2	3.596(7)	0.10	3.766(3)	0.09	3.467(2)	0.11	3.508(1)	0.12
A2 – M3	×2	3.426(3)	0.21	3.596(2)	0.17	3.340(2)	0.19	3.330(1)	0.20
A2 – M3	×2	3.693(1)	0.06	3.835(2)	0.05	3.562(2)	0.08	3.601(2)	0.10
M1 – M2	×2	3.152(3)	0.20	3.284(3)	0.28	3.235(2)	0.16	3.232(2)	0.29
M1 – M3	×2	2.997(7)	0.44	3.162(3)	0.45	3.033(2)	0.40	3.147(2)	0.30
M1 – M3[a]	×2	3.870(4)	–0.07	4.053(3)	–0.02	3.627(2)	0.04	3.575(2)	0.20
M2 – M1		3.152(3)	0.20	3.284(3)	0.28	3.235(2)	0.16	3.232(2)	0.29
M2 – M2[a]		3.413(3)	0.23	3.732(4)	0.14	3.165(3)	0.41	3.428(3)	0.29
M2 – M3	×2	3.011(2)	0.51	3.166(2)	0.52	3.053(2)	0.43	3.014(1)	0.57
M3 – M1		2.997(7)	0.44	3.162(3)	0.45	3.033(2)	0.40	3.147(2)	0.30
M3 – M1[a]		3.870(4)	–0.07	4.053(3)	–0.02	3.627(2)	0.04	3.575(2)	0.20
M3 – M2	×2	3.011(2)	0.51	3.166(2)	0.52	3.053(2)	0.43	3.014(1)	0.57

[a] Intercluster

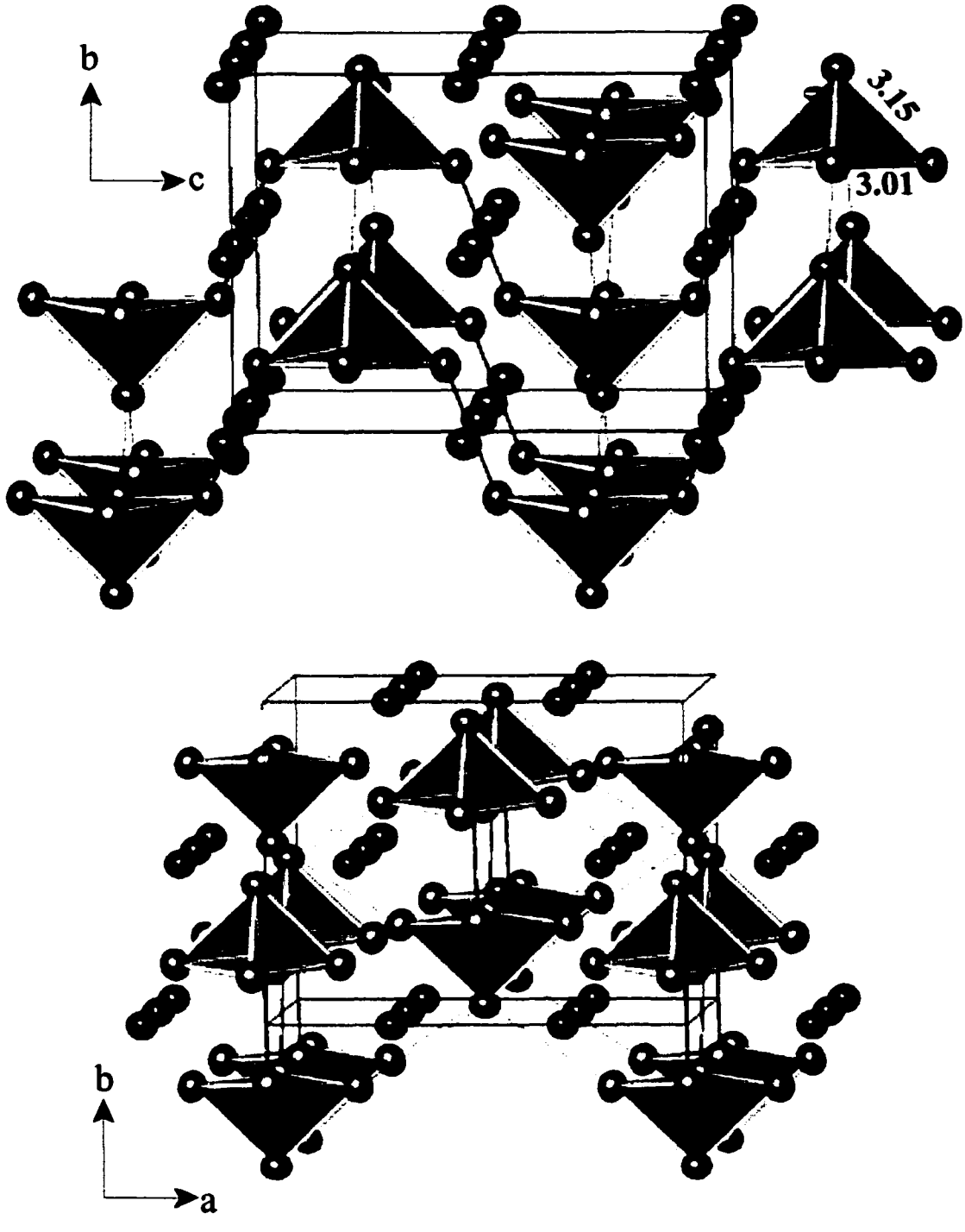

Figure 1. [100] (top) and [001] (bottom) views of the orthorhombic Pu_3Pd_5-type structure of Sr_3Sn_5. The square pyramidal Sn_5 units (C_{2v}) are blue and the isolated Sr1 and the more populous Sr2 atoms are red. Significant intercluster contacts are shown by light (Sn2–Sn2) and lighter (Sn1–Sn3) black lines, the latter being clearer in the bottom view. lines, the latter being clearer in the bottom view.

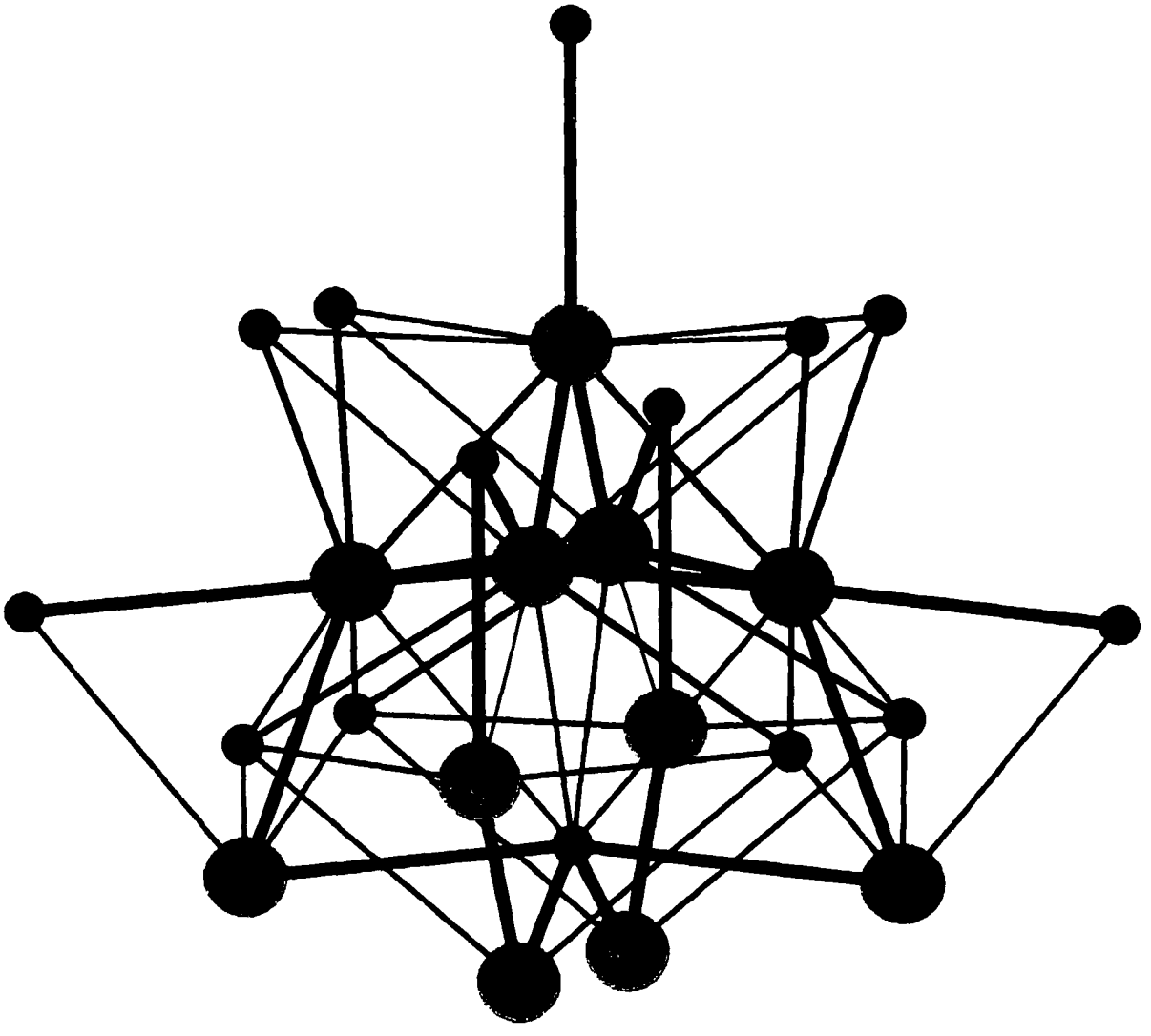

Figure 2. A single cluster in La_3Sn_5 (blue atoms, with Sn2 darker) plus parts of neighboring clusters to which it is bonded and the cations that interconnect these, La1 (orange) and La2 (red). Linewidths for the interconnections are proportional to overlap populations for the separate sets, Sn–Sn black and La–Sn, orange-red.

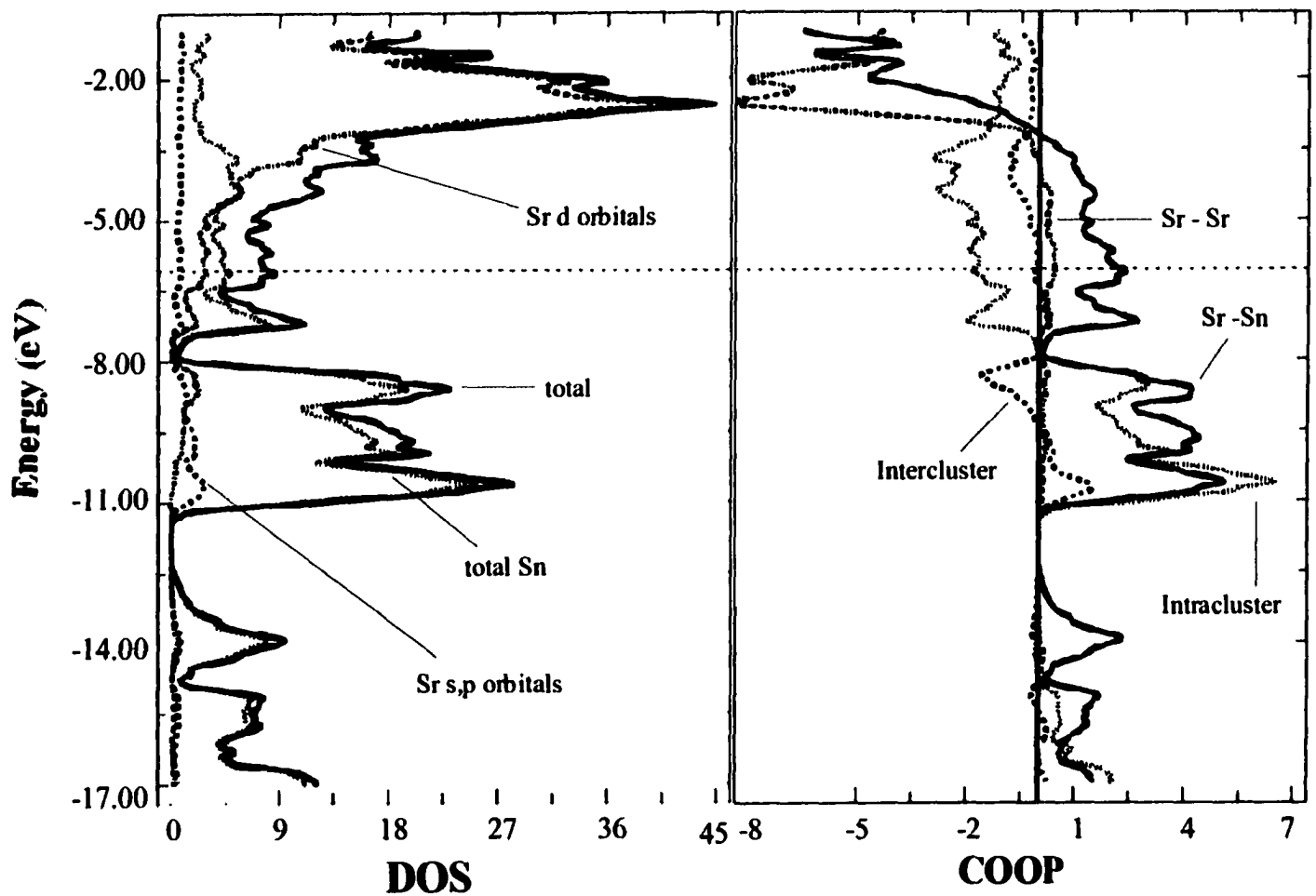

Figure 3. EHTB calculations results for Sr_3Sn_5. Densities-of-states (DOS) – left – include projections of partial values for Sn (dotted), Sr s,p (dashed) and Sr d (dash–dot). The COOP results on the right show total Sr–Sn (solid), intracluster Sn–Sn (dotted), intercluster Sn–Sn (dashed), and Sr–Sr (dash–dot).

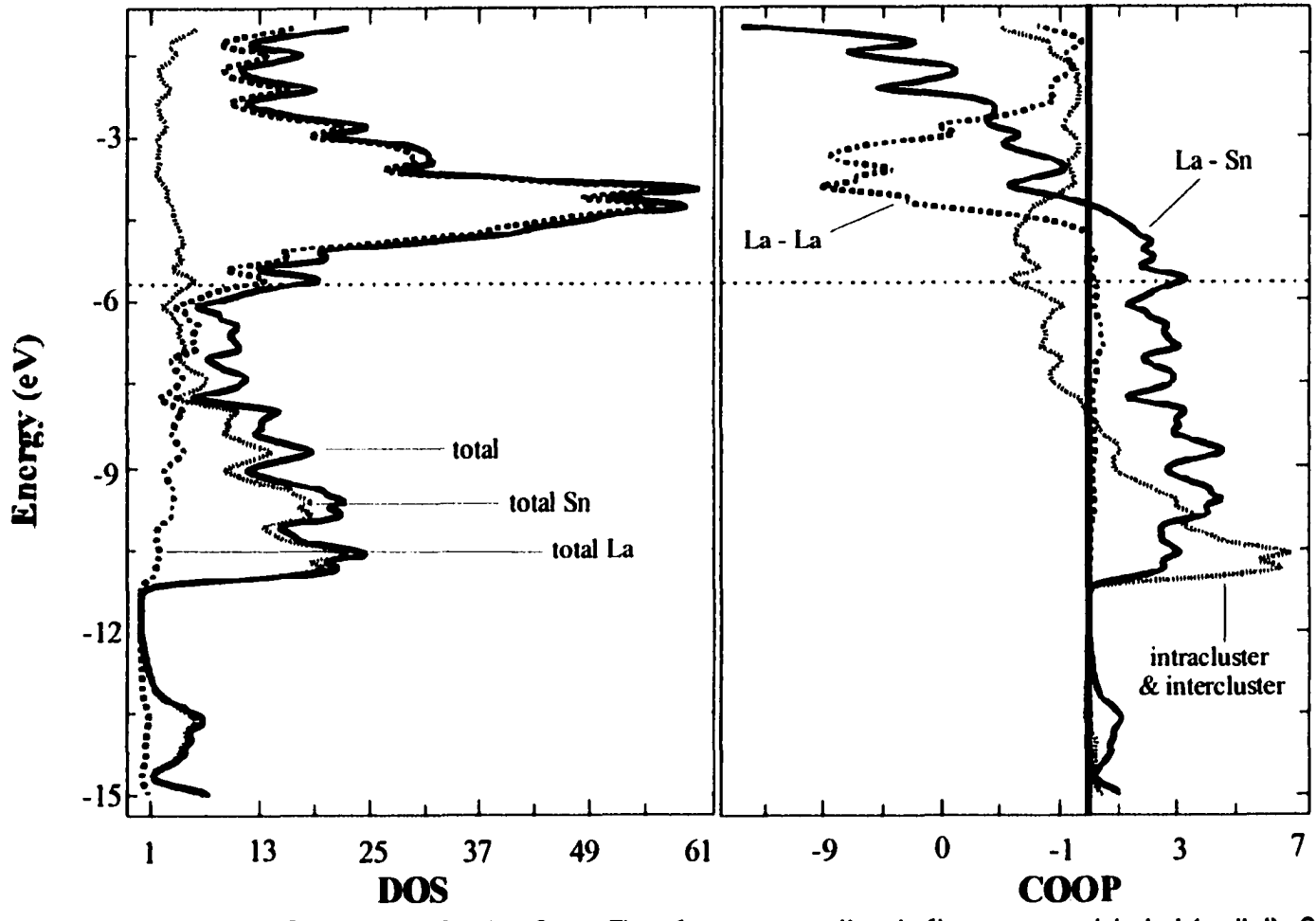

Figure 4. DOS and COOP results for La_3Sn_5. The former on the left represent total (solid), Sn (dotted), and La (dashed) components. In the COOP data on the right, the solid line represents the dominant La-Sn bonding, the dotted total Sn-Sn, and the dashed total La-La.

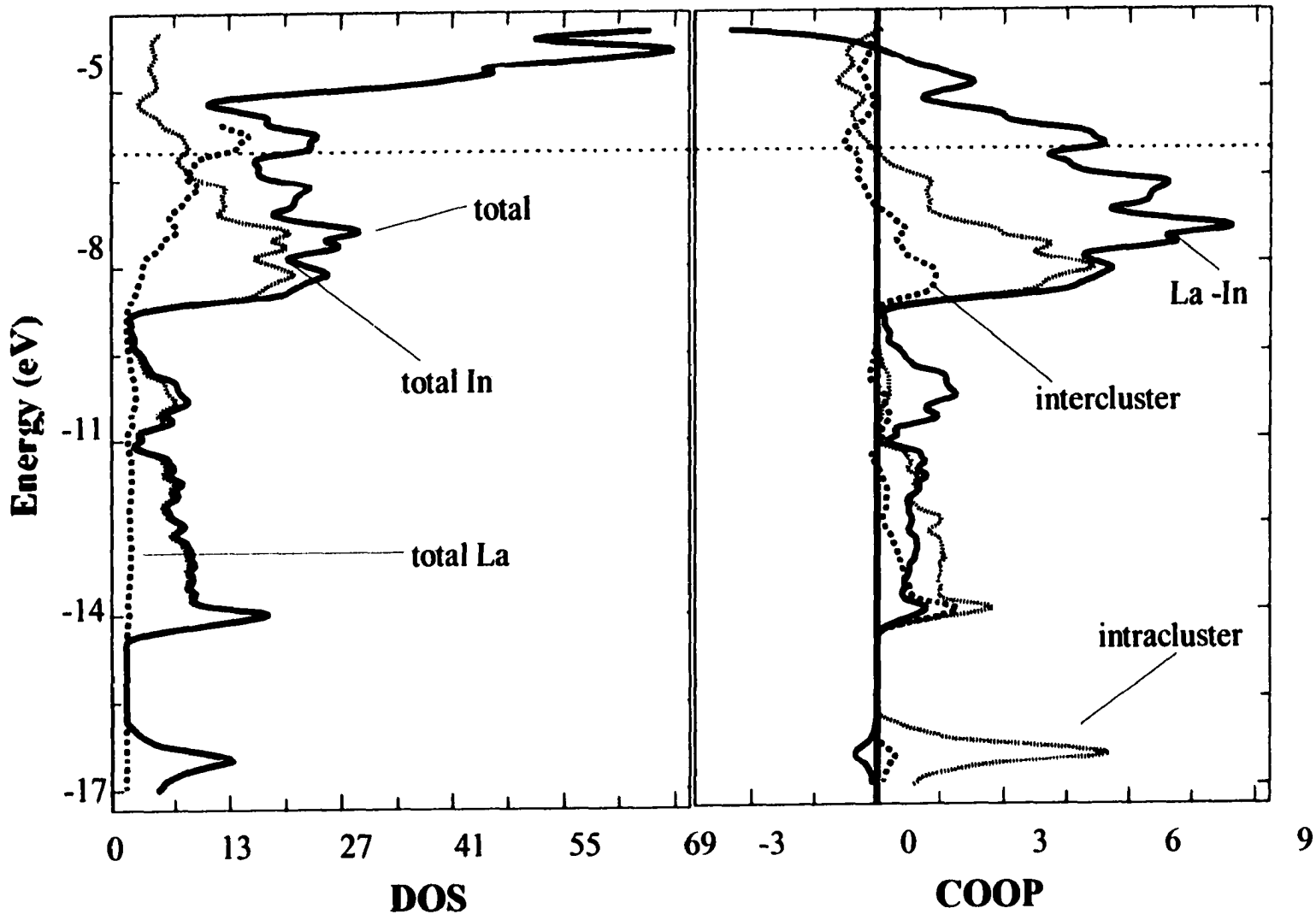

Figure 5. The DOS and COOP data for La_3In_5 with solid, dotted and dashed curves in the DOS showing total and partial In and La data, respectively. In the COOP results, the solid line gives the La–In data, and the dotted and dashed, In–In intra- and intercluster values, respectively.

Table S1. Details of data collection and refinement for Sr_3Sn_5, Ba_3Pb_5, La_3Sn_5

	Sr_3Sn_5	Ba_3Pb_5	La_3Sn_5
Formula Weight	856.31	1449.47	1018.18
Crystal system, space group, Z	orthorhombic *Cmcm* (No. 63), 4		
Unit cell dimensions (Å)[a]			
a	10.644(2)	11.154(7)	10.352(5)
b	8.588(1)	9.049(7)	8.290(6)
c	10.895(2)	11.370(5)	10.652(2)
V (Å^3)	995.9(3)	1147(1)	914(1)
Calculated density, g cm^{-3}	5.719	8.391	7.333
Diffractometer	Rigaku	Rigaku	Siemens P4
Octants, $2\theta_{max}$ (deg)	$\pm h,\pm k, l$; 55°	$h,\pm k,l$; 50°	h,k,l; 50°
Observ. refl.	2665		
unique	1813 ($2\sigma_I$)	1209 ($3\sigma_I$)	1040 ($3\sigma_I$)
indep. (>$3\sigma_I$) (R_{ave})	535 (9.8%)	420 (10.3%)	739
Absorp. coeffic. (Mo Kα, cm^{-1})	281.93	838.34	271.47
Rel. trans. coeff. range	0.559–1.00	0.365–1.00	0.496–1.00
variables	27	27	27
R, R_w[b]	0.036, 0.060	0.042, 0.051	0.036, 0.041
Largest ΔF, e$^-$/Å^3	3.63, 0.88 Å to Sn2	3.96, 1.6 Å to Pb2	2.8, 2.1 Å to La2
GOF	1.83	1.65	2.25

[a] Guinier powder pattern data, λ = 1.540.562, 23 °C.

[b] $R = \Sigma||F_o| - |F_c||/\Sigma|F_o|$; $R_w = [\Sigma w(|F_o| - |F_c|)^2/\Sigma w(F_o)^2]^{1/2}$; $w = \sigma_F^{-2}$.

Table S2. Anisotropic displacement parameters[a] for A_3M_5 phases

Sr_3Sn_5	U_{11}	U_{22}	U_{33}	U_{12}	U_{13}	U_{23}
Sn1	0.017(1)	0.0131(9)	0.0153(9)	0.0000	0.0000	0.0000
Sn2	0.0167(7)	0.0177(7)	0.0126(6)	0.0000	0.0000	0.0001(6)
Sn3	0.0152(7)	0.0188(7)	0.0153(6)	-0.0014(5)	0.0000	0.0000
Sr1	0.016(1)	0.014(1)	0.013(1)	0.0000	0.0000	0.0000
Sr2	0.0170(9)	0.0147(8)	0.0178(9)	0.0000	0.0000	-0.0003(7)
Ba_3Pb_5						
Pb1	0.009(1)	0.002(1)	0.006(1)	0.0000	0.0000	0.0000
Pb2	0.006(1)	0.007(1)	0.005(1)	0.0000	0.0000	-0.001(1)
Pb3	0.005(1)	0.011(1)	0.006(1)	-0.002(1)	0.0000	0.0000
Ba1	0.008(2)	0.003(1)	0.004(2)	0.0000	0.0000	0.0000
Ba2	0.006(2)	0.005(1)	0.005(1)	0.0000	0.0000	-0.001(1)
La_3Sn_5						
Sn1	0.012(1)	0.008(1)	0.0090(6)	0.0000	0.0000	0.0000
Sn2	0.0115(8)	0.0105(7)	0.0088(4)	0.0000	0.0000	-0.0002(5)
Sn3	0.0096(7)	0.0133(7)	0.0097(5)	-0.0023(6)	0.0000	0.0000
La1	0.0089(9)	0.0080(8)	0.0084(5)	0.0000	0.0000	0.0000
La2	0.0084(6)	0.0090(6)	0.0105(4)	0.0000	0.0000	0.004(4)

[a] $T = \exp[-2\pi^2(U_{11}h^2a^{*2} + U_{22}k^2b^{*2} + U_{33}lc^{*2} + 2U_{12}hka^*b^* + 2U_{13}hl^*c^* + 2U_{23}kl^*c^*)]$, $U_{12} = U_{13} = U_{23} = 0$.

Table S3. Details of data collection and refinement for $La_3Sn_{4.6}Ga_{0.4}$

	$La_3Sn_{4.6}Ga_{0.4}$
Formula Weight	856.31
Crystal system, space group, Z	orthorhombic *Cmcm* (No. 63), 4
Unit cell dimensions (Å)	
a	10.263(2)
b	8.2649(17)
c	10.506(2)
V (Å^3)	891.2(3)
Calculated density, Mg m^{-3}	7.164
Diffractometer	Rigaku
Octants, $2\theta_{max}$ (deg)	$\pm h, k, \pm l$; 55°
Observ. refl.	2212
unique	1800 (2σ)
indep. ($>3\sigma_I$) (R_{ave})	617 (15.9%)
Absorp. coeffic. (Mo Kα, mm^{-1})	27.936
Rel. trans. coeff. range	0.2475 - 1.0000
extinction coefficient	0.00110(16)
variables	28
R, R_w[a]	0.036, 0.10
Largest ΔF, e$^-$/Å^3	2.43, 0.54 Å to La2
GOF	0.774

[a] $R = \Sigma||F_o| - |F_c||/\Sigma|F_o|$; $R_w = [\Sigma w(|F_o| - |F_c|)^2/\Sigma w(F_o)^2]^{1/2}$; $w = \sigma_F^{-2}$.

Table S4a. Refined atomic positions for $La_3Sn_{4.6}Ga_{0.4}$

	x	y	z	U_{eq}	occupancy
$La_3Sn_{4.6}Ga_{0.4}$					
La1	0.0000	0.1413(1)	0.2500	13(1)	
La2	0.2979	0.0000	0.5000	13(1)	
Sn1	-0.2042(1)	-0.2122(1)	0.2500	15(1)	
Sn2	0.0000	0.5304(2)	0.2500	16(1)	
Sn3	0.0000	0.1827(1)	0.5491(1)	16(1)	79.72(4)%
Ga1	0.0000	0.1827(1)	0.5491(1)	16(1)	20.28(4)%

Table S4b. Anisotropic displacement parameters[a] for $La_3Sn_{4.6}Ga_{0.4}$.

$La_3Sn_{4.6}Ga_{0.4}$	U_{11}	U_{22}	U_{33}	U_{12}	U_{13}	U_{23}
La1	0.013(1)	0.010(1)	0.016(1)	0.0000	0.0000	0.0000
La2	0.012(1)	0.010(1)	0.016(1)	0.0000	0.0000	0.0000
Sn1	0.015(1)	0.015(1)	0.017(1)	0.002(1)	0.0000	0.0000
Sn2	0.017(1)	0.012(1)	0.018(1)	0.0000	0.0000	0.0000
Sn3	0.015(1)	0.016(1)	0.016(1)	0.0000	0.0000	0.001(1)
Ga1	0.015(1)	0.016(1)	0.016(1)	0.0000	0.0000	0.001(1)

[a] $T = \exp[-2\pi^2(U_{11}h^2a^{*2} + U_{22}k^2b^{*2} + U_{33}lc^{*2} + 2U_{12}hka^*b^* + 2U_{13}hla^*c^* + 2U_{23}klb^*c^*)]$, $U_{12} = U_{13} = U_{23} = 0$.

CHAPTER 4. A_5InPb_8 (A = K, Rb): A ZINTL PHASE WITH CLUSTERS OF Pb_4 TETRAHEDRA INTERBRIDGED BY μ_6-In ATOMS.

Michael T. Klem and John D. Corbett*

Department of Chemistry and Ames Laboratory —DOE,[1]

Iowa State University, Ames IA 50011

Abstract

Reaction of elemental In, Pb, and K or Rb within welded Ta containers at 900 °C followed by subsequent annealing at 350 °C gives the new phase A_5InPb_8 (A = K, Rb). The title phase crystallizes in the trigonal space group $R\bar{3}m$ (Z = 3) with the cell dimensions of a = 6.8835(6), 6.885(1) c = 37.591 (5), 37.64(2) Å for K_5InPb_8 and Rb_5InPb_8, respectively. The title compound contains clusters composed of two Pb_4 tetrahedra that are interbridged by a lone μ_6-In atom. The $InPb_8$ units, which in the isolated case would behave as ideal 40 electron Wade's rule cluster, are weakly interlinked into sheets in the *ab* plane by long intercluster Pb-Pb interactions. These long (~ 3.5 Å) interactions cause a broadening of the valence band and thus generate a number of states at the Fermi level. The compounds are metallic (ρ_{298} ~ 42 $\mu\Omega$·cm and $[(\delta\rho/\delta T)/\rho]$ of 1.4(2) × 10^{-1} K^{-1} for K_5InPb_8) which is in agreement with the expectations provided via the EHTB calculations.

Introduction

Large deltahedral clusters of the group 14 elements have been fairly limited in the solid state. The largest cluster to date is the Tt_9^{4-} anion which is now known for all tetrel elements except for carbon.[2] One of the limiting factors to the stability of deltahedral clusters of the heavy tetrel elements is the disproportionate size-to-charge ratio. Wade's rules for counting electrons states in a given class of clusters (closo, nido, etc.) indicate that the charge assigned to a deltahedral cluster is independent of its nuclearity, and therefore, large clusters would carry relatively small negative charges.[3] This can evidently set up situations where the number of cations is insufficient to separate large clusters. Molecular chemistry has in the past used large organic cations or units such as cryptated alkali-metal cations to achieve effective separation of clusters. In the solid state, larger alkali metal cations such as Rb and Cs, or cluster substitution with an electron poorer element has been used. It is the later approach, an attempt to substitute the electron poorer (and smaller) indium atom for lead into the Pb_9^{4-} cluster, that led to the synthesis of the title compound.

Experimental

The materials and general reaction techniques in welded tantalum tubes have been described elsewhere.[4,5] An improved method for sample mounting for powder pattern measurements was employed. Samples were held between sheets of aluminized polyester film by means of a thin centered film of vacuum grease that also served to seal the outer edge of the sheets and to prevent decomposition of the air sensitive products.[6] All transfers where completed in a N_2 or He-filled glove-box. Samples of A_5InPb_8 (A = K, Rb) where prepared by direct fusion of the elements in welded tantalum tubes followed by heat treatment.

Synthesis. The compounds A_5InPb_8 (A = K, Rb) were obtained by mixing stoichiometric amounts of potassium (Strem, 99.9995%) or rubidium (Strem, 99.999+%), indium (Aesar, 99.99%), and lead (Aesar, 99.9999%), allowing these to react 900 °C and then to anneal for 3 weeks at 350 °C. The results were brittle, black crystals. A quantitative yield (>95% by powder pattern) of K_5InPb_8 was obtained once the stoichiometry was known. In most cases, the yield of Rb_5InPb_8 was 80% according to Guinier powder pattern data with the remainder being elemental lead. Attempts to substitute Tl or Ga for In were unsuccessful as was the attempted use of the larger cation Cs.

X-ray diffraction. Powder diffraction data from an Enraf-Nonius Guinier camera and Cu $K_{\alpha 1}$ radiation were used for phase identification. The films were then first compared semiquantitatively with the patterns calculated for phases with known structures. The compositions of the products were then estimated visually from relative powder pattern intensities, considering the unit cell symmetry and contents as well. The cell dimensions of both phases as refined from powder data are listed in Table 1.

Several black crystals of K_5InPb_8 were isolated, sealed into thin-walled capillaries, and checked by Laue photographs. Diffraction data from one specimen were then collected at room temperature using a Rigaku AFC6 diffractometer with monochromated Mo Kα radiation. Routine indexing of 25 centered reflections gave a R-centered trigonal cell. The absence of other systematic extinctions led to the possible space groups $R\bar{3}m$, $R\bar{3}$, or R3. The space group $R\bar{3}m$ was chosen and this assignment was confirmed by a refinement carried out with the aid of the TEXSAN package.[7] The data were corrected for absorption empirically according to three ψ-scans of strong reflections with different θ values. The final residuals were R(F)/Rw = 5.7/7.0 % with the largest residual in the ΔF map of 3.02 $e^-/Å^3$

located 0.70 Å from K1. The phase Rb_5InPb_8 was identified via its powder pattern, and lattice parameters were refined using the K_5InPb_8 line assignments as a model.

Selected crystallographic and refinement data are given in Table 2, and more detailed information and displacement ellipsoid parameters are given in the Supporting Information, Tables S1, S2. Refined atom positions are listed in Table 3 and the bond distances are listed in Table 4.

Theoretical. Theoretical calculations were made over 326 k-points in the irreducible wedge with the aid of the CAESAR EHTB program of Whangbo, et al.[8] Only the lead and indium atoms were included (H_{ii} and ζ_i for Pb 6s: -15.70 eV and 2.35, for Pb 6p: -8.00 eV and 2.06, for In 5s: -12.60 eV and 1.903, and for In 5p: -6.19 eV and 1.677).[9] Calculations were carried out on the isolated cluster, the full structure, and a modified version of the full structure where the individual $InPb_8$ clusters were separated by over 5 Å in the *ab* plane.

Property Measurements. Resistivities of K_5InPb_8 were measured by the electrodeless Q method[10] on 44.3 mg that had been sieved to 250 – 425 μm powder and diluted with chromatographic Al_2O_3. Measurements were made at 34 MHz over 120 – 240 K. The resistivity of K_5InPb_8 extrapolated to 298 K was 42 $\mu\Omega\cdot$cm with a temperature coefficient $[(\delta\rho/\delta T)/\rho]$ of $1.4(2) \times 10^{-1}$ K^{-1}. The absolute resistivities may conceivably be off by a factor of two or three.

Results and Discussion

Description. The basic formula unit in this phase is pairs of Pb tetrahedra that are interbridged by a μ_6- In atom to form capped and centered $InPb_8$ trigonal antiprisms (D_{3d}) with the 3-fold axis along *c*. The unit cell is shown in figure 1. The Pb tetrahedra are non-

regular with the apex to base bond distance [(3*b*-Pb1) – (4*b*-Pb2)] 0.3 Å shorter (3.038 Å) than the corresponding Pb2-Pb2 distance (3.3329 Å). The Pb2-Pb2 basal contacts are also approximately 0.25 Å longer than the distances found in the Pb_4 tetrahedral clusters of KPb.[11] The In atom is positioned 3.14 Å between the clusters and sits on the $\bar{3}$ axis which also passes through the apical Pb1 atoms. The In1 atom links the Pb_4 tetrahedra in an antiprismatic fashion (D_{3d}) which gives rise to their staggered configuration, figure 2.

The cation arrangement about the $InPb_8$ clusters is also of interest. The A1 cation is situated between and coplanar with In in three parallel $InPb_8$ clusters and bridges In-Pb basal edges on each, figure 3. The A2 cation lies between three in-plane Pb_4 tetrahedra and caps a face on each cluster along with being terminal to a single Pb apex atom of a neighboring cluster. The A3 cation lies between two layers of $InPb_8$ clusters and bridges an apex–basal edge on 6 Pb_4 clusters (3 above, 3 below). The first two cations rest in voids with radii approximately 3.88 Å while the A3 cations with CN = 12 are in a void whose radius is 4.27 Å. This represents an increase in the void space volume of approximately 25% and is probably a contributing factor to the elongation of the A3 ellipsoid in the U_{33} direction, figure 3.

The occurrences of vertex-fused connections are uncommon in main group clusters. Some examples are known in molecular chemistry with aluminum or silicon as the central atom linking two caps of nido-carboranes in a monocapped square antiprism configuration or pentagonal bypyramids, respectively.[12] Geometric similarities exist in the solid state as well with examples including the mixed alkali metal compounds $A'_7A''E_8$ (E = Ge, Si) where the smaller cation occupies a μ_6-capping position between two E_4 tetrahedra (in a staggered configuration).[13,14] Analogous to the role of In here, recently two examples of transition

metal linked tetrel tetrahedra have been synthesized, Cs_6ZnGe_8 and K_6CdPd_8.[15,16] The former contains isolated clusters of two Ge_4 tetrahedra linked via a μ_6-Zn atom in which the Ge_4 tetrahedra are eclipsed and the later contains a $(Pb_4CdPb_4)Cd(Pb_4CdPb_4)$ dimer where the Pb_4 tetrahedra are staggered. Other known cases of heteroatomically linked tetrahedra of the tetrel elements include $K_4Au(TlSn_3)$ and the isoelectronic $A_3(AuTt_4)$ (A = K, Rb, Cs; Tt = Sn, Pb).[17,18] These phases contain infinite one-dimensional chains of M_4 tetrahedra that are interbridged on opposed edges by a μ_4-gold atoms to form $^1_\infty[Au(Tt_4)]^{x-}$.

Bonding. The electronic structure of an isolated $InPb_8^{5-}$ cluster can be understood with the aid of extended-Hückel calculations and Wade's rules. According to Wade, the number of skeletal electrons required for closed shell bonding in two nido-clusters of Pb_4 each (two tetrahedra) would be equal to 2 (2 x 4 + 4) = 24 electrons. Each lead atom contributes its two valence p-electrons, and the indium donates three electrons (essentially an In^{3+}) for a total of 19 skeletal electrons. In order to satisfy the bonding requirements, the cluster requires more electrons which come from the five alkali-metal cations. The molecular orbital calculation carried out confirms Wade's assumptions for the isolated cluster, figure 4.

The results of the molecular orbital calculation and Wade's rules analysis would suggest that this compound should be a valence compound, and hence a semiconductor. The measured resistivity for K_5InPb_8 was 42 $\mu\Omega$·cm with a positive temperature coefficient of 0.14 K^{-1} indicating metallic behavior, figure 5. This is in contrast to the expectations provided by the simple molecular orbital treatment and requires a deeper analysis.

Further calculations were then carried out on the full structure *minus the cations*. The density of states shows a clear separation between the s and p bands of lead with a small

contribution from the s and p orbitals of indium, figure 6. The density of states plot also reveals a small number of states at the Fermi level with no evidence of a band gap. The s band of lead dominates from -20 to about -13.5 eV with a small contribution from indium - 15.5 eV. The p band for lead starts at -12.5 eV and extends past the Fermi level. At the Fermi level, the p_x and p_y orbitals on lead are the dominating contributions.

In order to understand the results from the EHTB calculations, a more critical look at the full structure of A_5InPb_8 (A = K, Rb) is required. Upon closer examination, there are moderately long intercluster contacts between Pb2 atoms of neighboring clusters (at 3.55 vs 3.33 Å for the intracluster Pb2-Pb2 bonds). This results in $InPb_8$ clusters linked via Pb2-Pb2 intercluster bonds in the *ab* plane to form 2-dimensional sheets of clusters, figure 7. These long intercluster bonds still have a significant amount of overlap according to EHTB calculations (0.25 for each of the *intercluster* Pb2-Pb2 (3.6 Å) contacts versus 0.57 and 0.11 for each of the *intracluster* Pb1-Pb2 (3.0 Å) and Pb2-Pb2 (3.3 Å) respectively). The relatively low overlap population of the intracluster Pb2-Pb2 linkages is due to the occupation of antibonding states by the extra electrons. These conclusions were made using the default orbital coefficients for Pb and In as given by Alverez, and have been demonstrated to give meaningful results in related systems. Linkages of one sheet of clusters to another via the apical Pb1 atoms are precluded by the long separation of 4.90 Å in the *c* direction.

The intercluster contacts are responsible for a broadening of the valence band. This broadening is evident when calculations are carried out starting from a case where the clusters are isolated with a intercluster distance greater than 5 Å, figure 8. As the clusters are brought together, the p band visually broadens until the valence band crosses the Fermi level.

A similar type of behavior was noticed in K_6Pb_8Cd, a phase that contains $(Pb_4)_4Cd_3$ oligomers [essentially 2 $InPb_8$-like clusters with a additional cadmium atom linking the two together], where the oligomers themselves have relatively long intercluster bonds (3.57 Å between intercluster lead atoms). The calculation, without cations, also shows the optimization of the bonding within the $InPb_8^{5-}$ cluster, in accordance with the results from the MO and Wade's rules analysis.

With the intercluster bonding in mind, one can begin to understand the reason for having a positive density of states at the Fermi level, even though the isolated cluster itself conforms to a Wade's rules assignment. Each exobond between neighboring Pb2 atoms would lower the total number of electrons required for stabilization as predicted by Wade. One can think of this as taking the $InPb_8^{5-}$ and oxidizing it to form intercluster bonds. When the cluster is oxidized to form these linkages, it is not surprising that there is now a density of states at the Fermi level. Since the electron count has remained the same, the required number of electrons has decreased causing what were formerly empty antibonding orbitals to become filled.

The COOP curves clearly show that the cluster is filling up antibonding states around -8.2 eV, well before the Fermi level at -5.6 eV. These antibonding states are primarily within the Pb2-Pb2 intracluster bonds. This could account for the low overlap population of 0.11 for the shorter (3.33 Å) Pb2-Pb2 intracluster bonds over the longer Pb2-Pb2 intercluster bonds (0.25 at 3.55 Å). The In-Pb bonding appears to be unimportant around Fermi, but is a major bonding contributor to the peaks at -15.5, -14.5, and -10.5 eV. Interestingly enough, the intracluster bonding appears to be optimized at a point that is 6 electrons fewer than in

the isolated cluster. The extra electrons are assumed to be going into the 2-D net shown in figure 7.

Conclusions

The $InPb_8^{5-}$ cluster, in the isolated case, represents a new type of Zintl cluster in the heavy tetrel elements. The $InPb_8^{5-}$ cluster type is interesting because it is one of the few known vertex-fused polyhedra known in Zintl chemistry. The fact that the clusters are not isolated is probably because of packing effects introduced by the size and relatively few cations about the clusters. One's ability to rationalize the cluster geometry with the observed electron count enables one to make this assignment even though the compound is metallic due to intercluster interactions.

References.

(1) This research was supported by the Office of the Basic Energy Sciences, Materials Sciences Division, U. S. Department of Energy (DOE). The Ames Laboratory is operated for DOE by Iowa State University under Contract No. W-7405-Eng-82.

(2) Queneau, V.; Sevov, S. C. *Angew. Chem.* **1997**, *109*, 1818.; b) Schnering, H.G.v.; Baitinger, M.; Bolle, U.; Cabrera, W. C.; Curda, J.; Grin, Y.; Heinemann, L.; Llanos, L.; Peters, K.; Schmeding, A.; Somer, M. *Z. Anorg. Allg. Chem.* **1997**, *623*, 1037.; c) Queneau, V.; Sevov, S. C. *Inorg. Chem.* **1998**, *37*, 1358.; d) Todorov, E.; Sevov, S. C. *Inorg. Chem.* **1998**, *37*, 3889.; e) Queneau, V.; Todorov, E.; Sevov, S. C. *J. Am. Chem. Soc.* **1998**, *120*, 3263.

(3) Wade, K. *Adv. Inorg. Chem. Radiochem.* **1976**, *18, 1.*

(4) Corbett, J. D. In *Chemistry, Structure and Bonding in Zintl Phases and Ions*; Kauzlarich, S., Ed.; VCH: New York, **1996**; Chapter 3.

(5) Dong, Z.-C.; Corbett, J. D. *J. Am. Chem. Soc.* **1993**, *115, 11299.*

(6) Klem, M. T.; Vaughey, J. T.; Harp, J. G.; Corbett, J. D. *Inorg. Chem.* **2001**, *40*, 7020.

(7) *TEXSAN*, Windows version 1.02; Molecular Structure Corp.: The Woodlands, TX, **1997**.

(8) Ren, J.; Liang, W.; Whangbo, M.-H. *CAESAR*; PrimeColor Software, Inc.: Raleigh, NC, **1998**.

(9) Alvarez, A. Tables of Parameters for Extended Hückel Calculations, Parts 1 and 2, Barcelona, Spain, **1987**.

(10) Zhao, J.-T.; Corbett, J. D. *Inorg. Chem.* **1995**, *34*, 378.

(11) Hewaidy, I. F.; Busmann, E.; Klemm, W. *Z. Anorg. Allg. Chem.* **1964**, *328*, 283.

(12) Siriwardane,U.; Islam, M. S.; West, T. A.; Hosmane, N. S.; Maguire, J. A.; Cowley, A. H. *J. Am. Chem. Soc.* **1987**, *109*, 4600.; b) Bandman, M. A.; Knobler, C. B.; Hawthorne, M. F. *Inorg. Chem.* **1988**, *27*, 2399.

(13) Schnering, H. G.-v.; Schwarz, M.; Nesper, R. *Angew. Chem. Int. Ed. Engl.* **1986**, *25*, 566.

(14) Llamos, J.; Nesper, R.; Schnering, H. G.-v. *Angew. Chem. Int. Ed. Engl.* **1983**, *22*, 998.

(15) Queneau, V.; Sevov, S. C. *J. Am. Chem. Soc.* **1997**, *119*, 8109.

(16) Todorov, E.; Sevov, S. C. *Angew. Chem. Int. Ed. Engl.* **1999**, 38, 1775.

(17) Huang, D.; Corbett, J. D. *Inorg. Chem.* **1998,** *37*, 5007.

(18) Zachwieja, U.; Müller, J. Z. *Anorg. Allg. Chem.* **1998,** *624*, 853.

Table 1. Cell Parameters (Å, Å^3) of Trigonal A_5InPb_8-type phases (A = K, Rb)[a]

compound	*a*	*c*	*V*
K_5InPb_8[b]	6.8835(6)	37.591(5)	1542.5(5)
Rb_5InPb_8	6.885(1)	37.64(2)	1543(3)

[a] From Guinier data with Si as an internal standard, 23 °C, λ = 1.540562 Å.

Table 2. Selected Details of Data Collection and Structural Refinement for K_5InPb_8

	K_5InPb_8
Formula Weight	2959.19
Crystal system, space group, Z	trigonal, $R\bar{3}m$, 3
Calc. density, g cm^{-3}	8.508
Absorp. coeff. μ (Mo Kα, cm^{-1})	902.59
R, R_w[a]	0.057, 0.070

[a] $R = \Sigma||F_o| - |F_c||/\Sigma|F_o|$; $R_w = [\Sigma w(|F_o| - |F_c|)^2/\Sigma w(F_o)^2]^{1/2}$; $w = \sigma_F^{-2}$.

Table 3. Refined atomic positions for K_5InPb_8.

	x	y	z	B_{eq}
K_5InPb_8				
Pb1	0.0000	0.0000	0.12864(8)	2.35(4)
Pb2	0.1615(1)	1 – x	0.06592(4)	1.42(2)
In1	0.0000	0.0000	0.0000	1.19(7)
K1	0.6667	0.3333	0.0153(4)	1.5(2)
K2	0.0000	0.0000	0.2192(5)	2.1(2)
K3	0.0000	0.0000	0.5000	4.0(5)

[a]Site symmetries in K_5InPb_8 ($R\bar{3}m$): Pb1 6*c* 3*m*, Pb2 18*h* .*m*, In1 3*a* $\bar{3}m$, K1 6*c* 3*m*, K2 6*c* 3*m*, K3 3*b* $\bar{3}m$

[b]$B_{eq} = 8/3\ \pi^2(U_{11}(aa^*)^2 + U_{22}(bb^*)^2 + U_{33}(cc^*)^2 + 2U_{13}(aa^*cc^*)\cos\beta$

Table 4. Atom Separations (Å) out to 4 Å in K_5InPb_8.

Atom Pair	K_5InPb_8
Pb1 – Pb2 x3	3.041(4)
Pb2 – Pb2 x2	3.329(4)
Pb1 – K2 x3	4.004(4)
Pb1 – K2	3.40(2)
Pb2 – In1	3.135(2)
Pb2 – Pb2[a]	3.542(2)
Pb2 – K1 x2	3.93(1)
Pb2 – K1	3.67(2)
Pb2 – K2 x2	3.88(1)
In1 –K1 x6	4.008(4)

[a]intercluster

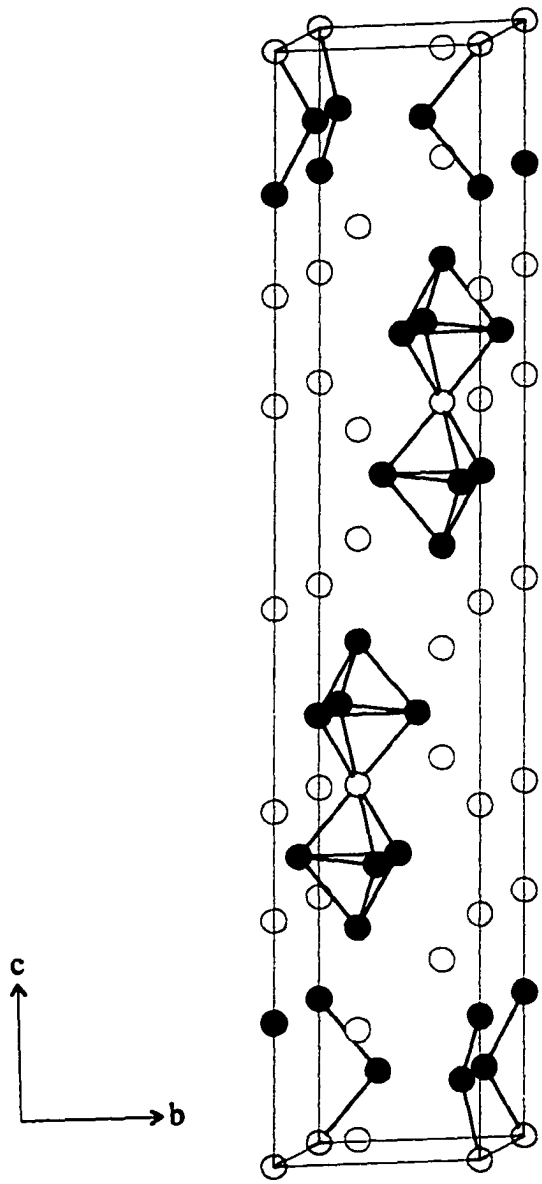

Figure 1. [$\bar{1}$00] view of the K_5InPb_8 structure type. The Pb, In, and K atoms are represented by black, grey, and white spheres respectively. The intercluster contacts between $InPb_8^{5-}$ clusters in the same plane are not shown.

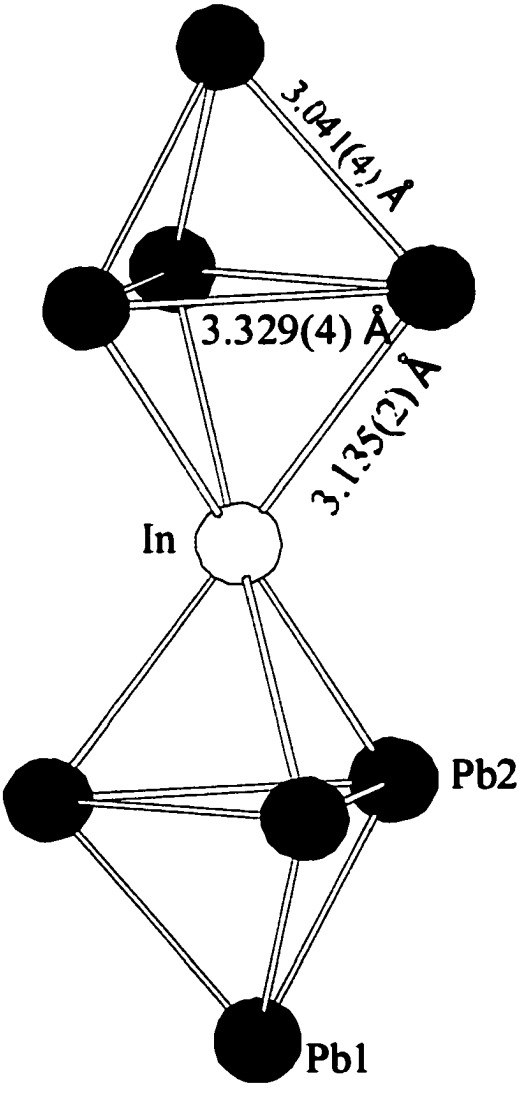

Figure 2. A view of the isolated cluster $InPb_8^{5-}$ the Pb2 atoms on each tetrahedra adopt a staggered configuration relative to one another. The In atom sits on a $\bar{3}$ axis that passes through the apical Pb1 atoms. This gives rise to a local D_{3d} point group symmetry.

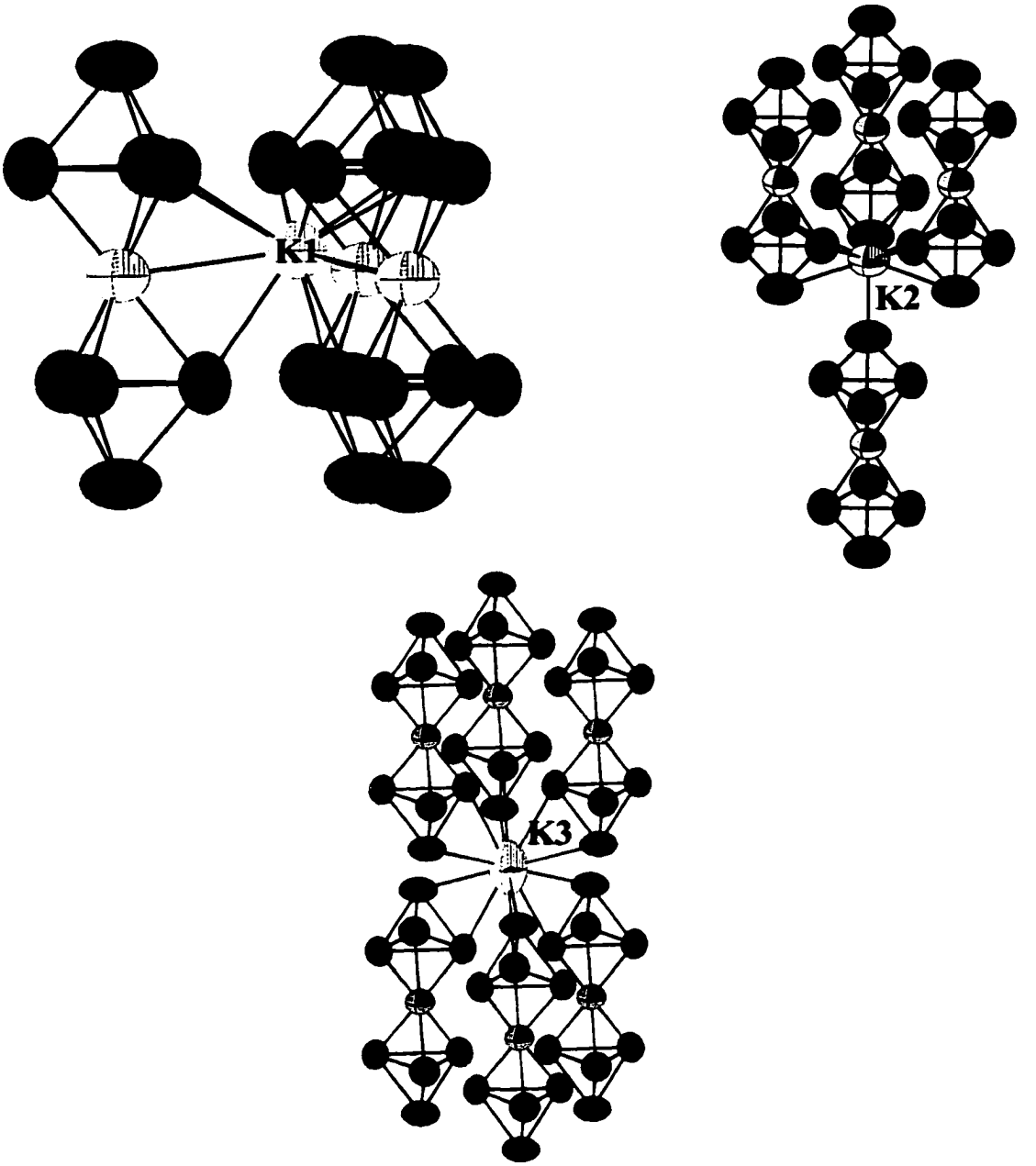

Figure 3. The cation coordination environments of K_5InPb_8 are illustrated above. The K1, K2, K3 environments are shown in the upper left, upper right, and lower middle respectively. The larger cavity of the K3 atom gives rise to a larger ellipsoid. The K2 ellipsoid is compressed slightly because of the short contact of the terminal Pb1 atom in the lower $InPb_8$ cluster. All ellipsoids drawn at 99.9%.

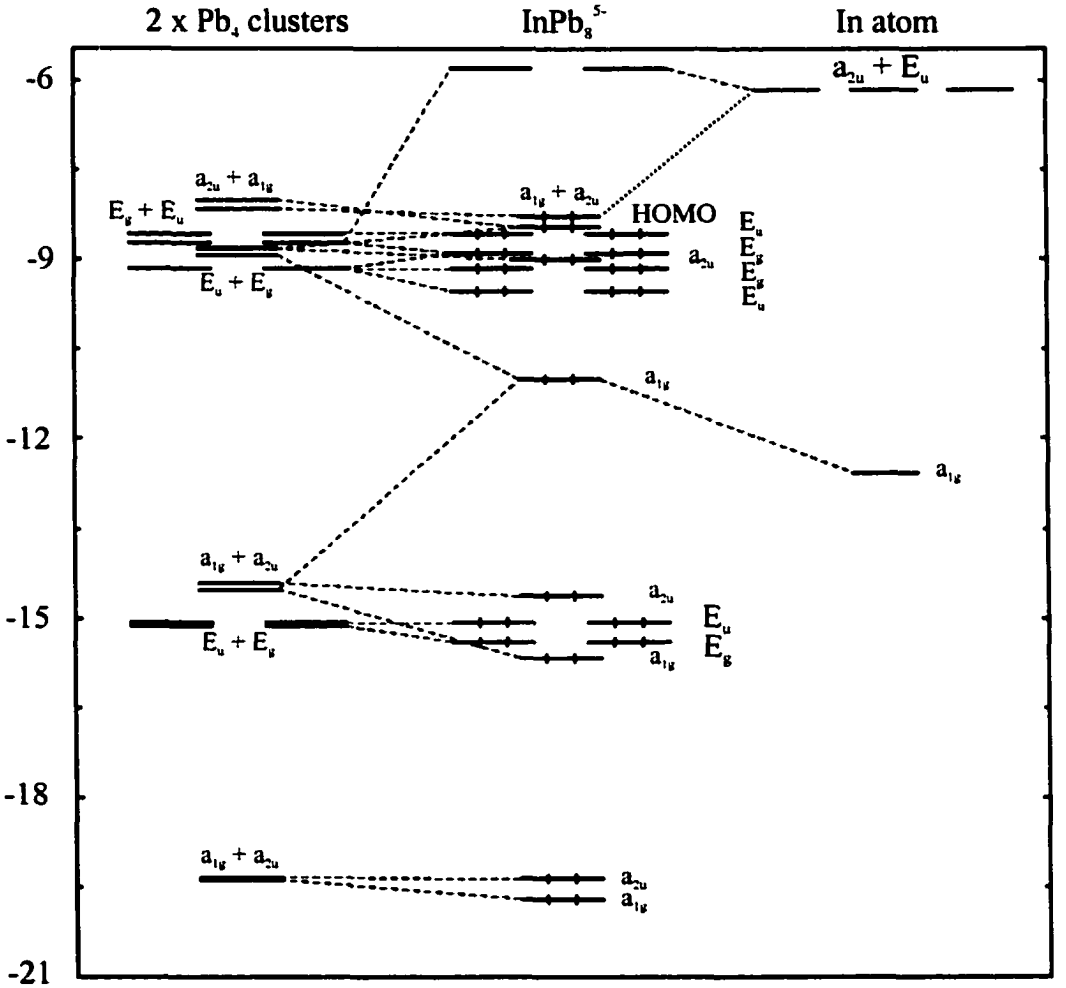

Figure 4. MO diagram for the isolated $InPb_8^{5-}$ cluster with the corresponding fragment orbitals from two Pb_4 tetrahedra and an isolated In atom.

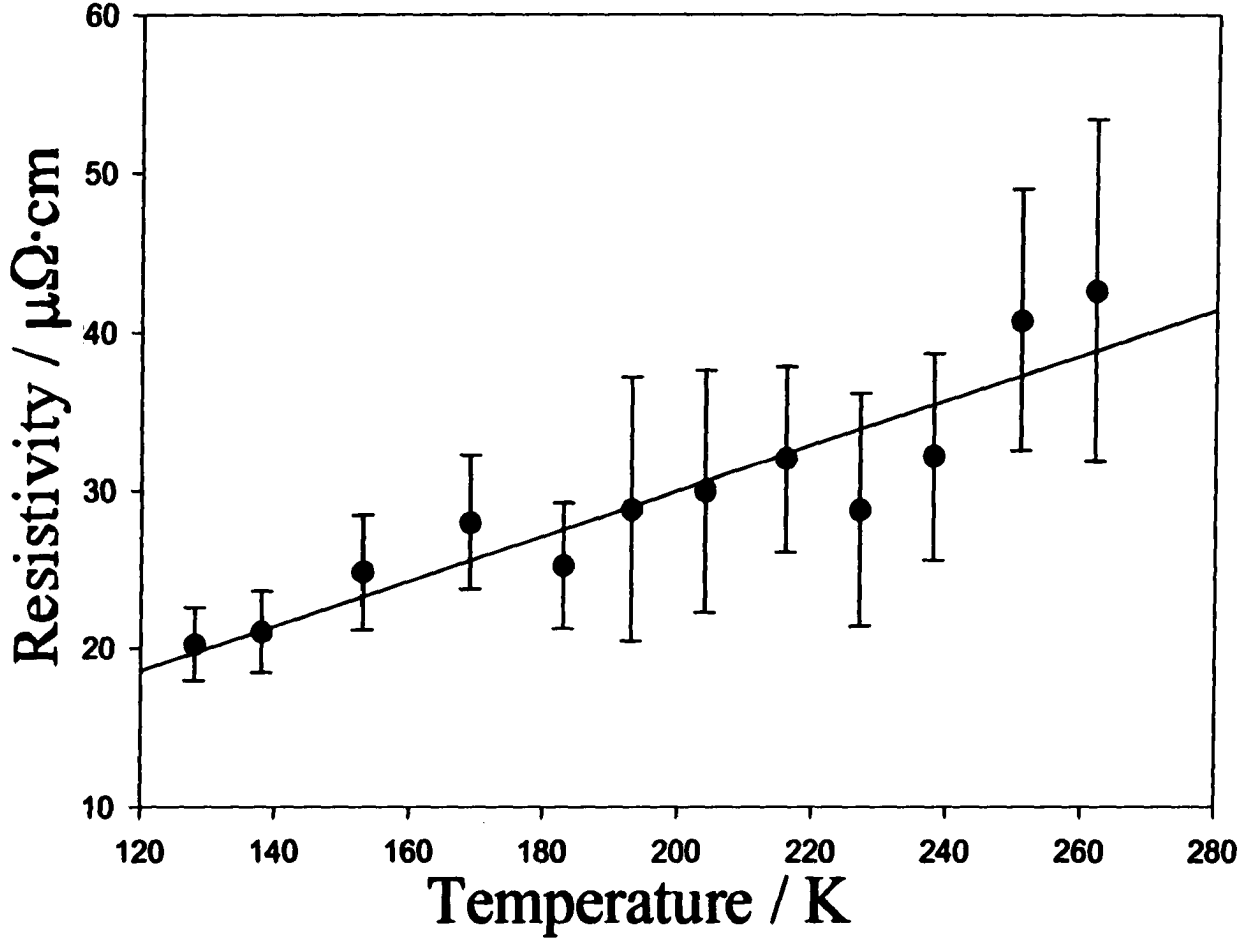

Figure 5. The microwave resistivity of a 44.3 mg sample of K_5InPb_8 with the best fit is shown above. The room temperature resistivity of the sample was extrapolated to be 42 μΩ · cm. The resistivities determined by this method are normally accurate within a factor of two, but gives good temperature dependencies.

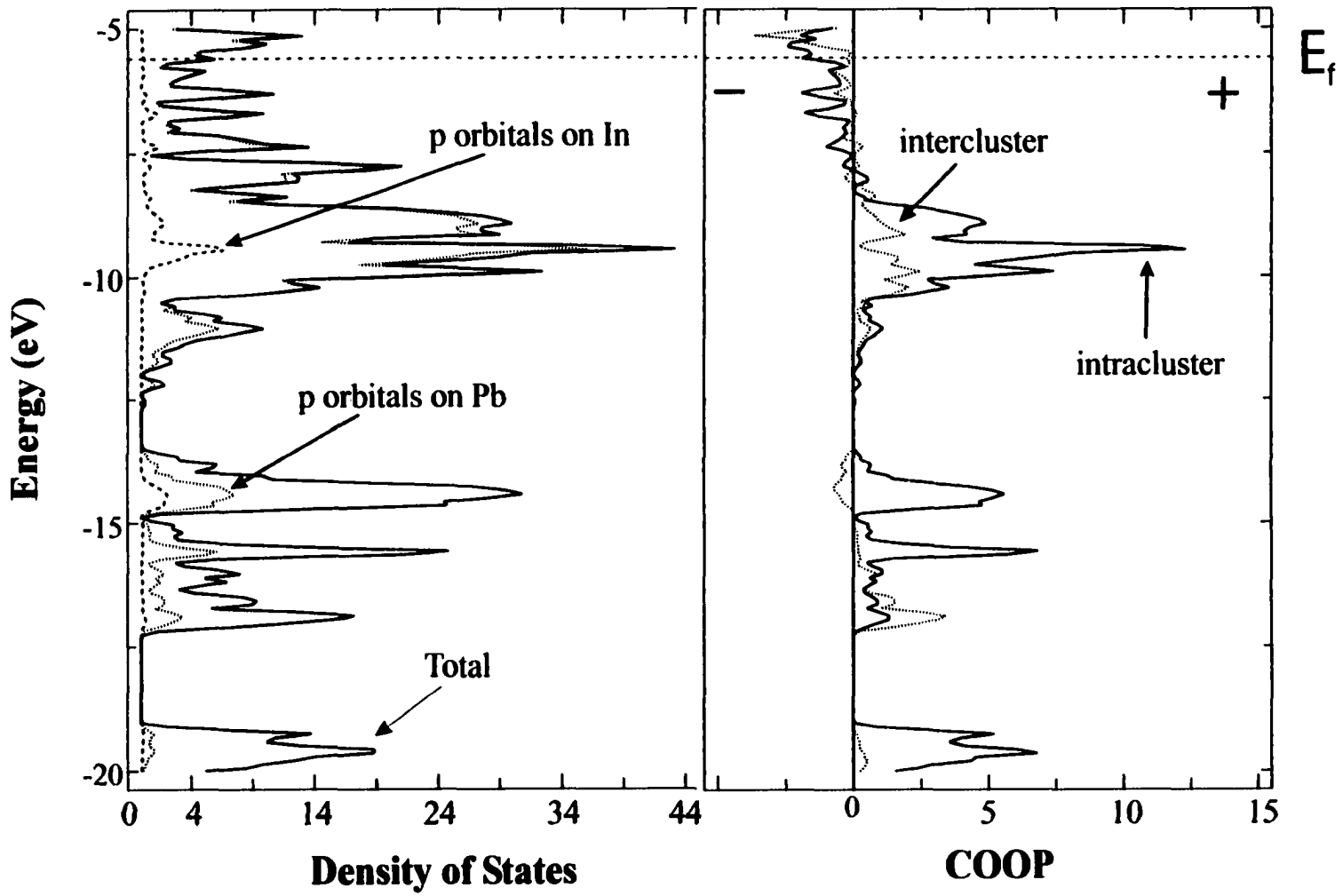

FIGURE 6: Density of States and COOP curves for $InPb_8^{5-}$ with the solid, dotted, and dashed lines showing the toal and partial Pb and In p data, respectively. In the COOP results, the solid line gives the total intracluster and the the dotted line representing the intercluster values.

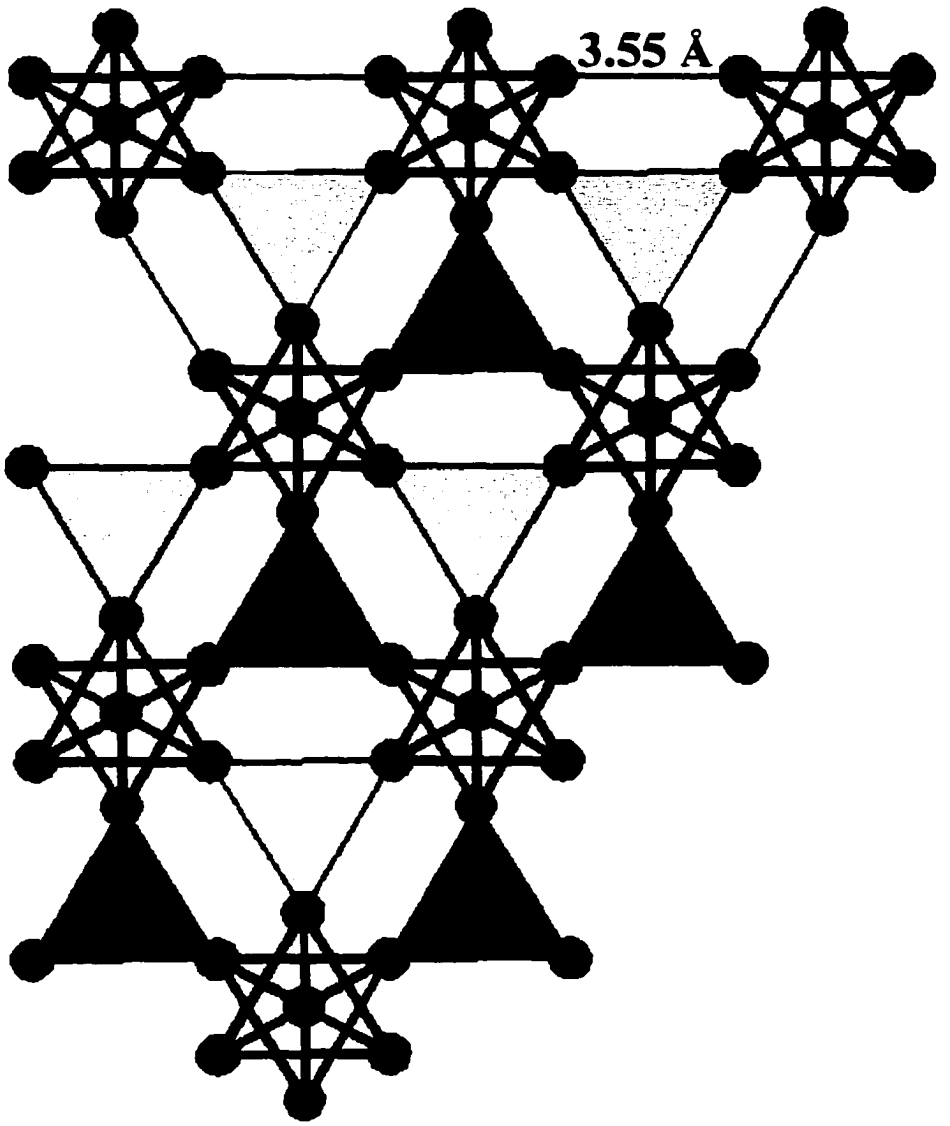

Figure 7. A partial layer of $InPb_8$ clusters at $z = 0$ (for the In atom) with the intercluster bonding shown. The intercluster bonding that is above and below the plane are represented by light and dark grey triangles, respectively. The Pb atoms are represented by black spheres and the In atoms by the lighter grey spheres. The intercluster seperation is 3.55 Å (vs 3.33 Å for the intracluster bonds) between neighboring Pb2 atoms.

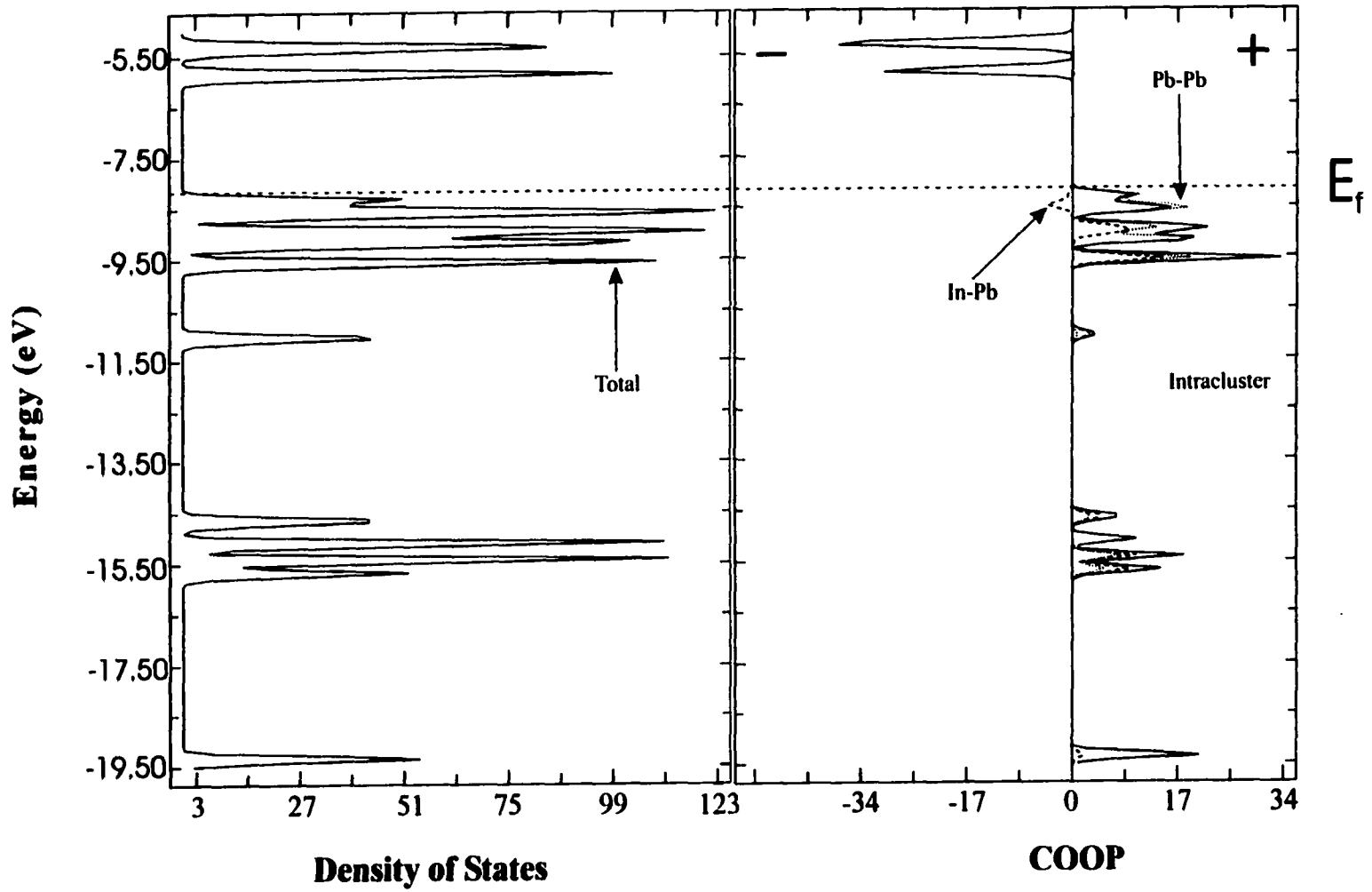

FIGURE 8: Densities of States and COOP curves for $InPb_8^{5-}$ in which the intercluster separation has been increased. The solid DOS line represents the total density of states. The solid, dotted, and dashed lines in the COOP represent intracluster overlap, Pb-Pb overlap, and In-Pb overlap respectively.

Table S1. Details of data collection and refinement for K_5InPb_8

	K_5InPb_8
Formula Weight	961.21
Crystal system, space group, Z	trigonal, $R\bar{3}m$, 3
Unit cell dimensions (Å)[a]	
a	6.8835(6)
c	37.591(5)
V (Å^3)	1543.9(2)
Calculated density, g cm^{-3}	8.508
Diffractometer	Rigaku
Octants, $2\theta_{max}$ (deg)	$\pm h, \pm k, l$; 55°
Observ. refl. ($> 2\sigma_I$)	2563
unique	502
Absorp. coeffic. (Mo Kα, cm^{-1})	902.59
Rel. trans. coeff. range	0.5678 – 1.0000
variables	20
R, R_w[b]	0.057, 0.070
Largest ΔF, e$^-$/Å^3	3.02, 0.70 Å to In1
GOF	1.69

[a] Guinier powder pattern data, $\lambda = 1.540.562$, 23 °C.

[b] $R = \Sigma||F_o| - |F_c||/\Sigma|F_o|$; $R_w = [\Sigma w(|F_o| - |F_c|)^2/\Sigma w(F_o)^2]^{1/2}$; $w = \sigma_F^{-2}$.

Table S2. Anisotropic displacement parameters for K_5InPb_8 phases

K_5InPb_8	U_{11}	U_{22}	U_{33}	U_{12}	U_{13}	U_{23}
Pb1	0.038(1)	0.038	0.012(2)	0.019	0.0000	0.0000
Pb2	0.0199(5)	0.020	0.0197(7)	0.0139(6)	0.0002	-0.0002(3)
In1	0.019(2)	0.02	0.007(4)	0.0095	0.0000	0.0000
K1	0.026(5)	0.026	0.007(8)	0.013	0.0000	0.00000
K2	0.031(5)	0.031	0.017(9)	0.0155	0.0000	0.0000
K3	0.04(1)	0.04	0.08(3)	0.02	0.00000	0.00000

[a] $T = \exp(-2\pi^2(a^{*2}U_{11}h^2 + b^{*2}U_{22}k^2 + c^{*2}U_{33}l^2 + 2a^*b^*U_{12}hk \_ 2a^*c^*U_{13}hl + 2b^*c^*U_{23}kl))$

CHAPTER 5. SYNTHESIS, STRUCTURE, AND BONDING IN THE APPARENT ZINTL PHASE $K_5As_3Pb_3$.

Michael T. Klem, and John D. Corbett*

Department of Chemistry and Ames Laboratory —DOE,[1]

Iowa State University, Ames IA 50011

Abstract

The title phase was synthesized by direct fusion of a stoichiometric amount of the elements at 900°C for 24 hours and then annealed at 650 °C for 3 weeks. The compound crystallizes in an orthorhombic space group, *Pnma*, Z = 4, with a = 19.451(6), b = 12.164(3), c = 6.581(1) Å. The compound is made up of $As_3Pb_3^{5-}$ crown clusters that can be likened to a 6-atom *hypho*-cluster based on the tricapped trigonal prism parent as the *closo* structure. These crowns are connected via intercluster bonds to form infinite chains down the b axis. Extended Hückel theory predicts that this phase should be semiconducting which is confirmed by microwave resistivity measurements (ρ_{298} = 103 $\mu\Omega$·cm; $(\delta\rho/\delta T)/\rho$ = -0.14(3) K^{-1}).

Introduction

Large deltahedral clusters of the tetrel elements have been fairly limited in the solid state. One of the largest cluster currently is the Tt_9^{4-} anion which is now known for all elements in Group 14 except for carbon.[2] One of the limiting factors to the stability of deltahedral clusters of the heavy tetrel elements is the disproportionate size to charge ratio. Wade's rules for counting electrons states that the charge assigned to a deltahedral cluster is independent of its nuclearity, and therefore, large clusters would carry relatively small negative charges.[3] This can set up situations where the number of cations is insufficient to separate large clusters. Molecular chemistry has in the past used large organic or cryptated alkali-metal cations to achieve effective separation of clusters. Alternatively, one can reduce the overall charge of a cluster by the substitution of an electron-rich element (e.g. a pnictogen) to contribute more electrons to the skeletal bonding of a cluster, and hence reduce its overall charge. This would lead to a reduction in the number of cations required for isolation and might provide a pathway for the synthesis of new heteroatomic clusters of the tetrel elements, but polymerization is a common alternative route to compensate for inadequate separations.

The heteroatomic anions of group 14 and 15 are relatively unexplored, but the triel (group 13) and group 15 systems are quite rich in phases.[4] The group 14/15 heteroatomics that are known for neat systems are the phosphide phases A_5GePn_3 (A = Li, Na; Pn = pnictogen).[5] Solution methods, however, have been successful in isolating tetrahedral clusters of $Sn_2Bi_2^{2-}$ and $Pb_2Sb_2^{2-}$ anions with cryptated K cations.[6] This approach has led to the formation of $K_5As_3Pb_3$, a new phase that consists of As_3Pb_3 crown shaped clusters that possess intercluster bonds to form 1-dimensional chains.

Experimental

Synthesis. The materials and general reaction techniques in welded tantalum tubes have been described elsewhere.[7,8] An improved method for sample mounting for powder pattern measurements was employed. Samples were held between sheets of aluminized polyester film by means of a thin centered film of vacuum grease that also served to seal the outer edge of the sheets and to prevent decomposition of the air sensitive products.[9] All transfers where completed in a N_2 or He-filled glove-box. The compound $K_5As_3Pb_3$ was obtained by allowing stoichiometric amounts of potassium (Strem, 99.9995%), arsenic (Aesar, 99.99%), and lead (Aesar, 99.9999%), allowing these to react at 900°C, quenched, and then the products annealed for 3 weeks at 650°C. The resulting products were brittle and black. Initially, single crystals were isolated from a reaction mixture that was loaded as K_5AsPb_8. Reactions loaded on stoichiometry typically yielded 80-90% of the title phase with the remainder being a combination of elemental Pb and KPb. There are 5 known As / Ta binaries, but there was no obvious indication that As was reacting with the Ta tubing.

X-ray diffraction. Powder diffraction data from an Enraf-Nonius Guinier camera and Cu $K_{\alpha 1}$ radiation were used for phase identification. The films were then first compared semiquantitatively with the patterns calculated for phases with known structures. The compositions of the products were then estimated visually from relative powder pattern intensities, considering the unit cell symmetry and contents as well.

Several black crystals of $K_5As_3Pb_3$ were isolated and placed into thin-walled capillaries, and checked by Laue photographs. Diffraction data from one specimen were then collected at room temperature using a Rigaku AFC6 diffractometer with monochromated Mo $K\alpha$ radiation. Routine indexing of 25 centered reflections gave a primitive orthorhombic

cell. Systematic extinctions led to the assignment of P*nma*. The space group assignment was confirmed by a refinement carried out with the aid of the TEXSAN package.[10] The data were corrected for absorption empirically according to three ψ-scans of strong reflections with different θ values. The final residuals were R(F)/Rw = 3.2/3.7 % with the largest residual in the ΔF map of 1.694 $e^-/Å^3$ located 0.86 Å from K2.

Selected crystallographic and refinement data are given in Table 2, and more detailed information and displacement ellipsoid parameters are given in the Supporting Information, Tables S1 and S2. Refined atom positions are listed in Table 2 and the bond distances are listed in Table 3.

Theoretical. Theoretical calculations were made over 326 k-points in the irreducible wedge with the aid of the CAESAR EHTB program of Whangbo, et al.[11] Only the lead and arsenic atoms were included (H_{ii} and ζ_1 for Pb 6s: -15.70 eV and 2.35, for Pb 6p: -8.00 eV and 2.06, for As 5s: -12.60 and 2.23, and for As 5p: -6.190 and 1.89).[12] Calculations were carried out on both an isolated $As_3Pb_3^{5-}$ cluster and the full anion structure.

Property Measurements. Resistivities of $K_5As_3Pb_3$ were measured by the electrodeless Q method[9] on 43.6 mg that had been sieved to 250 - 425 μm powder and diluted with chromatographic Al_2O_3. Measurements were made at 34 MHz over 120 - 240 K. The resistivity of $K_5As_3Pb_3$ extrapolated to 298 K was 103 $\mu\Omega$·cm with a temperature coefficient $[(\delta\rho/\delta T)/\rho]$ of -0.14(3) K^{-1}. The absolute resistivity may be off by a factor of two or three.

Results and Discussion

Description. The basic formula unit consists of As_3Pb_3 "crown" clusters that are linked via intercluster Pb1-Pb1 bonds to form chains that propagate down the *b* axis, figure 1. The crowns consist of a base formed by three Pb atoms with the points of the crown being defined by As atoms that bridge Pb-Pb edges, figure 2a. The cluster possesses C_s symmetry because of the unique function of As, but is close to the ideal C_{3v} assignment. The base of the lead triangle is 3.205(2) Å (Pb1-Pb1) and the sides are 3.324(2) Å (Pb1-Pb2). The arsenic atoms then cap each edge of the Pb triangle. The shorter Pb1-Pb1 edge is bridged by an As1 atom at 2.817(4), and the Pb2-Pb1 edges are bridged by As2 atoms at 2.761(3) Å and 2.854(3) Å to the neighboring Pb1 and Pb2 atoms respectively. The resulting crowns are then linked via longer Pb1-Pb1 intercluster bonds (3.366(2) Å) to form chains of As_3Pb_3 clusters along the *b* direction, figure 2b. The apical Pb2 atoms alternate pointing up and down with respect to the *a* axis as the chain propagates down *b*. The chains are well separated from one another with a minimum distance at 5.14 Å. The cations serve their expected role by bridging edges and faces about the As_3Pb_3 crown clusters. The K1 (CN 3) cations cap the triangular face defined by the three cluster As atoms, K2 (CN 6) caps 2 As and 1 Pb atom for two separate chains, K3 (CN 3) bridges the As2 atoms between two As_3Pb_3 clusters, and K4 sits in a void defined by 4 As_3Pb_3 clusters (3 within a chain and one above).

Similarities exist between the As_3Pb_3 motif in the title phase and the one present in $Cs_5In_3As_4$.[12] This phase contains both chains and layers with the same overall composition of $[In_3As_4]^{5-}$. This unit is quite similar in appearance to the title phase but contains an extra As atom that caps the open In_3 triangular face opposite the crown points.

Bonding. The electronic requirements for an isolated $As_3Pb_3^{5-}$ cluster can be deduced from Wade's rules. The $As_3Pb_3^{5-}$ crowns would correspond to a hypho cluster (i.e. 3 vertices removed from the closo D_{3h} parent) with the parent being the tricapped trigonal prism, Pb_6As_3. According to Wade's rules, the number of skeletal electrons required for closed shell bonding of a hypho-cluster would be equal to 2n + 8 or 20 electrons in this case. Each lead atom would contribute its 2 valence electrons and arsenic donates its 3 valence electrons for a total of 15 skeletal electrons. In order to satisfy the bonding requirements, the isolated cluster requires five more electrons which come from the alkali-metal cations. Molecular orbital calculations provide evidence for this assumption for an isolated cluster.

Complications arise when one takes into consideration the two intercluster bonds on each of the $As_3Pb_3^{5-}$ clusters. According to Wade (or anyone else), each exo-bond should lower the electronic requirements of the cluster by one. This leaves the compound two cluster electrons in excess, and to be accounted for. Additional calculations were carried out on the full structure minus the cations. The results (DOS AND COOP) are shown in figure 3. The density of states plot shows that at the Fermi level a small band gap is opening (solid line). This gap, it is hypothesized, should increase when K bonding / antibonding states are allowed to mix in. The As s band (dotted) starts before -20 eV and continues up to approximately -14 eV, and the Pb s band (dashed-dot) behaves similarly. There is clearly a substantial amount of mixing between the As s and Pb s orbitals. The As p band (dashed) begins around -15eV and continues up to -10 eV, and the Pb p band (dash-dot-dot) starts around -13 eV and continues to past Fermi. The As p orbital dominates from -13 eV to -10 eV at which point the Pb p gains dominance. There is a good amount of mixing between the As p and Pb p until about -8 eV above which point only Pb p is dominant.

The COOP curve for the $As_3Pb_3^{5-}$ cluster (solid line) show that weakly antibonding states are being populated around Fermi. These states are prominently antibonding between As-Pb (dash-dot) with the majority being As2-Pb2 antibonding states from -8 eV to Fermi level. There are also some antibonding states arising from the Pb1-Pb1 intracluster bonds from -9 to -8 eV. There is minimal contribution from antibonding states from In1-In1 intercluster bonds until Fermi. Interestingly, at approximately -9.5 eV, the $As_3Pb_3^{5-}$ cluster net bonding is optimized. This corresponds to 18 skeletal electrons per $As_3Pb_3^{5-}$ cluster. This is in agreement with the predictions afforded by Wade's rules for the six atom hypho-cluster with two exobonds.

The effect of populating these intracluster antibonding states is evident in the overlap populations. The overlap population for the intercluster Pb1-Pb1 contacts at 3.37 Å is 0.37, while for the average intracluster Pb-Pb contacts at 3.26 Å is 0.20. This is an 85% increase in overlap population for a 0.1 Å *increase* in bond distance. Since the intercluster Pb-Pb antibonding states are not being populated, this is not surprising. The average overlap population for As – Pb also remains relatively high at 0.47.

The results of the extended Hückel analysis would suggest that this phase has the potential to be a valence compound and exhibit semiconducting behavior. The measured microwave resistivity for $K_5As_3Pb_3$ was 103 $\mu\Omega$·cm with a negative temperature coefficient of -0.14 K^{-1} adding support for this assumption.

Conclusions

The $As_3Pb_3^{5-}$ cluster, in the isolated case, represents a new type of Zintl cluster in the heavy tetrel elements. The $As_3Pb_3^{5-}$ cluster type represents an expansion of the known

heteroatomic Zintl clusters of the tetrel elements. The large cluster atoms and the relatively few cations is a possible cause for the 1-dimensional chain formation.

References

(1) This research was supported by the Office of the Basic Energy Sciences, Materials Sciences Division, U. S. Department of Energy (DOE). The Ames Laboratory is operated for DOE by Iowa State University under Contract No. W-7405-Eng-82.

(2) Queneau, V.; Sevov, S. C. *Angew. Chem.* **1997**, *109*, 1818.; b) Schnering, H.G.v.; Baitinger, M.; Bolle, U.; Cabrera, W. C.; Curda, J.; Grin, Y.; Heinemann, L.; Llanos, L.; Peters, K.; Schmeding, A.; Somer, M. *Z. Anorg. Allg. Chem.* **1997**, *623*, 1037.; c) Queneau, V.; Sevov, S. C. *Inorg. Chem.* **1998**, *37*, 1358.; d) Todorov, E.; Sevov, S. C. *Inorg. Chem.* **1998**, *37*, 3889.; e) Queneau, V.; Todorov, E.; Sevov, S. C. *J. Am. Chem. Soc.* **1998**, *120*, 3263.

(3) Wade, K. *Adv. Inorg. Chem. Radiochem.* **1976**, *18*, 1.

(4) Eisenmann, B.; Cordier, G. In *Chemistry and Bonding in Zintl Phases and Ions*: Kauzlarich, S.M., Ed.; VCH Publishers: New York, **1996**; p 61. b..) Schäfer, H.; Eisenmann, B. *Rev. Inorg. Chem.* **1981**, *3*, 29.

(5) Juza, R.; Schulz W. *Z. Anorg. Allg. Chem.* **1954**, *275, 65.; b.)* Eisenmann, B.; Somer, M. *Z. Naturforsch., B: Chem. Sci,* **1985**, *40B*, 886.

(6) Critchlow, S.C.; Corbett, J.D. *Inorg. Chem.* **1982**, *21*, 3286.; Critchlow, S.C.; Corbett, J.D. *Inorg. Chem.* ***1985***, *24*, 97.

(7) Corbett, J. D. In *Chemistry, Structure and Bonding in Zintl Phases and Ions*; Kauzlarich, S., Ed.; VCH: New York, **1996**; Chapter 3.

(8) Dong, Z.-C.; Corbett, J. D. *J. Am. Chem. Soc.* **1993**, *115*, *11299*.

(9) Klem, M. T.; Vaughey, J. T.; Harp, J. G.; Corbett, J. D. *Inorg. Chem.* **2001**, *40*, 7020.

(10) *TEXSAN*, Windows version 1.02; Molecular Structure Corp.: The Woodlands, TX, **1997**.

(11) Ren, J.; Liang, W.; Whangbo, M.-H. *CAESAR*; PrimeColor Software, Inc.: Raleigh, NC, **1998**.

(12) Alvarez, A. Tables of Parameters for Extended Hückel Calculations, Parts 1 and 2, Barcelona, Spain, **1987**.

(13) Gascoin, F.; Sevov, S. C. *Inorg. Chem.* **2001**, *40*, 6254.

Table 1. Selected Details of Data Collection and Structural Refinement for $K_5As_3Pb_3$

	$K_5As_3Pb_3$
Formula Weight	1041.86
Crystal system, space group, Z	orthorhombic, Pnma, 4
Unit cell dimensions (Å)	
a	19.451(6)
b	12.164(3)
c	6.581(1)
V (Å^3)	1557.0(6)
Calc. density, g cm^{-3}	4.444
Absorp. coeff. μ (Mo Kα, cm^{-1})	400.37
R, R_w[a]	0.032, 0.037

[a] $R = \Sigma||F_o| - |F_c||/\Sigma|F_o|$; $R_w = [\Sigma w(|F_o| - |F_c|)^2/\Sigma w(F_o)^2]^{1/2}$; $w = \sigma_F^{-2}$.

Table 2. Refined atomic positions for $K_5As_3Pb_3$.

	x	y	z	B_{eq}
$\underline{K_5As_3Pb_3}$				
Pb1	0.04435(5)	0.11826(7)	0.4794(1)	1.55(2)
Pb2	0.19349(8)	0.2500	0.4397(2)	1.80(3)
As1	0.9567(2)	0.2500	0.2410(5)	1.46(7)
As2	0.1526(1)	0.0534(2)	0.2361(4)	1.51(5)
K1	0.0000	0.0000	0.0000	1.9(2)
K2	0.1033(5)	0.2500	0.950(1)	1.8(2)
K3	0.1788(3)	0.9545(5)	0.7293(8)	2.3(1)
K4	0.1215(6)	0.7500	0.261(1)	3.5(2)

[a] $B_{eq} = 8/3\ \pi^2(U_{11}(aa^*)^2 + U_{22}(bb^*)^2 + U_{33}(cc^*)^2$

Table 3. Atom Separations (Å) in $K_5As_3Pb_3$.

atom pair	distance	atom pair	distance
Pb1 – Pb1	3.205(2)	As1 – K3 x2	3.630(8)
Pb1 – Pb1	3.366(2)	As1 – K4	3.64(1)
Pb1 – Pb2	3.324(2)	As1 – K4	3.61(1)
Pb1 – As1	2.817(4)	As2 – K1	3.413(3)
Pb1 – As2	3.761(3)	As2 – K2	3.191(6)
Pb1 – K1 x2	3.573(1)	As2 – K3	3.582(7)
Pb1 – K2 x2	3.671(7)	As2 – K3	3.280(8)
Pb1 – K3	3.676(7)	As2 – K3	3.499(7)
Pb1 – K4	3.98(1)	As2 – K4	3.744(3)
Pb2 – As2 x2	2.854(3)	K1 – K2 x2	3.660(5)
Pb2 – K2	3.789(8)	K1 – K3 x2	3.947(7)
Pb2 – K2	3.668(8)	K1 – K4 x2	4.218(8)
Pb2 – K3 x2	3.778(7)	K2 – K3 x2	4.146(8)
Pb2 – K3 x2	4.078(6)	K2 – K4	4.59(2)
Pb2 – K4	4.18(1)	K3 – K3 x2	4.440(9)
As1 – K1 x2	3.532(2)	K3 – K4	4.11(1)
As1 – K2	3.44(1)	K3 – K4	4.44(1)

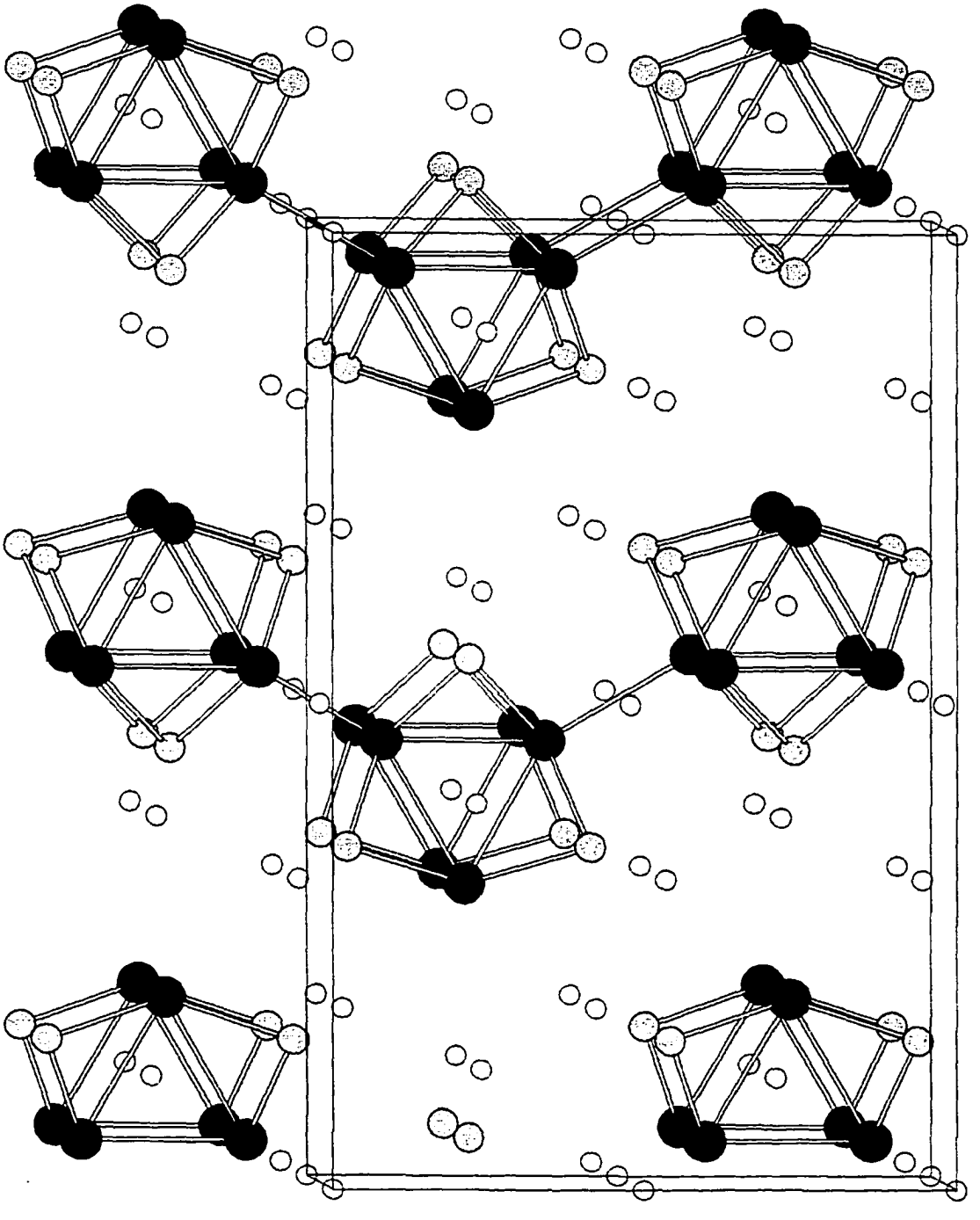

Figure 1. The [001] view of the full structure of $K_5As_3Pb_3$ is illustrated above. The Pb, As, and K are represented by black, grey, and white circles respectively.

A.)

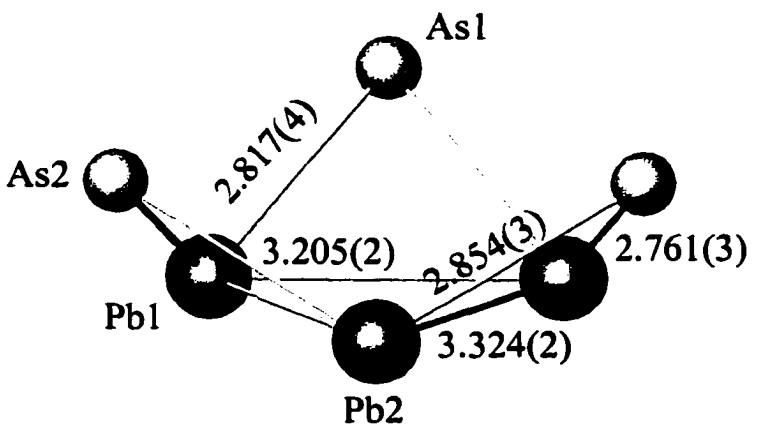

B.)

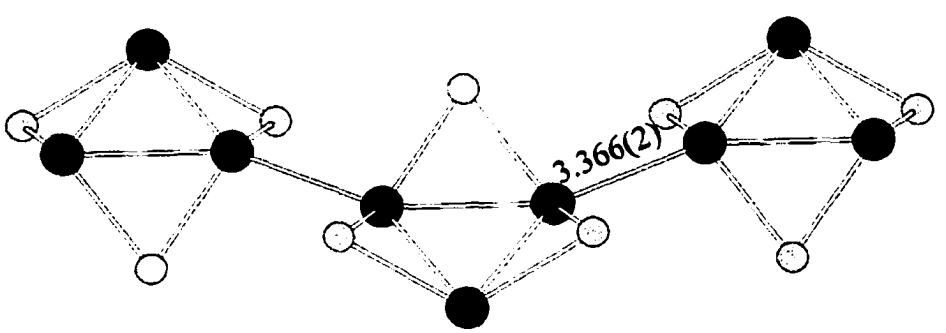

Figure 2. A.) The isolated cluster of $As_3Pb_3^{5-}$ is shown with Pb and As represented by black and grey spheres respectively. B.) The infinite chain running down the *b* axis is shown.

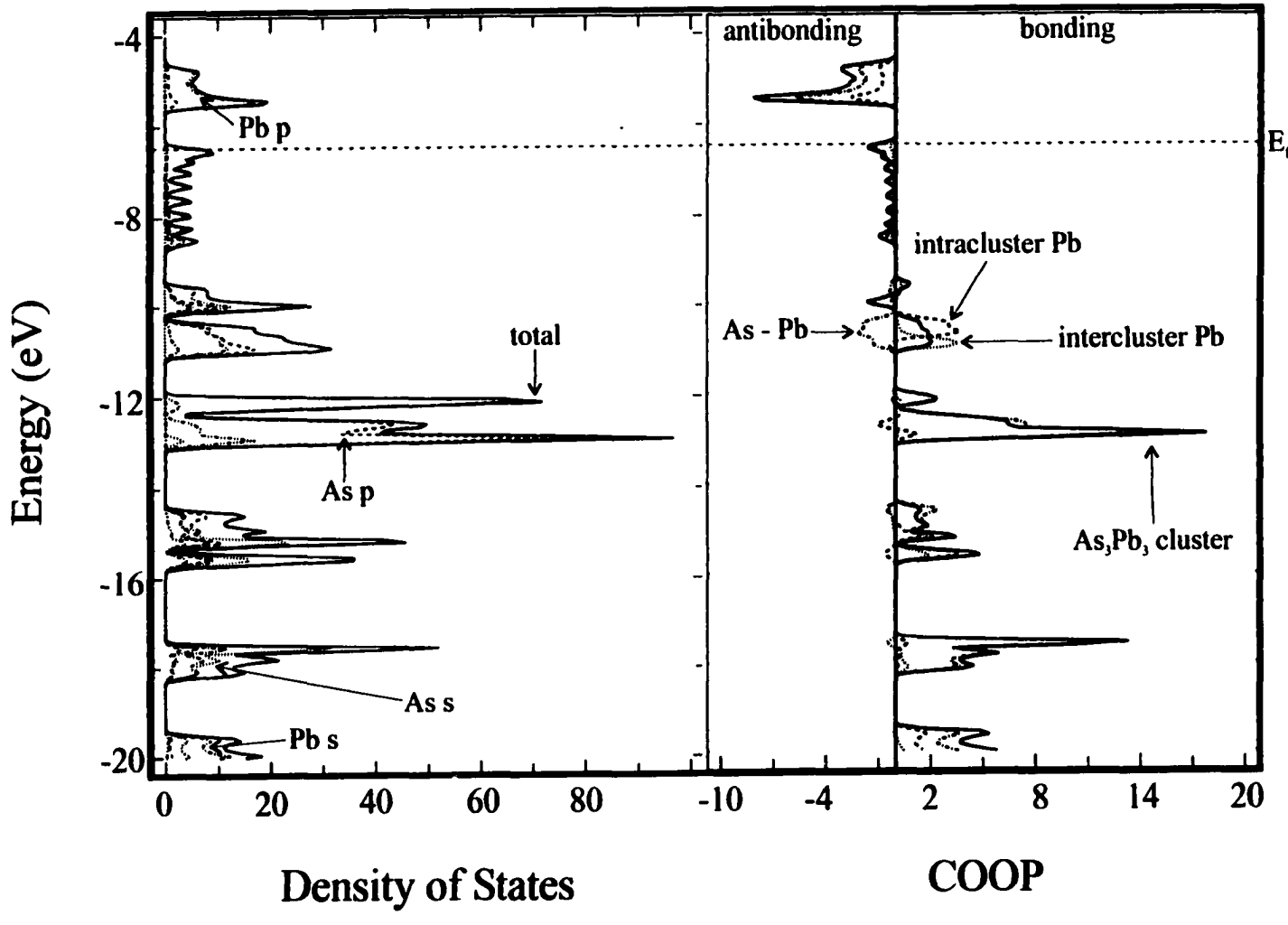

Figure 3. $As_3Pb_3^{5-}$ DOS and COOP curves. In the density of states plot, the As s, As p, Pb s, and Pb p orbital are represented by dotted, dashed, dash-dot, and dash-dot-dot lines respectively. In the COOP curve, the cluster is shown by the solid line, and the intracluster Pb, intercluster Pb, and As-Pb interactions are represented by dashed, dotted, and dash-dot curves respectively.

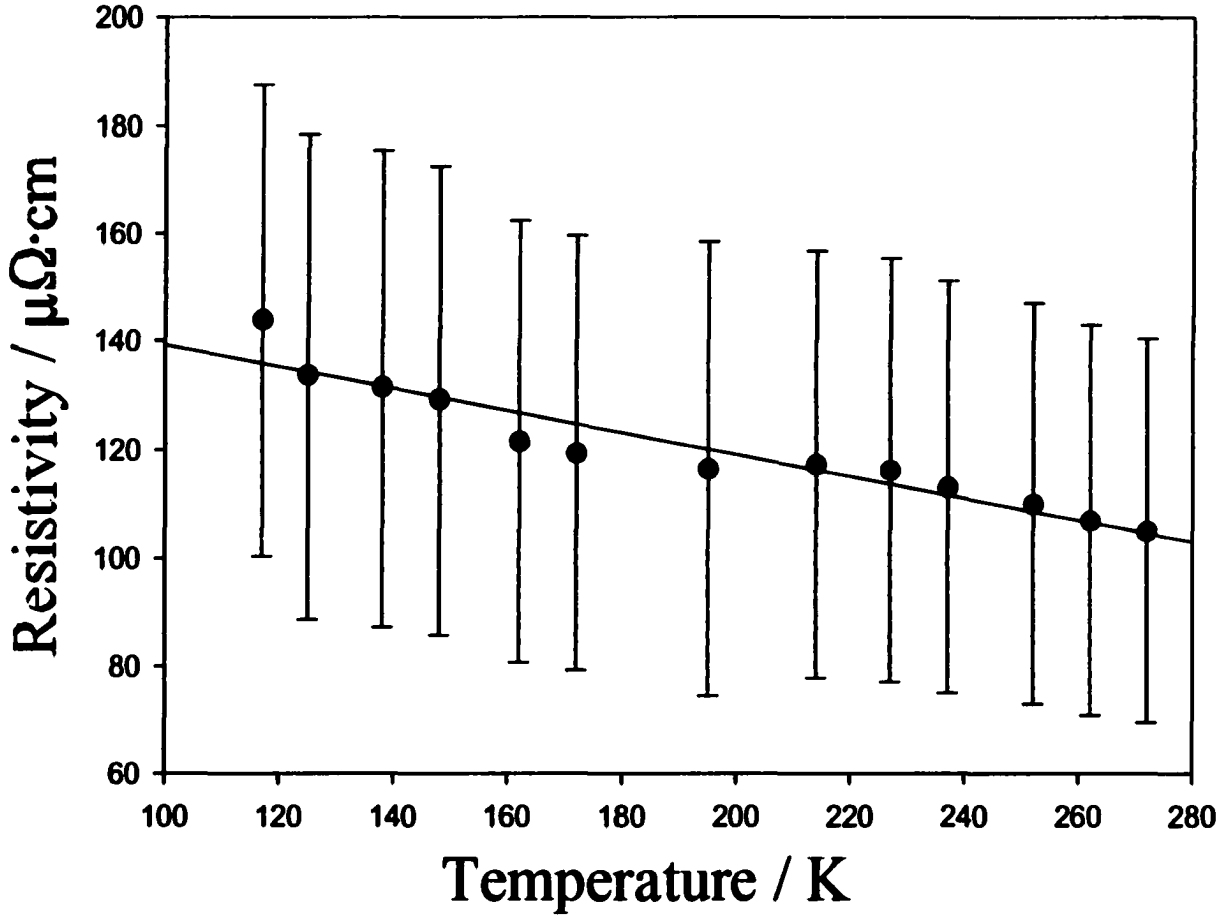

Figure 4. The microwave (Q's) resistivity of a 43.6 mg sample of $K_5As_3Pb_3$ with the best fit shown. The room temperature resistivity of the sample was an extrapolated 103 μΩ · cm.

Table S1. Details of data collection and refinement for $K_5As_3Pb_3$

Formula	$K_5As_3Pb_3$
Formula Weight	1041.86
Crystal system, space group, Z	orthorhombic, Pnma, 4
Unit cell dimensions (Å)	
a	19.451(6)
b	12.164(3)
c	6.581(1)
V (Å^3)	1557.0(6)
Calculated density, g cm^{-3}	4.444
Diffractometer	Rigaku
Octants, $2\theta_{max}$ (deg)	$\pm h, \pm k, l$; 55°
Observ. refl. ($> 2\sigma_I$)	9898
unique	2652 (R_{int} = 0.232)
Absorp. coeffic. (Mo Kα, cm^{-1})	400.37
Rel. trans. coeff. range	0.1839 – 1.0000
variables	58
R, R_w[a]	0.032, 0.037
Largest ΔF, e$^-$/Å^3	1.694 at 0.86 Å from K2
GOF	1.16

[a] $R = \Sigma||F_o| - |F_c||/\Sigma|F_o|$; $R_w = [\Sigma w(|F_o| - |F_c|)^2/\Sigma w(F_o)^2]^{1/2}$; $w = \sigma_F^{-2}$.

Table S2. Anisotropic displacement parameters for $K_5As_3Pb_3$ phase.[a]

$K_3As_3Pb_3$	U_{11}	U_{22}	U_{33}	U_{12}	U_{13}	U_{23}
Pb1	0.0209(5)	0.0217(3)	0.0162(3)	-0.0010(5)	0.0009(4)	0.0019(4)
Pb2	0.0177(8)	0.0289(7)	0.0219(6)	0.0000	-0.0043(6)	0.0000
As1	0.014(2)	0.022(2)	0.019(1)	0.0000	-0.003(2)	0.0000
As2	0.017(2)	0.022(1)	0.018(1)	0.004(1)	-0.001(1)	-0.002(1)
K1	0.021(5)	0.034(4)	0.019(4)	-0.004(4)	-0.001(4)	-0.004(4)
K2	0.030(5)	0.024(4)	0.014(3)	0.0000	-0.001(4)	0.0000
K3	0.019(3)	0.042(3)	0.028(3)	0.003(3)	0.001(3)	0.005(3)
K4	0.040(7)	0.064(7)	0.031(4)	0.0000	0.004(5)	0.0000

[a] $T = \exp(-2\pi^2(a^{*2}U_{11}h^2 + b^{*2}U_{22}k^2 + c^{*2}U_{33}l^2 + 2a^*b^*U_{12}hk + 2a^*c^*U_{13}hl + 2b^*c^*U_{23}kl))$

CHAPTER 6. $Na_{23}In_{40.4(1)}Pd_{2.51(2)}$, SOME UNRESOLVED PROBLEMS.

Michael Klem and John D. Corbett*

Department of Chemistry and Ames Laboratory —DOE,[1]

Iowa State University, Ames IA 50011

Abstract

Reaction of the elements within welded Ta containers at 800 °C followed by subsequent annealing for two weeks gave the new phase $Na_{23}In_{40.4(1)}Pd_{2.51(2)}$. The title phase crystallizes in the hexagonal space group P6/*mmm* (Z = 3) with cell dimensions of a = 16.233(2) and c = 15.852(3) Å. This phase appears to be isostructural to the unpublished $Na_{23}In_{38.4}Zn_{4.6}$. The major structural features include a 12-bonded-*closo*-In_{12} icosahedron, a 15-bonded-*closo*-In_{15} cluster, and an 18-bonded-21-atom spacer. If standard Zintl-Klemm/Wade's rules are applied, the title phase has 293.4(6) electrons per unit cell, while the predicted electron count is 292 or 296 depending on the occupation of a non-bonding orbital in the In_{15} cluster. This former is intermediate between the values inferred from the other known isostructural phases $Na_{23}In_{38.4(2)}Zn_{4.6}$ and $Na_{23}In_{39.8(1)}Au_{3.4}$, 294.8(1.2) and 291.6(1.2), respectively. The validity of the refinement has, to date, not been confirmed. The assignment of fractional occupancies to some sites and mixing of Pd on others can be sketchy at best. There are some unusually short cation-cation distances of approximately 3 Å that raise suspicions, and the phase width, if any, has yet to be established.

Introduction

The chemistry of indium in the reduced oxidation state has demonstrated a remarkable diversity. In the alkali-metal binary regime the structures range from simple isolated clusters of 3-bonded indium atoms in Na_2In,[1] networks of 8-bonded indium atoms in KIn_4,[3] and isolated cluster examples such as in K_8In_{11}.[4] When looking past the binary systems, two avenues of exploration have been undertaken, one the use of mixed cations, and the other the substitution of a third element for indium. The former approach has been used successfully in the synthesis of $Na_3A_{26}In_{48}$, A = K–Cs.[5] The later approach has been used with transition metals to synthesize cluster phases like $K_8In_{10}Hg$ containing $In_{10}Hg^{8-}$ (mercury disordered) units,[6] and to gain centered clusters like those found in $K_8In_{10}Zn$ and $K_{10}In_{10}M$, M= Ni, Pd, Pt.[7]

This chapter presents another structure in the ternary alkali-metal-indium-transition-metal system. The title phase is isostructural with $Na_{23}In_{38.4(2)}Zn_{4.6}$ and contains an electron count that is intermediate between the known Zn and Hg analogues.[8]

Experimental

The materials and general reaction techniques in welded tantalum tubes have been described elsewhere.[9,10] An improved method for sample mounting for powder pattern measurements was employed. Samples were held between sheets of aluminized polyester film by means of a thin centered film of vacuum grease that also served to seal the outer edge of the sheets and to prevent decomposition of the air sensitive products.[11] All transfers where completed in a N_2 or He-filled glove-box. Samples of $K_{23}In_{40.4(1)}Pd_{2.51(2)}$ were prepared by direct fusion of the elements in welded tantalum tubes followed by heat treatment.

Synthesis. The title phase was synthesized by combing stoichiometric amounts of Na (Fisher, 99.9%), In (Aesar, 99.99%), and Pd wire (Johnson Matthey, 99.995%) as Na_5PdIn_8. The resulting mixture was then heated to 800 °C and annealed for two weeks and then allowed to radiatively cool. Small black/grey crystals were obtained from the reaction mixture where the yield of the title compound was 75-80% and the balance was a combination of NaIn and In. Attempts to make the phase without Pd present were unsuccessful.

X-ray diffraction. Powder diffraction data from an Enraf-Nonius Guinier camera and Cu $K_{\alpha 1}$ radiation were used for phase identification. The films were then first compared semiquantitatively with the patterns calculated for phases with known structures. The compositions of the products were then estimated visually from relative powder pattern intensities, considering the unit cell symmetry and contents as well.

Several black crystals of $K_{23}In_{40.4(1)}Pd_{2.51(2)}$ were isolated and placed into thin-walled capillaries, and checked by Laue photographs. Diffraction data from one specimen were then collected at room temperature using a Rigaku AFC6 diffractometer with monochromated Mo $K\alpha$ radiation. Routine indexing of 25 centered reflections gave a primitive hexagonal cell. No systematic absences were observed, and the Wilson plot statistics suggested a centrosymmetric space group. The space group *P6/mmm* was chosen, and this assignment was confirmed by a refinement carried out with the aid of the SHELXTL package.[12] Attempts to refine the structure in a lower symmetry space group like *P6/m* gave thermal ellipsoids that were unreasonable. The data were corrected for absorption empirically according to three ψ-scans of strong reflections with different θ values. The final residuals were R(F)/Rw = 6.2/14.5 % with the largest residual in the ΔF map of 4.291 $e^-/Å^3$ located

0.55 Å from Na5. Refinement details are provided in tables 1-3 and bond distances are listed in table 4.

Initially, direct methods provided nine peaks with distances appropriate for indium atoms, except for one distance for In7 that was approximately 1.77 Å to its symmetry related position. This problem was caused by the 6-fold rotation axis of the space group. Lower symmetry trigonal space groups, like *P*3 were tried to alleviate this problem, but the PLATON software package[13] suggested that there were missing symmetry elements that when included would give rise to the original *P6/mmm* assignment. The distances about In1 are characteristically 0.15 Å shorter than the other indium distances. The peak heights of the last three atoms (In7-9) were also a little over half of the heights of the earlier indium atoms assigned (In1-6). All the positions where treated as fully occupied for the first few least square cycles. The difference Fourier map revealed all eight of the sodium atoms. When the sodium atoms were included in the refinement, the thermal parameters were about twice as large for In7-9 compared to the other indium atoms and the thermal parameters for In1 were also larger than average. If the occupancies of the indium atoms were allowed to vary, the occupancies of In1, 7-9 refined to 50-60% with all the other indium atoms, except In1, staying close to 100%. It appeared likely that In7 was half occupied (or incorrectly assigned) to avoid the short 1.765(4) Å contacts. This left the question of how much Pd was mixing in and where in the structure. It was stated for the isostructural $Na_{23}In_{39.8(1)}Au_{3.40(7)}$ that the transition metal was mixing in on the In1-3 sites, while the In7-9 sites remained fractionally occupied (i.e. In1-3 refined with occupancies greater than 100% and In7-9 refined with occupancies ranging from 50-60% indicating that Au was perhaps mixing in on the first three

positions). The present refinement was then carried out with a mixture of Pd on the In1 site and fractional occupancies on In7-9 to achieve the final results.

Results and Discussion

Description. The title phase is isostructural to the previously determined $Na_{23}In_{38.4}Zn_{4.6}$ and $Na_{23}In_{39.8}Au_{3.4}$ phases. The full unit cell of the title phase is shown in figure 1. The structure can be constructed from three basic building blocks, clusters of In_{12}, In_{15}, and an In_{21} atom spacer, all of which are interconnected via exo bonds. The first cluster type is a 12-bonded icosahedron with D_{2h} symmetry (figure 2a) and is centered on an *mmm* position. It is built up from In1–3 atoms with some mixing from Pd on the In1 site. The cluster is then bonded to four other In_{12} clusters through In1-In1 bonds, to four In_{15} clusters through In3-In4 bonds, and to four In_{21} clusters through In2-In5 bonds. The shortest of the intercluster distances is associated with the In1-In1 bonds (i.e. the site with the mixture of Pd).

The second building block is the 15-bonded *closo*-In15 cluster centered on the 2*c* position that possesses D_{3h} symmetry (figure 2b). This cluster is built up from In4, 6, and 9 positions. All of the atoms of the cluster are then exo-bonded to neighboring clusters, In4-In3 to six In_{12}, In6-In8 bonds to three In_{21} clusters, and In9-In9 to three other In_{15} clusters. The partial occupancy of the apparently 6-bonded In9 site on this cluster is not altogether unsurprising, because similar behavior has been noted in other large clusters, the 6-bonded *closo*-In_{16} in $Na_9In1_{6.8}Zn_{2.3}$, the 12-bonded *closo*-In18 unit in $Na_{49}In_{80.9}Sn_{9.1}$,[8] and the $(Ga,Cd)_{16}$ cluster units in $Na_{8.75}Ga_{14}Cd_{5.9}$.[14]

The final cluster type is the In_{21} spacer (figure 2c). This cluster is built up from In5, 7, and 8 positions. Figure 2c only shows one of two apparent orientations of the spacer. Half of the In7 and In8 positions belong to one orientation and the other half to the second. The two differing orientations are shown in figure 3. The In5 position is common to both orientations. The geometry of the cluster can be viewed as two truncated tetrahedra fused on one triangular face. It has 18 exo-bonds to 12 In_{12} clusters through In5-In2 and 3 In_{15} clusters (two In8-In6 to each In_{15}).

Electronic structure. A detailed analysis of the electronic structure has been done previously by Sevov.[8] The electrons required for each of the building blocks can be determined in the following manner. Each 12-bonded In_{12} cluster requires 26 (skeletal) + 12 (exo bonds) = 38 electrons. Each of the two 15-bonded In_{15} clusters requires 32 or 34 (skeletal electrons) + 15 (exo-bonds) = 47 or 49 electrons. The reason for the two possible electron counts is that there is a non-bonding orbital available to be filled. The In_{21} spacer has 21 4-bonded atoms requires 21 x 4 = 84 electrons. The sum per unit cell then becomes equal to 3 x 38 + 2 x 47 (or 49) + 84 so that 292 or 296 electrons needed.

The number of electrons available in $Na_{23}In_{40.4(1)}Pd_{2.51(2)}$ is 2 x (23 + 40.4 x 3 + 2.51) = 293.4(6). This number is similar to that obtained for $Na_{23}In_{39.8(1)}Au_{3.4}$ and $Na_{23}In_{38.4(2)}Zn_{4.6}$ which are 291.6(1.2) and 294.8(1.2) respectively. These numbers suggest that the Au compound could be balanced electronically while the Pd and Zn examples have extra electrons, presumably located on the non-bonding levels of the In_{15} cluster.

Conclusions

A variety of questions still exist with respect to these materials. In the title phase the Na1 Ueq is about half that of all the other Na atoms and the correctness of the assigned single occupancy is still in doubt. In regard to this feature, there is a short contact between Na1 and In9 of approximately 3.1 Å. Also the Na5-Na5 separation is only 3.0 Å, which is quite low for cation separation. All distances are on par with those reported by Sevov. The R factor is also high by modern standards especially when compared to the refinements of the isostructural examples (2.8 and 2.7 for the Zn and Au examples respectively). The phase width, if any, has yet to be determined for this and other related phases also.

References.

(1) This research was supported by the Office of the Basic Energy Sciences, Materials Sciences Division, U. S. Department of Energy (DOE). The Ames Laboratory is operated for DOE by Iowa State University under Contract No. W-7405-Eng-82.

(2) Sevov, S.C.; Corbett, J.D. *J. Sol. St. Chem.* **1993**, *103*, 114.

(3) Bruzzone, G. *Acta Cryst.* **1969**, *25B*, 1206.

(4) Sevov, S.C.; Corbett, J.D. *Inorg. Chem.* **1991**, *30*, 4875.

(5) Sevov, S.C.; Corbett, J.D. *Inorg. Chem.* **1993**, *32*, 1612.

(6) Sevov, S.C.; Ostenson, J.E.; Corbett, J.D. *J. Alloys Comp.* **1993**, *202*, 289.

(7) Sevov, S.C.; Corbett, J.D. *Inorg. Chem.* **1993**, *32*, 1059.; b.) Sevov, S.C; Corbett, J.D. *J. Am. Chem. Soc.*, **1993**, *115*, 9089.

(8) Sevov, S.C. *Ph.D. Dissertation,* Iowa State University, **1993**.

(9) Corbett, J.D. In *Chemistry, Structure and Bonding in Zintl Phases and Ions*; Kauzlarich, S., Ed.; VCH: New York, **1996**; Chapter 3.

(10) Dong, Z.-C.; Corbett, J.D. *J. Am. Chem. Soc.* **1993**, *115*, 11299.

(11) Klem, M.T.; Vaughey, J.T.; Harp, J.G.; Corbett, J.D. *Inorg. Chem.* **2001**, *40*, 7020.

(12) *Shelxtl*; Bruker AXS, Inc.; Madison, WI, **1997**.

(13) A. L. Spek (**2001**) PLATON, A Multipurpose Crystallographic Tool, Utrecht University, Utrecht, The Netherlands.

(14) Charbonnel, M.T.; Belin, C. *Mat. Res. Bull.* **1992**, *27*, 1277.

Table 1. Details of data collection and refinement for $Na_{23}In_{40.4(1)}Pd_{2.51(2)}$

Formula	$Na_{23}In_{40.4(1)}Pd_{2.51(2)}$
Formula Weight	1139.91
Crystal system, space group, Z	hexagonal, P6/*mmm*, 2
Unit cell dimensions (Å)	
a	16.233(2)
b	16.233(2)
c	15.852(3)
V (Å^3)	3617.4(10)
Calculated density, Mg m^{-3}	4.186
Diffractometer	Rigaku
Octants, $2\theta_{max}$ (deg)	$\pm h, \pm k, l$; 55°
Observ. refl. ($> 2\sigma_I$)	9128
unique	1693 (R_{int} = .1793)
Absorp. coeffic. (Mo Kα, mm^{-1})	11.053
Rel. trans. coeff. range	0.4881 – 1.0000
variables	87
R, R_w[a]	0.0620, 0.1452
Largest ΔF, e$^-$/Å^3	4.29 (0.55 Å from Na5) and -3.98 (1.52 Å from Na2)
GOF	1.133

[a] $R = \Sigma||F_o| - |F_c||/\Sigma|F_o|$; $R_w = [\Sigma w(|F_o| - |F_c|)^2/\Sigma w(F_o)^2]^{1/2}$; $w = \sigma_F^{-2}$.

Table 2. Refined atomic positions ($x10^4$) for $Na_{23}In_{40.4(1)}Pd_{2.51(2)}$

	x	y	z	U_{eq}	occupancy
$Na_{23}In_{40.4(1)}Pd_{2.51(2)}$					
In1	1611(2)	4937(2)	5000	30(1)	58.1(3)% In + 41.9%(3) Pd
In2	3447(1)	0	4047(1)	32(1)	
In3	5526(1)	2x	6549(1)	28(1)	
In4	6028(1)	2x	8154(1)	23(1)	
In5	1872(1)	0	3114(1)	21(1)	
In6	2239(1)	2x	9058(1)	29(1)	
In7	628(1)	2x	0	23(1)	52.0(8)% In
In8	1239(1)	2x	0.1519(2)	29(1)	59.8(8)% In
In9	5536(2)	2x	0	44(2)	58(1)% In
Na1	1/3	2/3	0	17(2)	
Na2	0	0	1906(16)	35(6)	
Na3	2072(3)	2x	6991(8)	34(3)	
Na4	1/3	2/3	6269(13)	37(4)	
Na5	0	0	4049(9)	30(3)	
Na6	3801(6)	0	1901(7)	38(3)	
Na7	1280(6)	2x	5000	40(4)	
Na8	2954(10)	0	0	47(4)	

Table 3. Anisotropic displacement parameters ($Å^2 \times 10^3$) for $Na_{23}In_{40.4(1)}Pd_{2.51(2)}$.[a]

$Na_{23}In_{40.4(1)}Pd_{2.51(2)}$	U_{11}	U_{22}	U_{33}	U_{23}	U_{13}	U_{12}
In1	25(1)	45(1)	28(1)	0	0	23(1)
In2	24(1)	53(1)	27(1)	0	-3(1)	27(1)
In3	29(1)	29(1)	27(1)	-5(1)	-2(1)	15(1)
In4	19(1)	18(1)	32(1)	-4(1)	-2(1)	9(1)
In5	17(1)	15(1)	31(1)	0	-4(1)	7(1)
In6	37(1)	18(1)	26(1)	1(1)	1(1)	9(1)
In7	24(2)	16(2)	25(3)	0	0	8(1)
In8	29(1)	24(2)	32(2)	10(1)	5(1)	12(1)
In9	51(3)	23(3)	48(4)	0	0	12(1)
Na1	15(6)	15(6)	19(11)	0	0	8(3)
Na2	41(9)	41(9)	22(14)	0	0	21(4)
Na3	24(4)	17(4)	58(7)	1(4)	1(2)	9(2)
Na4	25(5)	25(5)	61(12)	0	0	13(3)
Na5	34(4)	34(4)	21(7)	0	0	17(2)
Na6	35(4)	43(6)	37(7)	0	-17(4)	21(3)
Na7	26(5)	46(9)	55(11)	0	0	23(5)
Na8	54(7)	98(14)	5(7)	0	0	49(7)

[a] $T = \exp(-2\pi^2(h^2 a^{*2} U^{11} + \ldots + 2\,h\,k\,a^{*} b^{*} U^{12}))$

Table 4. Atom Separations in (Å) for $Na_{23}In_{40.4(1)}Pd_{2.51(2)}$.

Atom pair	Distance
In1 – In1 x2	2.785(4)
In1 – In1 x2	2.820(5)
In1 – In2 x2	2.940(2)
In1 – In3 x2	2.938(2)
In1 – Na3 x2	3.62(1)
In1 – Na4 x2	3.45(1)
In1 – In7	3.62(2)
In2 – In2	3.022(4)
In2 – In3 x2	3.071(2)
In2 – In5	2.953(2)
In2 – Na3 x2	3.390(7)
In2 – Na7 x2	3.415(6)
In3 – In3	2.957(3)
In3 – In4	2.910(2)
In3 – Na3 x2	3.462(5)
In3 – Na4	3.238(3)
In3 – Na6 x2	3.466(9)
In4 – In4 x2	3.111(3)
In4 – In6 x2	3.036(2)
In4 – In9	3.236(3)
In4 – Na1	3.433(2)
In4 – Na3 x2	3.583(9)
In4 – Na4	3.48(2)
In4 – Na6 x2	3.485(6)
In5 – In5 x2	3.039(2)
In5 – In8 x2	3.070(3)
In5 – Na2	3.59(1)
In5 – Na3 x2	3.540(8)
In5 – Na5	3.382(6)
In5 – Na6	3.67(1)
In5 – Na7 x2	3.491(5)

Atom pair	Distance
In6 – In6	2.988(4)
In6 – In8	2.955(3)
In6 – Na1 x2	3.421(2)
In6 – Na3	3.30(1)
In6 – Na6 x2	3.568(5)
In6 – Na8 x2	3.545(3)
In7 – In7 x2	3.057(7)
In7 – In7 x2	1.765(4)
In7 – In8 x2	2.958(4)
In7 – Na2 x2	3.50(2)
In7 – Na8 x2	3.38(2)
In8 – In5 x2	3.070(3)
In8 – In6	2.955(3)
In8 – In7 x2	2.958(4)
In8 – Na2	3.538(5)
In8 – Na3	3.32(1)
In8 – Na6 x2	3.653(9)
In8 – Na8 x2	3.463(8)
In4 – In9	3.236(3)
In9 – In9	3.016(9)
In9 – Na1	3.178(5)
In9 – Na8 x2	3.64(2)
Na2 – Na5	3.40(3)
Na3 – Na6 x2	3.583(9)
Na5 – Na5	3.02(3)
Na6 – Na8	3.31(1)
Na7 – Na7 x2	3.59(2)

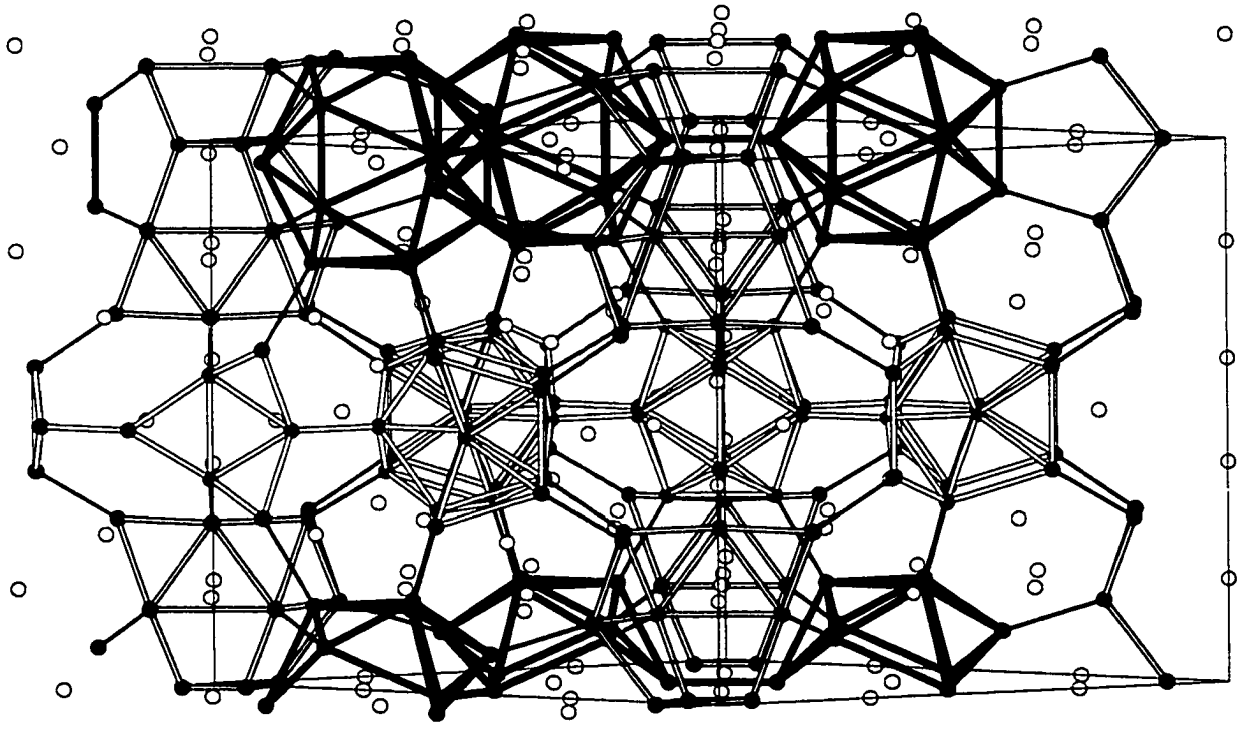

Figure 1. Structural view of $Na_{23}In_{40.4(1)}Pd_{2.51(2)}$. The In/Pd and Na atoms are represented by grey and white spheres respectively. The In_{12}, In_{15}, and In_{21} clusters are drawn with thicker white, black, and grey lines respectively.

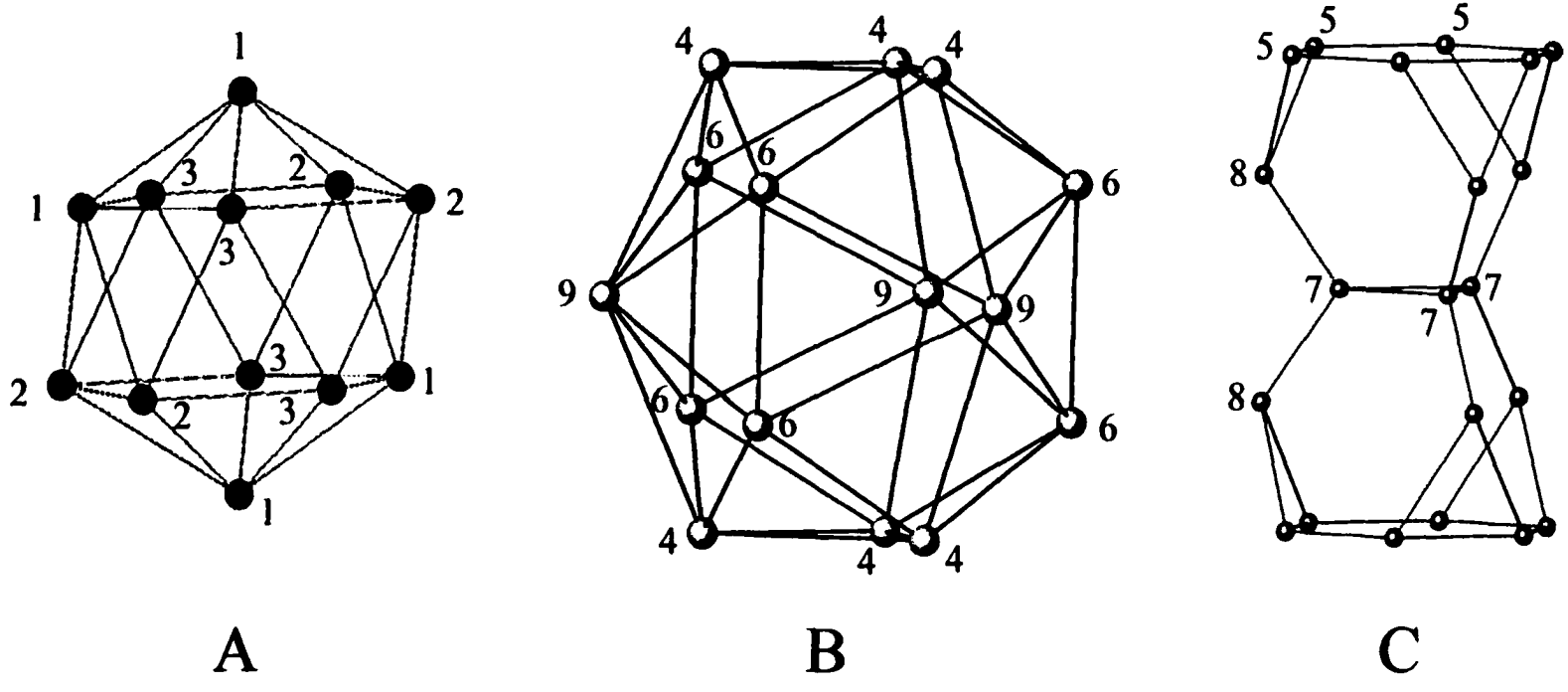

Figure 2. The three structural building blocks of $Na_{23}In_{40.4(1)}Pd_{2.51(2)}$. A.) 12-bonded icosahedron, B.) 15-bonded *closo*-In_{15}, C.) 18-bonded 21 atom spacer in one of two possible orientations. All atoms contain exo-bonds to other clusters except for the triangular waist in the In_{21} spacer.

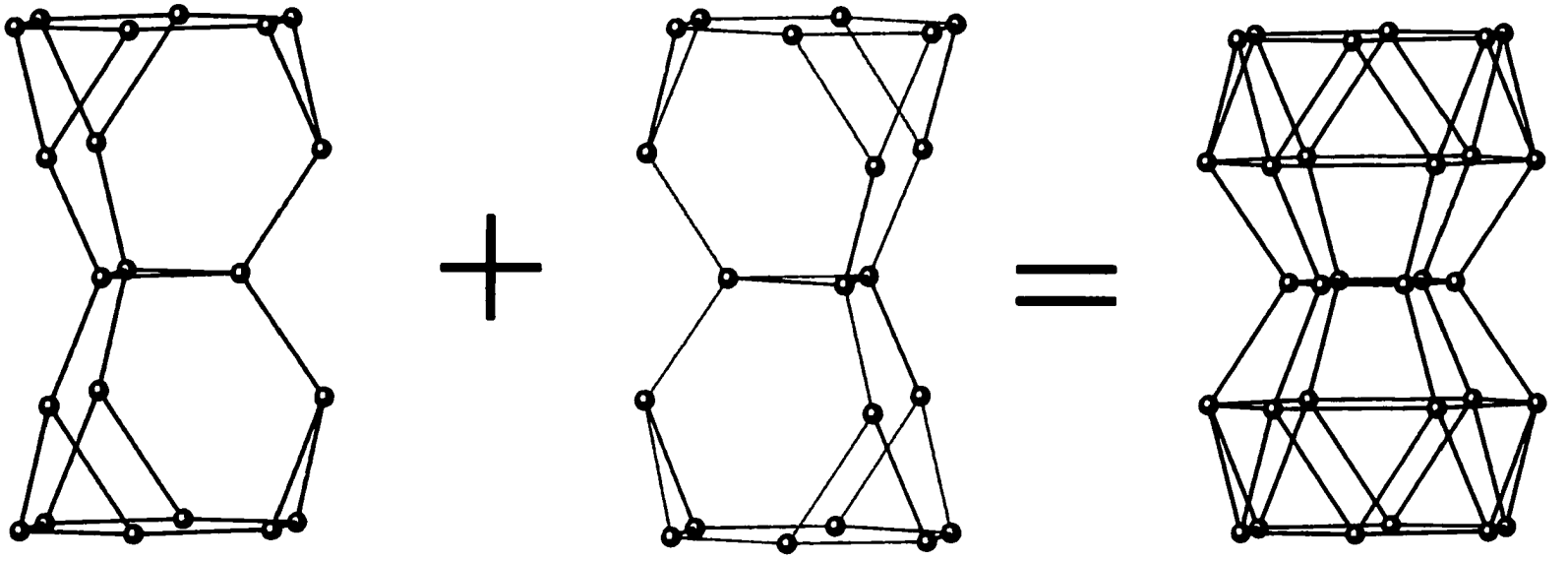

Figure 3. The refined formation (right) with D_{6h} symmetry is generated by superimposing two 21-atom spacers with two possible orientations. The atoms in the two end hexagons are common for both orientations while the rest belong to one orientation.

FUTURE WORK

A large amount of research remains possible in the ternary alkali metal (or alkaline-earth metal)/lead/main group element systems. The use of mixed cations has not been effective in the alkali-metal–Pb systems as only one known example has been produced, $Cs_{10}K_6Pb_{36}$.[1] Other ternaries may exist in the alkali-metal/tetrel/main group systems and more work should be done to determine if Ge or Sn may be suitable tetrel elements to explore. Their smaller size makes cluster separation easier with the fewer number of cations generally available. With this approach, the number of known Zintl phases in non-transition-metal containing heteroatomic clusters may be extended.

Further work is necessary with $K_{23}In_{40.4(1)}Pd_{2.51(2)}$ along with the isostructural $Na_{23}In_{38.4(2)}Zn_{4.6}$ and $Na_{23}In_{39.8(1)}Au_{3.4}$ to answer some of the lingering questions that remain about their structure refinements. The search for lower symmetry space group possibilities and a superstructure may be greatly aided by the acquisition of CCD data sets.

Explorations into the Ba/Sb/Pb system have shown an unknown phase present in the powder pattern, but no successful single crystal refinement has been successful as of yet. A few crystals have been isolated and tentatively indexed to a body-centered tetragonal cell (a = 12.4976, c = 18.2022 Å), but refinements ceased at a point that leaves approximately 22 e^-/Å^3 peaks left in the Fourier map 0.5 Å from a neighboring Pb atom left. Further work could include a search for lower symmetry and/or a superstructure.

Reference

(1) Bobev, S.; Sevov, S.C., *Polyhedron*, **2002**, *21*, 641.

ACKNOWLEDGMENTS

The years I have spent at Iowa State University have been challenging, exciting, and fulfilling, but would have been impossible without the help from many people. I would like to thank Dr. John D. Corbett for his support, understanding, and guidance during my time here. I would like to acknowledge Dr. Gordon Miller for his help, advice, and conversations on a variety of topics not always related to chemistry. I would also like to thank the rest of the inorganic faculty members at Iowa State. The guidance during classes and advice they contributed to my research will long be remembered and appreciated.

I am also grateful to Jerome Ostenson and Serguei Bud'ko for magnetic susceptibility measurements and aid in interpreting the results, and to Warren Straszheim for EDS measurements, and to Dr. Robert Jacobson for advice on refinements and the diffractometers.

I am also indebted to Shirley Standley, K.G. Baikerikar, and James Anderegg who have contributed to my work here by offering their friendship, advice, and performing basic maintenance duties, without which the lab would cease to function. I also have to acknowledge the past and present members of Dr. Corbett's and Dr. Franzen's group. Without them, I could never have completed my studies.

Finally I have to thank my family, especially my parents, Mary and Charles Klem, for encouraging my interest in science and supporting me emotionally during my time at Iowa State.